# Electrorheology for Smart Landing Gear

Final Technical Report

Grant No. NAG-1-1410
UMTRI No. UMTRI-96-16

Submitted to:
NASA/Langley

By:

Robert D. Ervin
Engineering Research Division
University of Michigan Transportation Research Institute

Zheng Lou
Electrical and Fuel Handling Division
Ford Motor Company

Frank E. Filisko
Material Science And Engineering
University of Michigan Transportation Research Institute

Christopher B. Winkler
Engineering Research Division
University of Michigan Transportation Research Institute

2901 Baxter Road
Ann Arbor, Michigan 48109-2150

April 30, 1996

UMTRI The University of Michigan Transportation Research Institute

**Technical Report Documentation Page**

| 1. Report No. | 2. Government Accession No. | 3. Recipient's Catalog No. |
|---|---|---|
| UMTRI-96-16 | | |

| 4. Title and Subtitle | 5. Report Date |
|---|---|
| Electrorheology for Smart Landing Gear | April 30, 1996 |
| | 6. Performing Organization Code |
| 7. Author(s) | 8. Performing Organization Report No. |
| Ervin, R.D., Lou, Z., Filisko, F.E., Winkler, C.B. | UMTRI-96-16 |
| 9. Performing Organization Name and Address | 10. Work Unit No. (TRAIS) |
| The University of Michigan<br>Transportation Research Institute<br>2901 Baxter Road, Ann Arbor, Michigan 48109-2150 | 11. Contract or Grant No.<br>NAG-1-1410 |
| | 13. Type of Report and Period Covered |
| 12. Sponsoring Agency Name and Address | Final Report |
| NASA Langley Research Center, Grants Office<br>Mail Stop 126<br>Hampton, VA 23665-5225 | 14. Sponsoring Agency Code |

15. Supplementary Notes

16. Abstract

Electrorheological (ER) technology was explored for its suitability to the continuous control of force and motion in aircraft landing gear. Although the state of knowledge on all types of active suspensions was examined, the analytical and experimental portions of the study focused upon the control of damping, alone. A specific class of ER damper designs was selected by means of a generalized analysis that modeled the ER fluid as a "bingham" plastic material. This analysis reveals the advantage of ER damping devices that minimize shear rates such that static shear stresses tend to dominate the damper's response. A prototype damping device in this class was constructed and simplified response parameters of the device were measured. Alternative formulations of the ER fluid are discussed and the employed test fluid is described. An analysis of the landing transient for an example military aircraft was performed so that the nominal performance of an ER-based damping controller could be estimated. The study observes that although ER technology offers promise over the long term, current limitations in fluid performance severely constrain the application to aircraft landing gear.

| 17. Key Words | 18. Distribution Statement |
|---|---|
| Electrorheology, landing gear, semi-active suspension, aircraft, dampers | Unrestricted |

| 19. Security Classif. (of this report) | 20. Security Classif. (of this page) | 21. No. of Pages | 22. Price |
|---|---|---|---|
| | | 62 | |

# Table of Contents

# 1. Introduction

This document constitutes the final report on a research study entitled "Electrorheology for Smart Landing Gear," sponsored by the National Aeronautics and Space Administration (NASA), Langley Research Center, under grant No. NAG-1-1410. The purpose of the project was to explore the suitability of electrorheological (ER) technology for creating adaptive control of the strut forces in aircraft landing gear during landing and taxiing. Insofar as ER fluids offer an inherent electrical-to-mechanical interface, the technology is of interest wherever the need exists for the active electronic control of a mechanical function. In the case of aircraft landing gear, a semiactive strut damping mechanism offers a means of adapting to the extant conditions of loading and vertical velocity such that peak values of airframe loads are minimized. Without an active damping function, for example, a fixed damping device must be designed for the mean operating condition, offering *too much damping* under some conditions and *too little damping* under others. It is also not possible, using a passive device, to phase the delivery of damping forces so that strut displacements are opposed optimally within a single cycle of motion. Although the traditional tools of electrohydraulics have been examined for creating active strut controls, the control devices have typically been rather complex, and the broad set of system requirements have generally militated against their frequent application.

Since ER fluids offer an inherent medium for mechanical control, there has been an interest in exploring the suitability of this technology for active landing gear control. The basic concept that was explored in this project is to operate on instantaneous signals representing acceleration, sink velocity, or strut displacement to derive an electrical signal that is applied as a *command signal* to the ER-controlled device. The instantaneous *thickening,* causing an increase in shear strength of the fluid, with increasing signal level produces a resistance to motion that is calculated to manage the strut forces and perhaps ride vibrations that accrue.

The work reported here covers a range of development tasks including a parametric analysis upon which one can select a generic type of ER device design, an analysis of the landing problem as addressed with semi-active ER control of strut damping forces, the identification of an example design that demonstrates the ER application principle, and generation of example data on an analogous, but not quite strut-worthy, ER damper. Because funding for this project was curtailed due to budget limitations in the last two years, it was not possible to build a semi-active ER control device specifically scaled for a landing gear application. Nevertheless, in a companion study funded by the U.S. Army's Tank Automotive Command (TACOM), [Lou, 1994] a reasonable approximation of the device intended for aircraft application was built and tested and is presented by way of reference here.

This report presents, in Section 2, a Technical Discussion of the general problem of controlling dynamic forces appearing in aircraft landing gear or automotive suspensions, including consideration of damping by electrical control of an ER fluid within a suitable semi-active device. Section 3 presents a consideration of alternative formulations of the ER

fluid, itself, for satisfying a suspension-type control application. In Section 4, the corresponding discussion of an ER device is presented, based upon design considerations that are, strictly speaking, scaled to the mentioned Army application, but that also apply reasonably well to a light-duty aircraft application that is more or less in the class of the F-106B nose wheel strut that has been examined in prior active control studies through Langley research. In Section 5, results of dynamic tests performed on the illustrative ER device are presented. These results serve to document the basic performance characteristics of the prototype ER damper that was, by cooperation with TACOM, delivered to NASA Langley for use in drop-test experimentation by the Landing Gear Research Group.

The report also appends copies of two technical papers that were produced in the course of this work. The first is entitled, "An Electrorheologically Controlled Semi-Active Landing Gear" and provides an analysis of an ER-control approach applied to the F-106B nose wheel problem in the landing mode of strut actuation. A second paper is entitled, "A Preliminary Parametric Study of Electrorheological Dampers." It develops the basis for preferring a certain class of mechanical designs for ER dampers, given the peculiarity that an ER fluid responds to an imposed electric field condition by changing its *static shear stress*, although the damping application calls for control of dynamic shear stresses.

# 2. Technical Discussion

## 2.1 Landing Gear Technology

The development of aircraft landing gear has evolved through various stages from the initial configuration of bicycle-type wheels carried in cycle forks to suspended wheels supported on rubber-and-spring devices, oleo-pneumatic shock absorbers, and later developments, such as the jump strut gear (Anon. 1987d) and active or semiactively-controlled landing gear systems (Wignot *et al.* 1971) (Bender *et al.* 1971) (McGehee and Carden 1976) (Ross and Edson 1979) (McGehee and Carden 1979) (McGehee and Dreher 1982) (Wigotsky 1984).

A modern landing gear typically consists of a wheel, a brake, a motion damper, an energy storage medium, and a retraction mechanism. While each component deserves its own share of attention, this project addresses only the damping function of absorbing and dissipating energy during landing and taxiing.

Vibrating forces and rigid body motions during landing and taxiing tend to hinder the pilots' manipulative and visual tasks, cause damage to the aircraft, and make the ride uncomfortable. To counter this general problem, various shock-absorbing packages have been designed, incorporating steel springs with or without oil damping, rubber springs with viscoelastic damping perhaps supplemented by an oil damper, pneumatic-only absorbers, oleo-pneumatic absorbers, and liquid-spring or oil-in-compression types. Among them, the oleo-pneumatic type is the most commonly used because of its light weight, high (energy absorption) efficiency, and effective recoil damping. In oleo-pneumatic and other oil-based shock absorbers, damping is induced by throttling the hydraulic fluid through mechanical orifices.

### 2.1.1 Energy absorption in the landing gear

During landing, the vertical kinetic energy of an aircraft is absorbed primarily by the tires and shock absorbers. Tires serve mainly as a spring for storing energy and for low-pass filtering of pavement irregularities, while the shock absorber package both stores and dissipates the bulk energy associated with vertical velocity and potential energy. The total reaction force from an oleo-pneumatic shock absorber is equal to the sum of the air spring force, the damping force associated with liquid pressure drop across the orifice, and other minor forces. The spring force increases with net deflection while the damping force is determined by the speed of the deflection. The deflection rate is typically the highest right at touchdown and then declines to zero as the aircraft settles toward (and perhaps overshoots) the static deflection state. Thus it is obvious that, with fixed orifice hardware, the damping forces will peak almost immediately upon first contact, resulting in a very nonuniform distribution of the energy absorption task over the full deflection transient.

### 2.1.2 The energy storage and absorption efficiencies

In a classic text on landing gear design, Conway (1958) presented the following definition: "the ratio of the actual energy storage to the full area bounded by the maximum load and deflection ordinates is called the energy storage or absorption efficiency." For our work, however, we need to distinguish the storage vs. dissipation components through these definitions:

(a) the energy storage efficiency: the ratio of the actual energy storage to the full area bounded by the maximum *spring* load and deflection ordinates; and

(b) the energy dissipation efficiency: the ratio of the actual energy dissipated to the full area bounded by the maximum *damping force* and deflection ordinates. (At least in concept, an optimally design ER damper would be able to approach the 100 percent level of energy dissipation efficiency.)

An air spring is nonlinear, and it is normally prepressurized in landing gear applications to reduce the required stroke needed to obtain maximum suspension forces. The preloading approach increases the storage efficiency by yielding a rather "boxy" force/deflection curve. If damping forces could be developed to yield comparably boxy force/deflection shapes, notwithstanding the declining velocity profile as deflection increased, dissipation efficiencies would likewise be improved.

### 2.1.3 The peak landing force

Increasing energy dissipation through damping will, of course, serve to minimize the deflection overshoot, thus resulting in shorter stroke and lower peak spring force. However, increased damping will not necessarily reduce the peak strut force if the overall time history of strut force is simply dominated by the initial damping spike at touchdown. The ultimate design goal relative to managing the landing transient, therefore, is to minimize the peak strut force for a given value of stroke, i.e., having high values of both storage and dissipation efficiency. To achieve this goal, it is ideal to control both the damping and spring forces during the landing. In this project, however, the scope of attention to ER control was limited to that of damping devices, only.

### 2.1.4 Taxiing

Since the main goal during taxiing is to reduce vibration during a period of near-static loading, energy storage is not a major concern. Rather, the focus is upon the regulation of damping coefficient in order to minimize transmissibility, from pavement irregularity into the airframe. The problem is thus more-or-less identical to that faced in other shock absorber applications, such as with automotive suspensions and engine mounts. The damping function during taxiing, however, must be provided by the same landing gear package, which satisfies the especially demanding requirements of the landing transient. Therefore, the need for parameter control spans a broad range of functionality. In the following discussion, we review prior work on the control of landing gear characteristics, recognizing that its emphasis upon the landing problem involves devices and principles that can be applied to the taxiing mode, as well.

### 2.1.5 Classifications of orifices

Damping in a conventional landing gear is realized by throttling hydraulic fluid through an orifice. There are three types of orifices: short, medium, and long. Across a short orifice, the main pressure loss is due to the formation of a jet, and it can be calculated by,

$$\Delta p = \frac{\rho}{2}\left(\frac{Q}{AC_q}\right)^2$$

where dp is the pressure drop, rho, the density; Q, the flow rate; A, the cross section area; and Cq, the discharge coefficient. Through a long orifice, the main pressure loss is due to the wall shear stress and is calculated from the following equations

$$\Delta p = \frac{128\mu l Q}{\pi d^4} \qquad \text{for a laminar flow}$$

$$\Delta p = 0.18809\rho\left(\frac{Q}{A}\right)^{7/4} v^{1/4} d^{-5/4} l \qquad \text{for a turbulent flow}$$

where d is the diameter; m, the dynamic viscosity, and n, the kinematic viscosity. For an intermediate-length orifice, the calculation is more involved.

The viscosity has no influence on the pressure drop in short orifices since the primary stresses are inertial. The viscosity does have strong influence however, in regions of laminar flow through long orifices, but only marginal influence when the flow in long orifices becomes turbulent.

The orifices used in conventional landing gear are typically short, such that damping forces due to viscous shear are minimal and the fluid viscosity is of little consequence to energy dissipation, per se (although it may have importance to other aspects of fluid handling within the device). Damping in conventional landing gear is thus normally controlled by selection of the orifice area.

## 2.2 Classification of dampers—and the generic option for real-time control of suspension/strut damping forces

Dampers are generally classified into passive, active, and semi-active varieties. A passive damper does not have any real-time control during the operation, although its damping characteristics may vary under changing load conditions and/or through a predesigned mechanism. In an active damper, the instantaneous position, speed, or force is directly controlled by a servo-actuation system, drawing from an independent energy source. The idea of using active devices to generate suspension forces dates back at least to the 1960s, and this interest has remained until the present, because of the large potential market in automotive applications (Karnopp, 1990). From a control theory point of view, the introduction of active damping forces would be expected to increase system performance. The idea that various active forces really need to be generated by some sort of servomechanism, however, is a strongly negative factor in most cases. Most force generators are complex, inefficient, and limited in frequency response. With their necessary power supplies, they tend to be much more expensive, bulky, massive, and delicate than

passive elements. This led to the consideration of semiactive force generators such as the semiactive damper (Alanoly and Sankar, 1987; Karnopp, 1990; Karnopp et al., 1974). The idea is to modulate the dissipation of energy in a basically passive damper by means of a control medium as a function of sensed variables such as mass velocities. Each of the three damping approaches will be discussed briefly below.

### 2.2.1 Passive damper

A passive damper can be designed to be optimum only at a fixed set of parameters, although real landing conditions vary greatly. Even under the optimum conditions, the performance may not be optimum due to other design constraints, e.g., stroke, weight, and size limitations. Clearly, the damping coefficient should be relatively small in the early phase of the landing transient, when vertical velocity is greatest, but would ideally rise as velocity declines. The current technique used to address such objectives provides mechanical means for changing orifice area using a needle or plunger with a variable area, a so-called "taxiing slot," or other more complex mechanisms such as the Chausson system or Katz systems (Conway 1958). For adjusting to other damping coefficients during recoiling (rebounding, in automotive parlance,) recoil orifices are engaged when fluid flow reverses.

The fundamentals of the passive vehicle suspension are reasonably well understood. Nevertheless, good design requires compromise among passenger ride comfort, requirement for suspension working space, variation in tire/ground contact-force variation, and vehicle attitude control (Sharp and Crolla, 1987b).

A conventional passive suspension consists of a fixed set of components, which implement predetermined spring and damping functions. These spring and damping functions may be complex, incorporating discontinuous responses in differing ranges of speed and stroke, but the operation is entirely mechanical and involves no external energy source. Selection of damper settings is a compromise between ride vibration isolation and control of wheel-hop resonance. Optimal design can be made only under a defined set of conditions, although combinations of pavement condition, vehicle loading, tire inflation pressure, etc. may vary greatly. In other words, off-optimality is incurred when the system state moves away from the assumed design conditions, which is unavoidable.

### 2.2.2 Active Suspensions

An active suspension is a system in which an actuator either totally replaces the conventional spring and damper elements or acts in parallel with a spring. Active suspensions require external power to drive the actuators, which are normally hydraulic cylinders, to generate the desired forces in the suspensions. Such systems can be further classified into two categories: slow-active and fast-active suspensions. The bandwidth of a slow-active system provides for actuation at frequencies higher than that of sprung-mass resonance but lower than that of the fundamental wheel-hop vibration, while the bandwidth of a fast-active system extends beyond the domain of wheel-hop frequencies. The bandwidth of active systems is mainly limited by the type of actuators used, although the control strategy also plays an important role. The slow-active systems would typically have a bandwidth around 3 hz and would employ pneumatic actuators (Cho and Hedrick, 1985), oleo-pneumatic actuators (Crolla *et al.*, 1987), d.c. motor-driven lead screws (Sharp and

Crolla, 1987b), and hydraulic actuators controlled by relatively inexpensive proportional valves (Inagaki *et al.*, 1992). Successful fast-active systems have generally required stiff hydraulic actuators controlled by expensive, precision servo valves.

Among the slow-active types of actuators, pneumatic devices have served to trim out static loads, acting in parallel with mechanical springs. Such actuators perform simply as soft springs when exercised at load frequencies that are beyond their response bandwidth, such that the suspension spring rate stays at the base rate. Stiff hydraulic actuators, as well as motor-driven lead screws, have also been employed in relatively slow-active systems, being mounted in series with mechanical springs (Sharp and Crolla, 1987b) when load trimming is, again, the objective. Among these variations, pneumatic actuators are treated as variable-force actuators, while hydraulic and mechanical lead screw devices are seen as displacement producers changing the preload on a conventional spring. If the spring is highly nonlinear, as with most multileaf springs, a higher preload also avails a higher local value of spring-rate.

The actuators required for fast-active suspensions are often not suitable for use in mass produced vehicles such as cars and trucks (Karnopp and Heess, 1991). Since the energy-input requirements are high, especially when addressing high frequency suspension activity, the fast-active alternative is adverse to fuel economy goals. The Toyota Motor Corporation, for example, recently abandoned its prototype work on fast-active suspensions as impracticable for the foreseeable future and moved, instead, to develop slow-active systems (Inagaki *et al.*, 1992).

In a slow-active suspension, the active component generally performs the leveling function only, while its conventional spring-damper subsystem is specially tailored for high frequency performance. Therefore, the functions of attitude control and isolation are separated. Slow-active systems have been shown to be competitive with fast-active systems in certain constrained applications (Cho and Hedrick, 1985; Pollard and Simons, 1984; Sharp and Crolla, 1987a). However, a slow-active system may exhibit deficiencies when the range of condition variables is large and, yet, performance expectations are high (Sharp and Crolla, 1987a). In particular, slow-active systems fail to handle wide-ranging conditions when no mechanism of variable damping control is provided.

### 2.2.3 Semiactive suspensions

The most common semiactive suspensions are those whose damping characteristic is adaptively controlled, although some have also entailed direct control of the spring characteristic (Mizuguchi *et al.*, 1984). In the spring case, however, varying the stiffness without, at the same time, effectively varying the free length of the spring produces the undesirable results of having unpredictable distribution of load on a four-wheeled vehicle. Solving this problem may be more difficult than solving those of a fully active system (Sharp and Crolla, 1987b). Recognizing this issue, the following discussion is limited to semiactive suspensions having controllable damping. Such systems can be further classified into two sub categories: force-controlled and resistance-controlled (Karnopp, 1990).

In the force-controlled semiactive system, the damping force is made to be dependent only upon the sign of the relative velocity; that is, the damping force is rendered more or less

independent of the magnitude of the relative velocity. The damping force is raised to a step function in the tension portion of the cycle and set to zero on the compression stroke. This kind of control can be accomplished by (a) using hydraulic shock absorbers with electromagnetically loaded pressure control valves (Hamilton, 1985; Karnopp *et al.*, 1974; Krasnicki, 1980a; Krasnicki, 1980b), or (b) incorporating a force sensor and a force control feedback loop (Karnopp, 1990), or (c) using an electromagnetic damper (Karnopp, 1987).

In the resistance-controlled semiactive system, the control target is the ratio of the damping force and relative velocity. In a hydraulic type of system, the damping force can be controlled by changing either the fluid viscosity or the orifice area. Control utilizing fluid viscosity variation will be effective only with long-orifice designs. Since the viscosity of conventional hydraulic fluids can be controlled only by thermal regulation, no feasible control techniques using conventional fluids exist. Two other possible approaches toward viscosity modulation involve ferromagnetic and electrorheological fluids. The use of ferromagnetic fluids is generally eliminated from automotive consideration by their demand for high levels of electric power, although recent research has indicated a promising new approach (Pinkos *et al.*, 1993). ER fluids offer a solution that avoids both thermal and power-based adjustments in viscous response and that may be practicably scaled for automotive application.

As for changing orifice area to effect semiactive control, the function can be implemented either continuously or discretely. The continuous approach is to regulate the cross-sectional area or opening of a short orifice or valve port. The most developed technologies in this regard involve electrohydraulic servo valves. In such devices, actuation energy is needed to drive a valve spool, typically through either electromagnetic or piezoelectric media. The discrete approach is to control the availability of flow passages (each of which has a fixed resistance property) to obtain various discrete increments in a control law governing total resistance. This approach can be realized using solenoid-controlled on-off valves, although there tend to be transient disturbances during the on-off switching (Karnopp *et al.*, 1974; Margolis and Goshtasbpour, 1984).

With its much simpler design, better efficiency, and lower cost, a semiactive suspension may compete well against active suspensions in practical terms while delivering performance that is much superior to that of passive suspensions (Hrovat *et al.*, 1980; Karnopp, 1990; Katsuda *et al.*, 1992; Kimbrough, 1986; Margolis, 1982; Margolis, 1983; Redfield, 1991). As far as controlling body motion due to roadway unevenness is concerned, semiactive systems can be virtually as effective as fully active systems using state variable feedback (Karnopp, 1990).

## 2.3 Control of Damping by Means of ER Fluid Devices

Although a variety of rather complex changes in the mechanical and electrical properties of electrorheological fluids have been observed in response to an imposed electrical field, the primary characteristic upon which most ER devices seek to operate is the static shear resistance that arises exponentially with increasing field strength. This phenomenon accounts for the common observation that ER fluids can exhibit the properties of a solid,

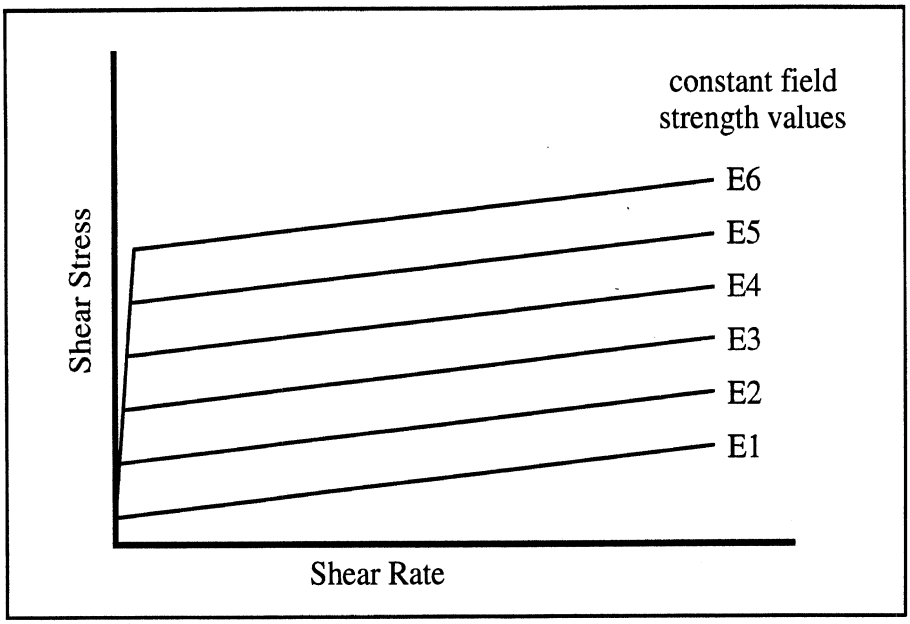


**Figure 1. Electrorheologic response per the classical Bingham model**

when "energized," and a liquid when de-energized. The electrical field condition is imposed upon a sample of fluid by containing the sample between two opposing electrodes that are energized to some voltage. In order to realize a mechanical stress response from the fluid, a mechanical shear condition is established—typically by inducing flow of the fluid between the electrodes or by translating one electrode relative to the other.

Figure 1 shows the basic characteristic of the so-called *Bingham plastic* model of electrorheological response. As field strength increases, an essentially static stress response to shear is observed. Exceeding the static strength level causes the fluid to shear more or less according to the behavior of Newtonian liquids, assuming that a Newtonian fluid medium has been employed as the liquid phase of the material.

Since the imposed field strength has virtually no influence on the shear stress levels developed at increasing levels of shear rate (i.e., the slopes in the figure are virtually the same across the range of E values, indicating that viscosity, per se, is essentially unaffected by the electric field), it is desirable practice to design devices to operate in the regime of low shear rates. By this approach, variation in the electrical signal level more directly controls the mechanical (stress-based) response, thus increasing the control efficiency of the system package. The shear rate regime can be modified, of course, by changing the nominal gains or gear ratios that directly determine either the flow of the fluid through an electrode gap or the translational movement of the electrodes causing uniform shear across the gap.

The particular variety of semiactive suspension that has been pursued in this study involves an ER controllable damper having parallel rotating disks. It is noted that a simple prototype of ER damper with concentric-cylinder electrodes has also been tested by Coulter (Coulter, 1993) at Lehigh University within the same time frame as the current Michigan research.

# 3. An Electrorheological Test Fluid

Within this project, alternative formulations of electrorheological fluid were examined in an attempt to improve upon fluid shear strength capability and to reduce settling of the particulate component in ER suspensions. Four alternative fluid categories were examined, namely, 1) homogenous solutions, 2) colloidal dispersions or gels, 3) amorphous substituted alumino-silicates, and 4) a zeolite-based suspension that was ultimately used as the fluid specimen for testing the automotive damping device in this study. The consideration of each will be discussed below.

## 3.1 Homogenous Solutions

ER active *solutions* present the ideal conceptual approach for solving the problem of settling that is otherwise seen in the multiphase (suspension) materials most commonly used as ER fluids. That is, a solution is, by definition, a single phase system that is inherently stable in terms of the physical distribution of its constituents. Recent discoveries have shown that solutions of poly gamma benzyl-L-glutamate (PBLG) and poly n-hexyl isocyanates (PHIC) exhibit an ER-active behavior. The PBLGs, although ER active in many solvents, are known to be soluble only in polar solvents, resulting in relatively high levels of conductivity and thus requiring rather high levels of electrical power for sustaining the electric field condition.

For this and other reasons, PHIC systems were examined in this study, seeking 25 to 30 percent concentrations of this solute in nonpolar solvents such as xylene and toluene. The selected solvents are also attractive because of their substantially lower cost than the PBLGs. Unfortunately, since the PHIC materials are not commercially available, it was necessary to develop procedures for preparing them in the laboratory. Initial plans were for preparing samples of PHIC from the monomer form, hexyl isocyanate, but it was discovered that only small quantities were available, from a single U.S. vendor, and that the highly costly material could be obtained only when ordered with a nine-month lead time. Accordingly, steps were taken to synthesize the monomer in our laboratories from more readily available base materials (heptanoyl chloride and sodium azide). Published procedures for this synthesis were substantially modified to yield the product quantities and the quality of molecular weight control that the ER application required. Approximately 1000 grams of PHIC was prepared, yielding 4 liters of an ER solution. The solutions thus prepared were found to be substantially ER-active, but exhibited properties that were poorer than those of more common fluids prepared by other methods. Since it was not possible, within this project, to further improve the materials by synthetically modifying the components, the search for a suitable ER solution was discontinued.

## 3.2 Colloidal Dispersions/Gels

By a second approach, steps were taken to prepare ER fluids that, under quiescent or static conditions, would constitute a gel that inherently resists settling of a particulate phase of the

materials. The desired gel formulation, of course, would exhibit an ER response to an electric field but would otherwise have a very low viscosity when deformed over a range of shear rate values. Various colloidal, as opposed to soluble, gelling agents were used primarily because the colloidal systems produce gels that are highly shear-thinning. By this approach, the gel effect would hold the fluid in a semisolid state, at rest, presenting an essentially zero static shear strength in the absence of an electric field. Upon even very slight initial loading, the gel would yield and thereafter exhibit a very low viscosity (i.e., thinning) response to increasing shear rate.

Although many colloidal agents were studied, the most promising was a montmorillonite clay modified so that it could be readily dispersed into an organic liquid. The ER-active behavior was achieved by using standard zeolite particles dispersed into paraffin oil with 1 to 2 percent organo-clay added. The fluids had the appearance of jelly but were seen to be highly thinning, even at shear rates down to 0.001 per second. This approach is not known to have been reported previously. Although it is believed to offer a promising approach to achieving stable ER-active suspensions, it was found that the gelled fluid could not be easily loaded into the ER damping device considered here. That is, since the gel-based fluid retains a static shape, it was not possible to fill a complex device with the fluid without entraining a great number of small air pockets. Entrained air is problematic in ER devices because the high field strengths required for the ER effect produce ionic breakdown and arcing across the bubbles. The arcing, in turn, tends to saturate the supply amplifier and thereby disturb the continuous nature of the ER energization voltage. Also, arcing can lead to breakdown of many insulating materials and to the introduction of metallic "spatter," which, itself, can form bridges for further short circuit paths through the fluid. Additionally, optimization of properties of these fluids and techniques for dispersing the clays into the liquids are not straightforward and will require substantial research for their refinement.

## 3.3 Amorphous Substituted Alumino-Silicates

The term *zeolite* applies to a crystalline form of alumino-silicates (Al/Si) that was observed by University of Michigan researchers to be an effective ER-active particulate. Amorphous forms of Al/Si as the dispersed phase in ER fluids have also been shown to produce ER-active suspensions. The amorphous materials are intrinsically more attractive because the chemistry can be much more radically varied without concern for constraints on the crystalline structure and because the materials are much less hydrophilic than the crystalline (note that water entrainment on ER particulates is undesirable because of the higher conductivity level that accrues). Seeking the combined qualities of ready synthesis and dry particles, efforts were taken to develop amorphous ER materials during this study. While this task was carried out only to a preliminary level of achievement, the effort was successful in varying the Al/Si ratio over large ranges and in combining the silicon atoms with a wide variety of elements other than Al. These include boron, germanium, cesium, and silver. Although much work remains to be done, small fluid samples were produced showing ER shear strengths three to four times greater than those that have been achieved customarily using the crystalline materials (zeolites). Research continues in this area, given indications that further increases in static stress capability are possible.

## 3.4 A Zeolite-based ER Fluid Used in the Illustrative Damper

Toward the conclusion of this study, a relatively conventional form of (nominally-dry) ER fluid was prepared using commercial zeolite particulate dispersed into a medium of transformer oil. The fluid was quite low in conductivity and yielded a shear strength of approximately 0.15 psi in response to an electric field of 3000 volts per millimeter. The very crucial shear strength question is only modestly addressed in this fluid sample. Indeed it is generally accepted that fluid strengths in excess of 1 psi will be needed before ER fluids are broadly attractive for automotive and aircraft applications, such as in active damping devices. Nevertheless, as the following sections of this document will show, a workable device was created and demonstrated here.

The particulate phase of the test fluid did tend to settle when left on the shelf, requiring substantial agitation to redisperse the thick layer that would form within a few days or so. When loaded into the test device, the system was kept in a mild state of agitation so as to simply avoid the settling problem for the duration of testing. The ancillary research thrusts outlined in the previous subsections indicate that while various approaches exist for resolving specific shortcomings in ER fluids, a substantial degree of further refinement is still needed.

# 4. Design of an ER Damper for use in Semiactive Control of Suspension/Strut Loading

In this chapter, substantive issues of the ER application to suspension or strut damping will be addressed. These issues begin with the basis for an ER damper concept given certain generic features of ER fluid behavior. Next, we address the configuring of a prototype damping device which, although scaled originally to meet the physical constraints of the suspension on the Army's High-Mobility Multipurpose Wheeled Vehicle (HMMWV), was later delivered to NASA/Langley for examination as an aircraft strut damper. Finally, the dynamic response of this device was tested in a generic way so as to characterize its basic properties as an electroncially-controllable damper. In the first subsection, a parametric study of the basic design options establishes the principle that ER damper performance is optimized in devices that shear the fluid at relatively low rates. This finding derives from the observation that the electrical field condition controls a *static shear stress* characteristic of the fluid. Given this principle, the discussion proceeds to lay out a design in which the fluid in a specialized ER damper is sheared at low rate, throughout an illustrative operating range. The device in question comprises a screw mechanism that is advanced through a carrier *nut* that, in turn, serves to rotate a number of disks between which ER fluid is sheared. The screw/nut mechanism provides a major reduction in the velocities over which fluid shear is imposed, thus keeping shear rates low so that the statically-derived ER stresses dominate.

## 4.1 Generic Design Options and Parameters for the ER Damper

In approaching the design of an ER-based, semiactive suspension control, the ER component can be built as either a flow-mode (figure 2a), mixed-mode (figure 2b), or shear-mode (figure 2c) type of damper. The configurations illustrated in figure 2 are essentially generic concepts that contain simplified features to facilitate the design analysis. In practical hardware, for example, the cylinder is likely to be single-ended, rather than double-ended, and the ER control valve or area is likely to be comprised of multiple parallel or concentric plates. Among the three conceptual modes, the flow-mode damper is most similar to the traditional shock absorber, except that it replaces the conventional orifice with an ER control gap or valve. The source of the damping force in this mode is exclusively from flow-induced pressure drop across the piston. The ER valve can be placed outside the cylinder (as in figure 2a) or within the piston component. For the sake of compact packaging, the external approach could be implemented by forming a flow chamber along the outside of the cylinder wall (Petek, 1992).

In the mixed-mode damper, the ER control is realized in the gap between the piston side-wall and the cylinder liner. The fluid shear stress at the shear surface also contributes to the damping force, while the flow-induced pressure drop is still present as a force component on the piston.

If a large by-pass port is cut through the piston of a mixed-mode damper, the device becomes a simple shear-mode element. Since the fluid can flow freely through the by-pass, the pressure drop across the piston becomes negligible and only shear stresses developed along the wall contribute to the damping force.

Our analysis (see appendix B) indicates that the shear-mode damper achieves better dynamic response and more effective control than the flow- or mixed-mode types. Because certain principles in ER design support the prospect of a package that is mechanically simple, durable, low in cost, and exhibits a broad bandwidth, it appears that an ER semiactive suspension may be superior to conventional types of semiactive and active suspensions for automotive applications. Although the fluid's behavior is complex, it has also been sufficiently well defined at this point that its codification on cheap and reliable memory devices is straightforward. Improvement in mechanical strength of the fluid's energized, shear-stress response remains the most important factor in determining whether or not ER devices will become practical in this application.

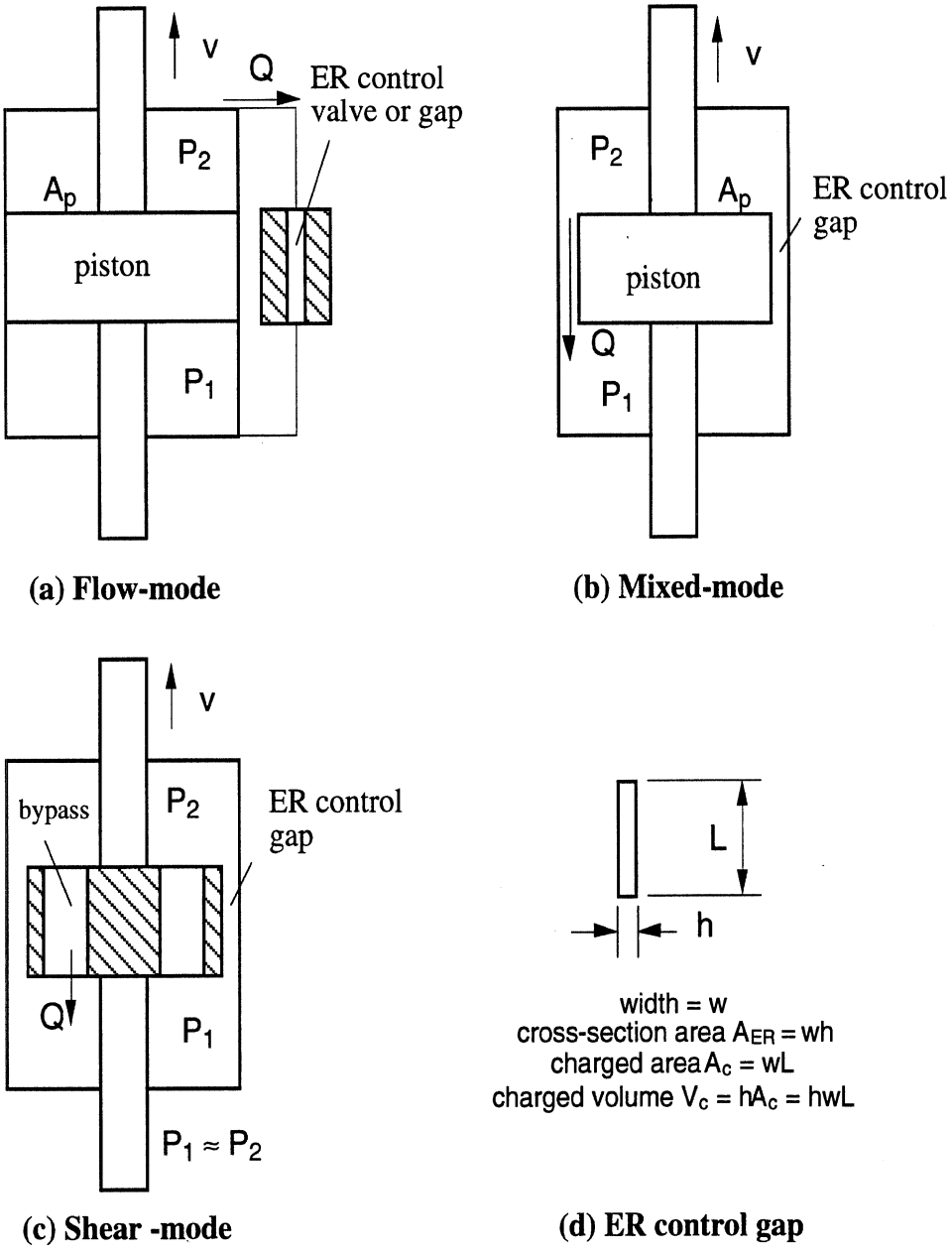


**Figure 2. The generic concepts of the three modes of electrorheological dampers**

## 4.2 Selected Design of the ER Shock Absorber

A shear-mode damper, as indicated in the above section, achieves better dynamic response and more effective control than the flow- or mixed-mode types and is thus selected as the damper mode for this project. The general concept of the proposed design is shown in figure 3. The control in the ER damper is realized through a medium of an ER fluid. The shear-mode damper uses, instead of translational plates, a plurality of rotational shearing disks (hot electrodes and cold electrodes), which form a total control (or shearing) surface area that is constant and independent of the relative position of the actuator, resulting in a

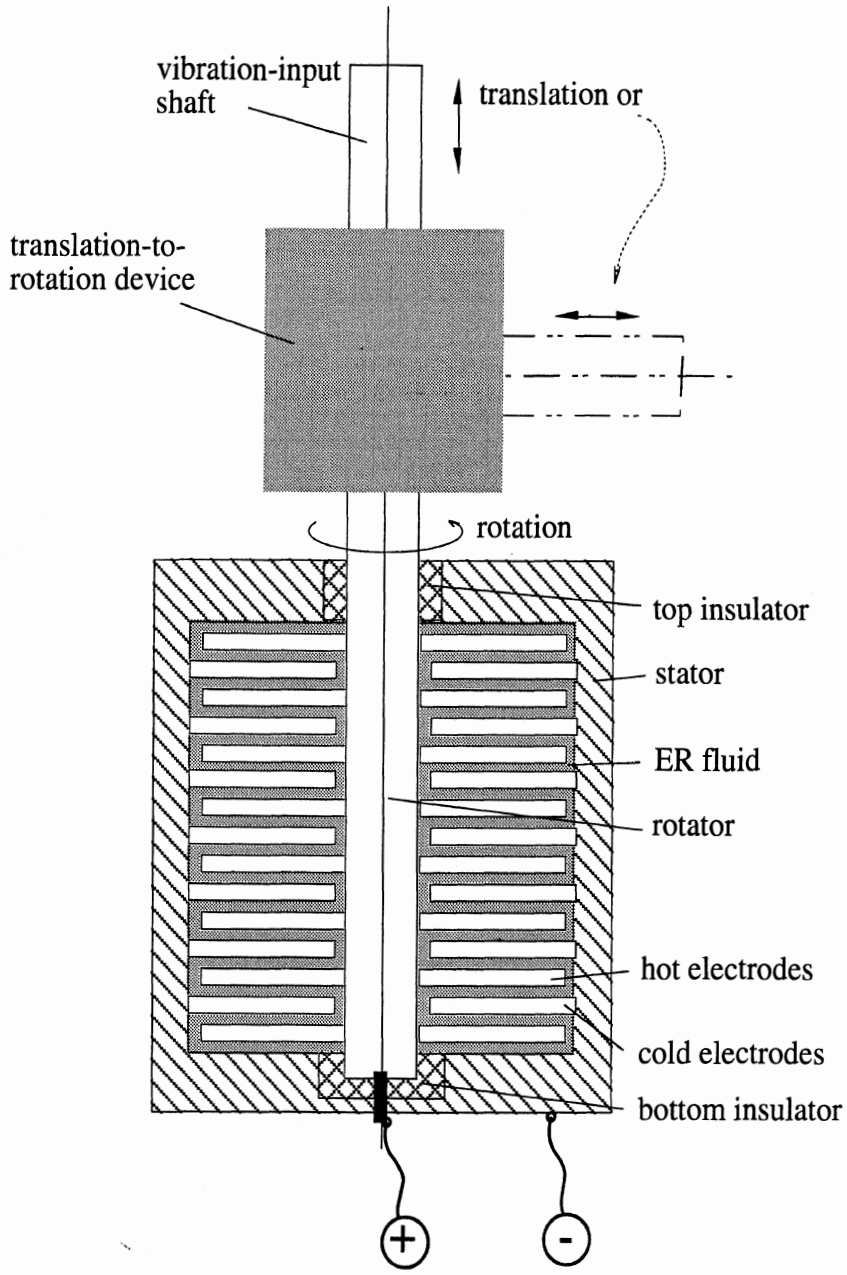


**Figure 3. The general concept of the proposed design**

good control and a compact size. A translation-to-rotation device converts the translational motion of the vehicle vibration into the rotational motion of the shear-mode damper, and vice versa.

The actual ER damper developed in this project is show in figure 4. In this design, thirty-nine ground electrodes, separated from each other by spacers, are mechanically fixed and electrically connected to a stator through stator feather keys. The stator is grounded electrically and fixed rigidly onto the unsprung mass. Forty elevated-voltage, or "hot," electrodes, also separated from each other by spacers, are mechanically attached to a rotator

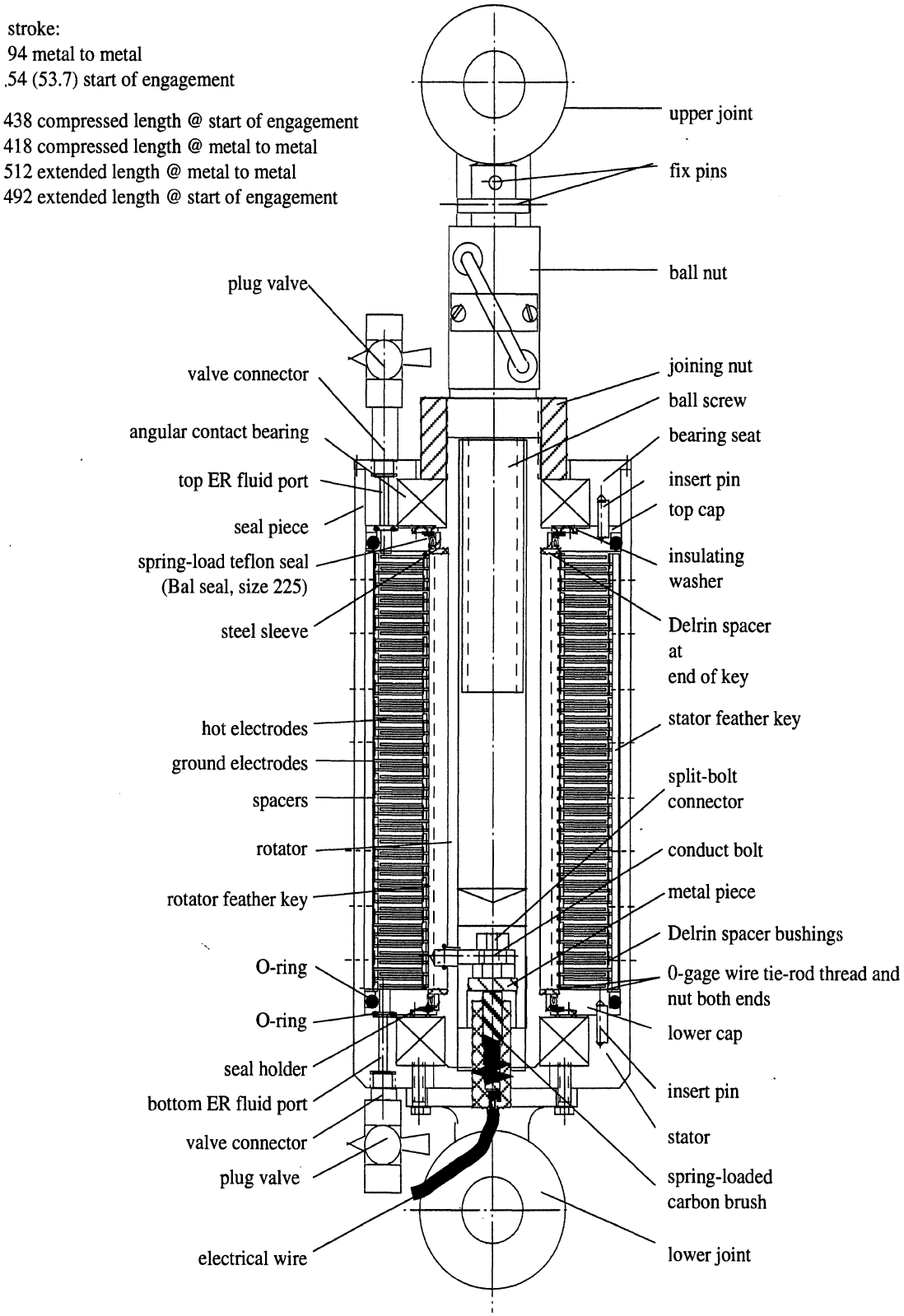


**Figure 4. Assembly of the demonstration ER damper**

through rotator feather keys, and electrically connected to the high voltage source through a spring-loaded carbon brush. The rotator is mechanically supported by top and bottom bearings that can sustain both radial and axial loads. The rotator is made from glass epoxy G-11, a dielectric material with high mechanical strength. Interelectrode gaps are filled with an ER fluid through top and bottom ports.

The translational relative motion is converted through a ball screw mechanism, which is tightly connected on top of the rotator with a joining nut. The use of the ball screw provides for a very low-friction transmission of power and motion. The complete set of drawings of the ER damper is contained in appendix C.

### 4.2.1 Number of Electrode Plates

The influence of the inertia force is small in a shear-mode damper, such that the damping force in the strut can be approximated with a Newtonian damping force ($F_{dN}$) and an ER damping force ($F_{dER}$), corresponding to the effects of the plastic viscosity (h) and the yield shear stress ($\tau_y$), respectively, in the Bingham model. The two damping forces are derived as

$$F_{dN} = \frac{4\pi n\eta(r_o^4 - r_i^4)}{ehD_p^2 \tan^2\lambda}\Delta v \tag{4}$$

and

$$F_{dER} = \frac{\Delta v}{|\Delta v|}\frac{8\pi n(r_o^3 - r_i^3)}{3eD_p \tan\lambda}\tau_y \tag{5}$$

with

$$\Delta v = \frac{dx_U}{dt} - \frac{dx_S}{dt} \tag{6}$$

$$e = \frac{\cos\phi - \frac{f}{\tan\lambda}}{f\tan\lambda + \cos\phi} \tag{7}$$

where $n$ is the number of hot electrodes, $h$ ( = 0.001 m) the gap size between the electrodes, t the time, Dv the strut deflection velocity, $x_S$ the sprung mass displacement, $x_U$ the unsprung mass displacement, $r_o$ (= 0.0483 m) and $r_i$ (= 0.0285 m) the outer and inner radii of the effective shearing surface of the electrodes, respectively. The parameter $D_p$ ( = 0.0254 m) is the pitch diameter, f (standard at 29 degrees) the thread angle , l ( = 17.657 degrees) the lead angle, $e$ ( = 90 percent) the ball screw efficiency, and $f$ ( = .033) the friction coefficient for the screw-nut mechanism. The variables $v_s$ and $v_u$ are the sprung and unsprung mass velocities, respectively, and Dv is the strut deflection velocity. The Newtonian and ER damping forces here are completely uncoupled and additive. While this approach provides only a first-order estimation, the formulation is convenient and insightful for a preliminary parametric study. However, a complete solution of the problem will demand a full solution of the fluid flow problem (Lou *et al.*, 1993).

### 4.2.2 Filling the Damper with ER Fluid

In order to avoid arcing when high voltages are applied across the plates of the damper, it is important to insure that little or no air is entrained in the ER fluid. Therefore, a special effort was undertaken to fill the damper with fluid.

The fluid sample was first put into a closed vessel and subjected to a 29-in hg. vacuum for a period of twenty-four hours. Still under a vacuum, the fluid was agitated to insure an even distribution of the particulate material. The fluid was then immediately forced into the damper under three to five psi pressure. In this process, the fluid was withdrawn from the bottom of the external vessel and fed into the damper through its bottom port so that air was not drawn into the system. Air was simultaneously evacuated from the damper through the top port.

In all of the subsequent operations of the damper, the internal fluid space of the damper was plumbed to a small bladder-accumulator containing the same ER fluid. By this means, ER fluid was maintained at about three psi gage pressure. Thus, the fluid in the damper was maintained at a positive pressure, preventing air ingestion through the seals of the damper while permitting expansion and contraction with heating and cooling.

Whenever the damper was not active, the sealed system of damper and external accumulator was removed from the testing apparatus and placed in a tumbler in order to prevent settling of the particulates in the ER fluid. (The tumbler was simply a tube lined with foam padding, turning slowly in a lathe.)

# 5. Dynamic Tests of the Illustrative ER Damper

A short series of dynamic tests were conducted on the ER damper (also called an "ER shock" in data figures, below) to determine its coulomb and viscous friction response and to characterize the response time of the controlled force to applied voltage.

The test arrangement involved a simple displacement cylinder arranged in line with the ER damper on a bed plate. The actuating cylinder stroked the damper directly through a load cell, which measured the damper rod force. An LVDT was used to measure the damper stroke.

Tests were conducted with three voltage wave forms: (1) $v_c = 0$ v for a complete run; (2) $v_c = 500$ v for a complete run; (3) $v_c = 500$ v at $t = 0$, stepping up to 2,500 volts at one third of the compression stroke and returning to 0 volts at two thirds of the compression stoke. For each wave form, four tests were run with the stroke speeds of 2, 4, 6, and 8 in/s. Data were used from the compression stroke only because the special plastic fittings used to electrically isolate the ER damper from the load cell were not strong enough in tension to handle reverse loading.

Tests conducted with the first wave form ($v_c = 0$ v) were intended to characterize the viscous, unenergized, behavior of the damper. The intent was to measure the steady-state response of the ER damper at the four velocity levels. Test results showed, however, that fairly large mechanical vibrations existed throughout the stroke. An example of the time history of damper (labeled "shock") force during one such test is shown in figure 6. After some informal experiments, the second test series, using a command voltage of 500 volts, was added with the hope of providing less noisy data. This was not particularly successful. In the end, steady state results were derived from both of these test series simply by processing the time histories through the appropriate low-pass filters. The filter-processed data corresponding to the example test of figure 6 are shown in figure 7.

The third test series involved step changes in command voltage from 500 volts to 2500 volts and back to 0 volts during the stroke. The resulting time histories of damper force were (1) low-pass filtered to obtain the steady-state response at 2500 volts, and (2) examined to characterize the response quality of the ER damper.

The steady-state results from the three test series are summarized in figure 8. This figure also includes the appropriate zero velocity data taken at electric field intensities corresponding to 0, 500, and 2500 volts. These static values represent the sum of the damper forces produced by coulomb friction (at zero volts) and the so-called Bingham yield stress of the ER fluid.

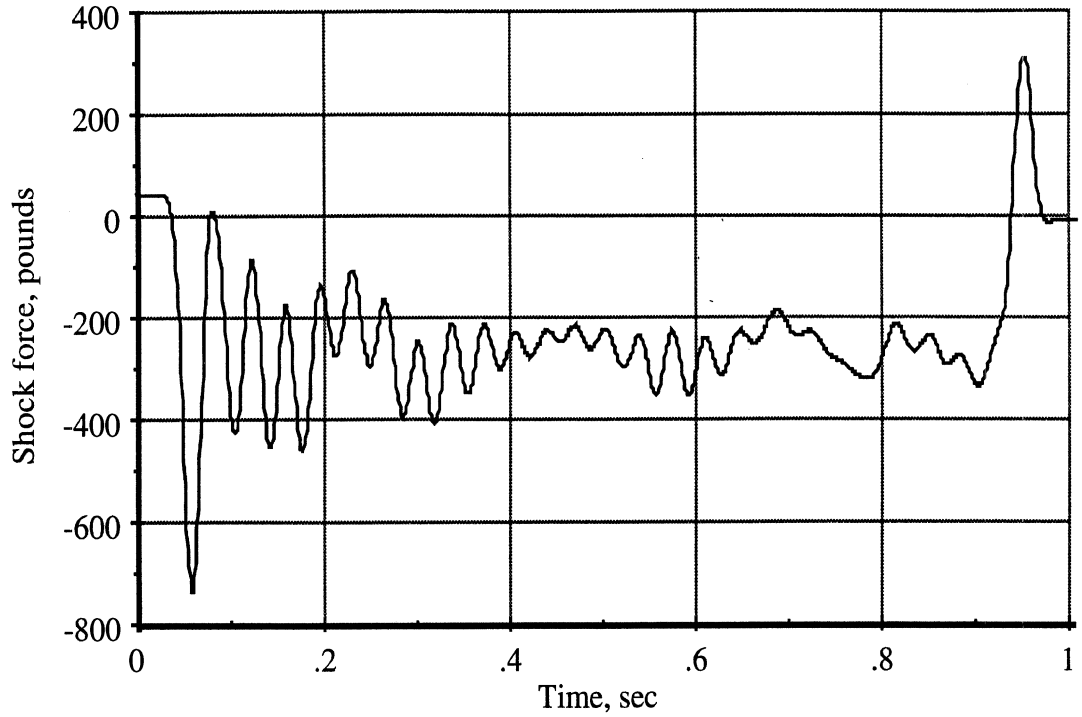


**Figure 6. Time history of ER damper force during a steady state test (4 inches per sec, 0 volts)**

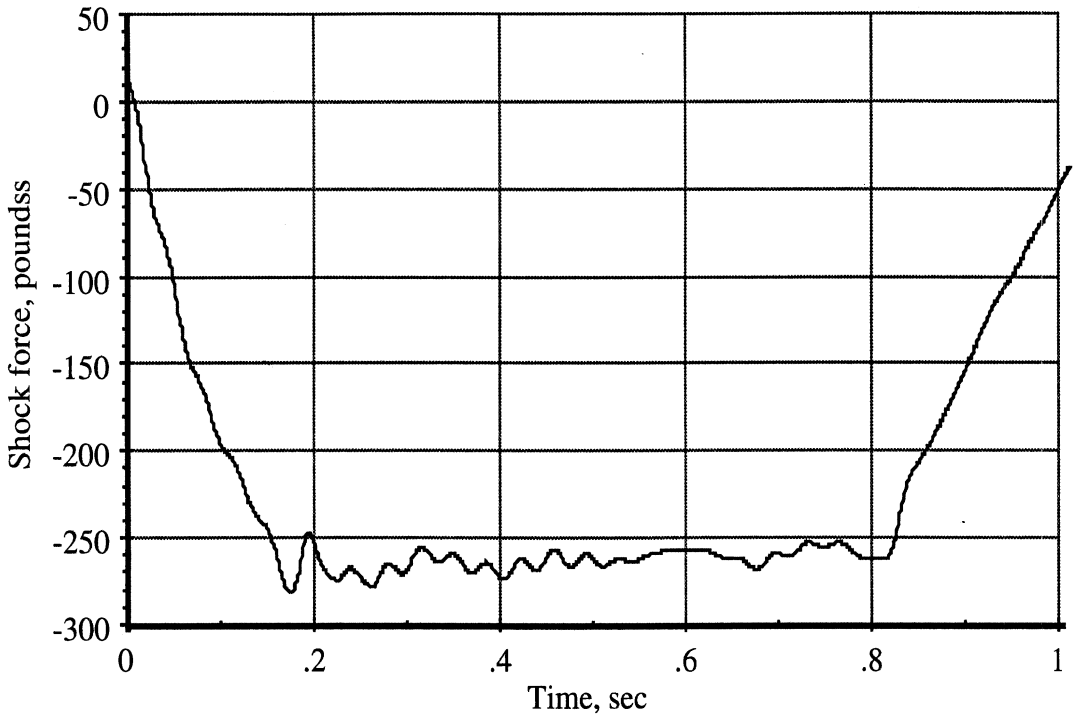


**Figure 7. Example of a heavily filtered time history of ER damper force during a steady state test (4 in/sec, 0 volts)**

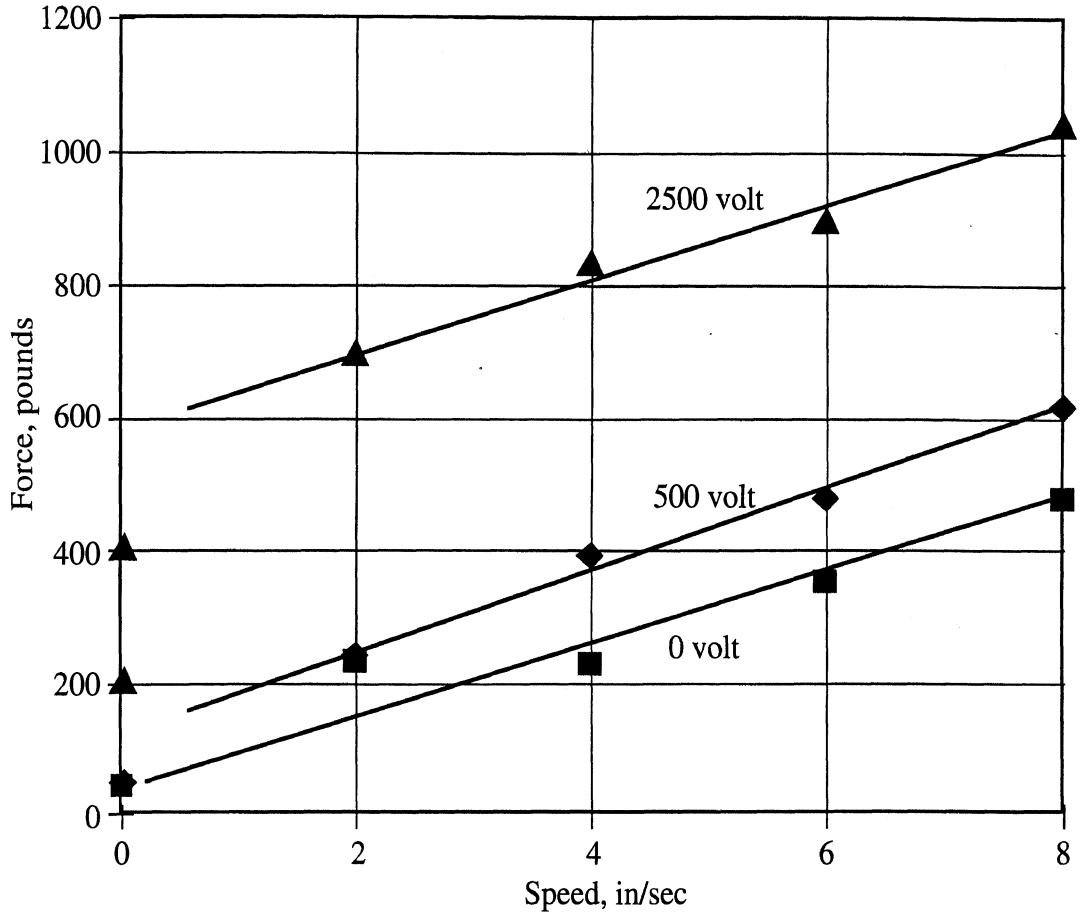


**Figure 8. Summary of average force values from steady-state tests**

Among the steady-state data, the damper force at 2 in/sec and 0 volts deviates from the trend and almost coincides with the damper force at 2 in/sec and 500 volts. If this point is removed from the plot, a line fitted to the 0-volt line will be nearly parallel to the lines fitted to the 500- and 2500-volt data, respectively.

The slope of these fitted lines is indicative of the viscous response of the damper. The viscous damping forces are substantial, and larger than we had intended within the original design. This result is largely because of the change from kerosene as the originally-intended, low-viscosity, base fluid to a higher-viscosity transformer oil.

The vertical separation of the lines in figure 8 is related to the ER behavior of the damper. The damper forces at 2,500 volts are roughly two times higher than the zero-field forces. The damper forces at 4,500 volts, if achievable without arcing, would be approximately 4 times those at 2,500 volts (i.e., approximately 4,000 pounds) according to the $2.5^{th}$ power law, which roughly approximates the shear stress vs. field strength relationship for this fluid.

The dynamic response of the ER damper absorber is illustrated in the time histories of figures 9 and 10. Each figure includes the time history of control voltage and current and the resulting damper force. Figure 9 shows the portion of a single test when

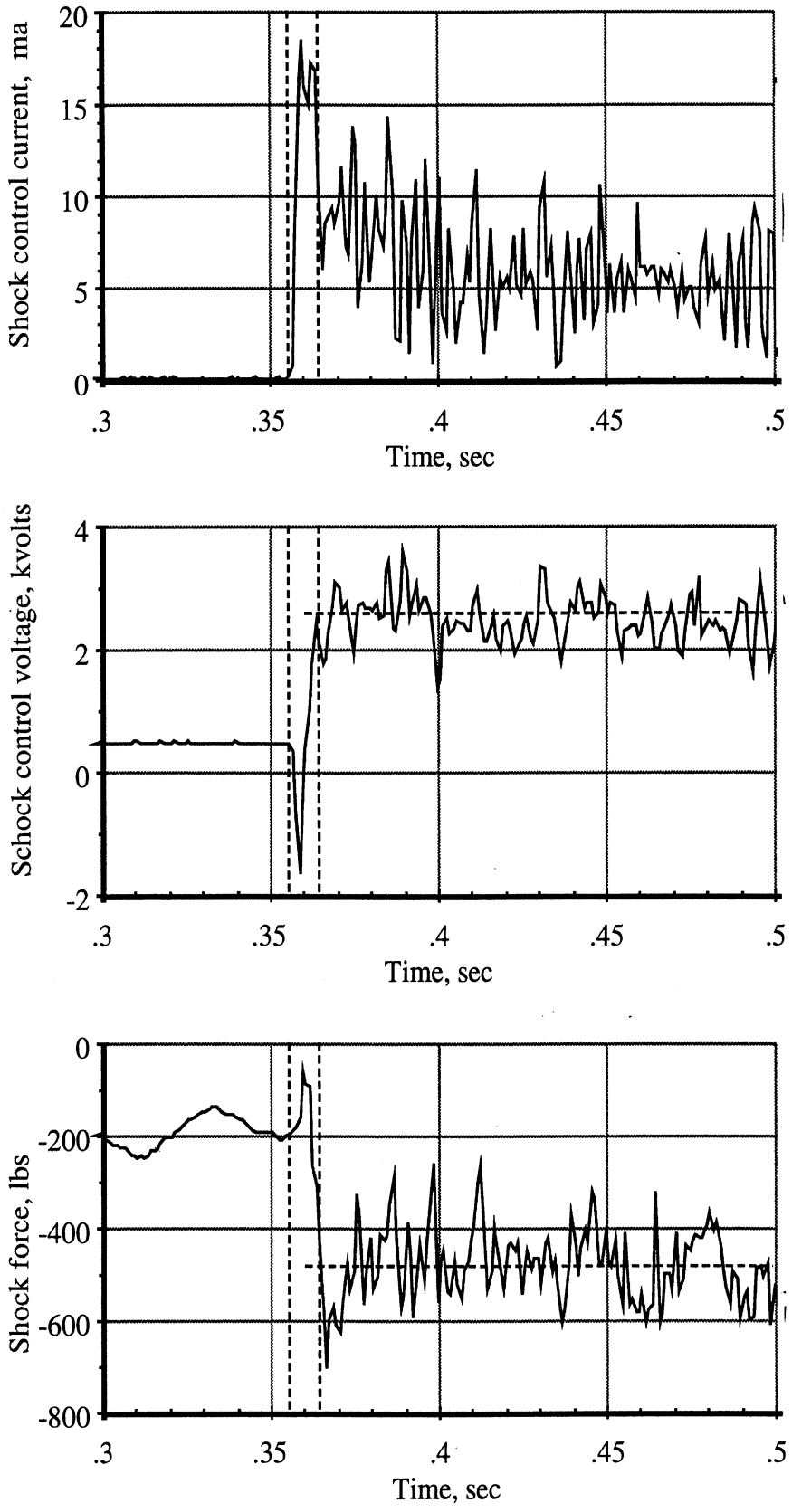


**Figure 9. Timing of the ER damper control current and voltage, and damper force upon a step change of voltage command from 500 volts to 2500 volts**

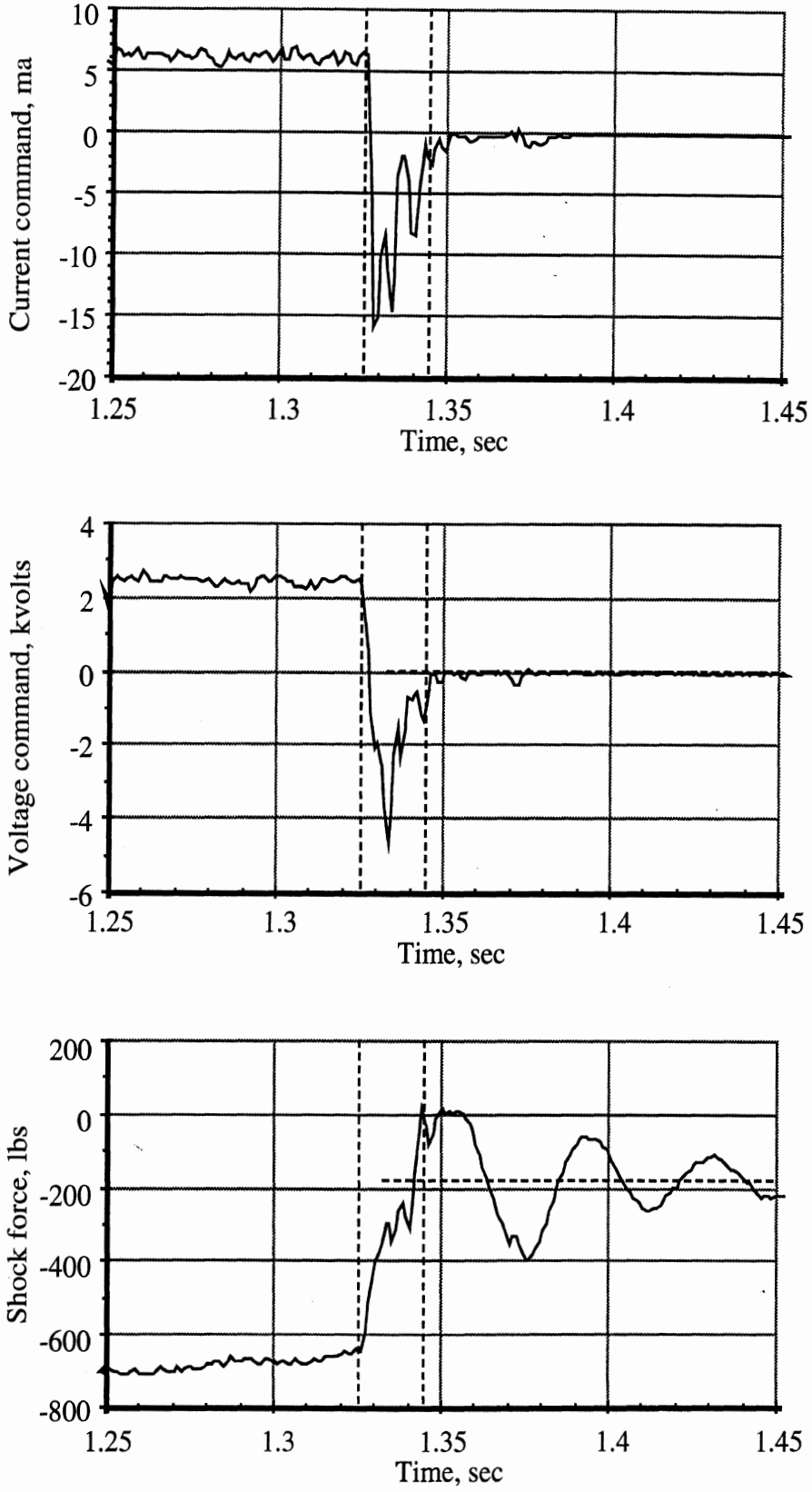


**Figure 10. Timing of the ER damper control current and voltage, and damper force upon a step change of voltage command from 2500 volts to 0 volts**

voltage stepped from 500 to 2500 volts. Figure 10 is from the same test at the time when the command voltage was stepped back down to 0 volts.

These time histories seem to show that when the step change in command voltage is requested, the change in current flow is very rapid, but the change in actual voltage lags slightly due to the need to charge the plates inside the ER damper. The force appears to develop virtually in phase with control voltage. Thus, it appears that the dynamic response of this system is limited by the response of the high-voltage amplifier, and the force responds to the voltage without appreciable lag.

# 6. Conclusions

The semiactive control of strut damping forces in an aircraft landing gear poses a challenging application for which electrorheology offers a feasible, although insufficiently developed, solution at present. Clearly, working prototypes can be built that at least demonstrate the functional benefits of ER control, if not in an attractive overall package.

In this project and a companion study under Army sponsorship, a working prototype of an electrorheological damper was developed, demonstrated, and later delivered to Langley's Landing Gear Research Group. In its Army application, this device showed a level of suspension control that was superior to that of conventional shock-absorber damping, (Lou, 1994) although performance limitations and fluid handling problems served to illustrate the constraints faced by many ER applications. Some argue that the fluid handling issues will all be resolved when fluids are finished for commercial usage and supplemented with additives that otherwise suppress bubble-entrainment, particulate settling, arc-induced breakdown, etc.

It is also fair to say that parallel advancements in ER fluid technology are offering to extend the fluid performance range and to make possible entirely different design approaches for configuring semiactive damper devices. For example, an American chemical supplier is advertising ER fluids with a shear strength capability of 1.0 pounds per square inch (i.e., six times the level achieved in the prototype fluid formulated here). The advertised fluids are comprised of cross-linked polyurethane particles in silicone oil. If such a fluid was found to exhibit other suitable attributes, it would allow alternative designs that avoid the relatively high complexity and weight of the ER damper that was prototyped in this study.

Finally, while this study borrowed from the extensive literature on semiactive suspension control, it did serve to illustrate the merits of the broad bandwidth capability of ER technology. With proper design of the electrical system so as to minimize device capacitance and heighten the current delivery capability of the high-voltage amplifier, ER dampers could be made to act in better than a 10 msec response time. The very high speed response of ER fluids does, indeed, offer a powerful mechanism for achieving the rapid modulation in damping forces that would be required for high absorption efficiency in an aircraft landing gear.

# 7. References


Alanoly, J., and Sankar, S., 1987, "A new concept in semiactive vibration isolation," *Journal of Mechanisms, Transmissions, and Automation in Design*, Vol. 109, pp. 242-247.

Cho, D., and Hedrick, J. K., 1985, "Pneumatic actuators for vehicle active suspension applications," *Journal of Dynamic Systems, Measurement and Control*, Vol. 107, pp. 67-72.

Coulter, J. P., 1993, "An investigation of electrorheological material based controllable damping devices," *The Fluids Engineering Conference: Electrorheological Flows -1993,* Siginer, D. A., Kim, J. H., and Bajura, R. A., ed., FED-Vol. 164, ASME, New York, pp. 143-156.

Crolla, D. A., Horton, D. N. L., Pitcher, R. H., and Lines, J. A., 1987, "Active suspension control for an off-road vehicle," *Proceedings of Institution of Mechanical Engineers*, Vol. 201, pp. 1-10.

Hamilton, J. M., 1985, "Computer optimized adaptive suspension technology (COAST)," *IEEE Transaction on Industrial Electronics*, Vol. IE-32, pp. 355-363.

Hrovat, D., Hubbard, M., and Margolis, D. L., 1980, "Suboptimal semiactive vehicle suspensions," *Proceedings of Joint Automatic Control Conference,* pp. WA10-H.

Inagaki, S., Inoue, H., Sato, S., Tabata, M., and Kokubo, K., 1992, "Development of feedforward control algorithms for active suspension," Paper No. 920270, SAE, Inc., Warrendale, PA.

Karnopp, D., 1987, "Force generation in semiactive suspensions using modulated dissipative elements," *Vehicle System Dynamics*, Vol. 16, pp. 333-343.

Karnopp, D., 1990, "Design principles for vibration control systems using semiactive dampers," *Journal of Dynamic Systems, Measurement and Control*, Vol. 112, pp. 448-55.

Karnopp, D., Crosby, M. J., and Harwood, R. A., 1974, "Vibration control using semiactive force generators," *Journal of Engineering for Industry, Transactions of the American Society of Mechanical Engineers*, no. 96, pp. 619-626.

Karnopp, D., and Heess, G., 1991, "Electronically controllable vehicle suspensions," *Vehicle System Dynamics*, Vol. 20, pp. 207-217.

Katsuda, T., Hiraiwa, N., Doi, S., and Yasuda, E., 1992, "Improvement of ride comfort by continuously controlled damper," Paper No. 920276, SAE, Inc., Warrendale, PA.

Kimbrough, S., 1986, "Bilinear modelling and regulation of variable component suspensions," *ASME Monograph*, Vol. AMD-80, DSC-2.

Krasnicki, E. J., 1980a, "Comparison of analytical and experimental results for a semiactive vibration isolator," *The Shock and Vibration Bulletin*, Vol. 50, Part 4, pp. 69-76.

Krasnicki, E. J., 1980b, "The experimental performance of an 'on-off' active damper," *The Shock and Vibration Bulletin*, Vol. 51, The Shock and Vibration Information Center, Naval Research Laboratory, Washington D.C.

Lou, Z., Ervin, R. D., and Filisko, F. E., 1990, "The feasibility of using electro-rheological fluids in aircraft flight controls-Phase 1 report," UMTRI-90-10, The University of Michigan Transportation Research Institute, Ann Arbor.

Lou, Z., Ervin, R. D., and Filisko, F. E., 1992, "Behaviors of electrorheological valves and bridges," *Proceedings of the International Conference on Electrorheological Fluids: Mechanism, Properties, Structure, Technology, and Applications,* Tao, R., ed., World Scientific, River Edge, NJ, pp. 398-423.

Lou, Z., Ervin, R. D., and Filisko, F. E., 1993, "The influence of viscometer dynamics on the characterization of an electrorheological fluid under sinusoidal electric excitation," *Journal of Rheology*, Vol. 37, pp. 55-70.

Lou, Z., Ervin, R. D., Filisko, F. E., and Winkler, C.B., 1993, "An electrorheoligically controlled semi-active landing gear," SAE Paper No. 931403, 1993 Aerospace Atlantic Conference & Exposition, Dayton, Ohio.

Lou, Z., Ervin, R. D., and Filisko, F. E., 1993, "A preliminary parametric study of electrorheological dampers," pp. 143-156.

Lou, Z., Winkler, C.B., Ervin, R.D., Filisko, F.E., Venhovens, P.J.Th., Johnson, G.E., 1994, "Electrorheology for Smart Automotive Suspensions", UMTRI Final Report No. 94-15 to the U.S. Army Tank Automotive Command under Contract DAAE07-92-C-R078.

Margolis, D. L., 1982, "Semiactive heave and pitch control for ground vehicles," *Vehicle System Dynamics*, Vol. 11, pp. 31-42.

Margolis, D. L., 1983, "Semiactive control of wheel hop in ground vehicles," *Vehicle System Dynamics*, Vol. 12, pp. 317-330.

Margolis, D. L., and Goshtasbpour, M., 1984, "The chatter of semiactive on-off suspensions and its cure," *Vehicle System Dynamics*, Vol. 13, pp. 129-144.

Mizuguchi, M., Suda, T., Chikamori, S., and Kobayashi, K., 1984, "Chassis electronic control systems for the Mitsubishi 1984 Galant," Paper No. 840341, SAE, Inc., Warrendale, PA.

Petek, N. K., 1992, "An electronically controlled shock absorber using electrorheological fluid," Paper No. 920275, SAE, Inc., Warrendale, PA.

Pinkos, A., Shtarkman, E. M., and Fitzgerald, T., 1993, "An actively damped passenger car suspension system with low voltage electro-rheological magnetic fluid," SAE Paper No. 930268, SAE, Inc., Warrendale, PA.

Pollard, M. G., and Simons, N. J. A., 1984, "Passenger comfort-the role of active suspensions," *Proceedings of Institution of Mechanical Engineers*, Vol. 198D, pp. 1-15.

Redfield, R. C., 1991, "Performance of low-bandwidth, semiactive damping concepts for suspension control," *Vehicle System Dynamics*, Vol. 20, pp. 245-267.

Sharp, R. S., and Crolla, D. A., 1987a, "Intelligent suspensions for road vehicles - current and future developments," *Procedings of the European Automobile Engineers Cooperation. International Conference on New Developments in Power Train and Chassis Engineering*, Vol 2, pp. 579-601.

Sharp, R. S., and Crolla, D. A., 1987b, "Road vehicle suspension system design - a review," *Vehicle System Dynamics*, Vol. 16, pp. 167-192.

Venhovens, Paul J. Th., 1994, "Optimal control of vehicle suspensions," PhD thesis, Delft University of Technology, Faculty of Mechanical Engineering, pp. 69-84.

# APPENDIX A

931403

# An Electrorheologically Controlled Semi-Active Landing Gear

**Zheng Lou, Robert D. Ervin, Frank E. Filisko, and Christopher B. Winkler**
University of Michigan

## ABSTRACT

This study is to explore the application of electrorheology (ER) to the real-time control of damping forces that are transmitted through the nose landing gear for an F-106B aircraft. The main part of the landing gear is a strut that consists of a pneumatic spring and an ER controlled damper that is situated on the strut centerline and applies a force directly opposing the vertical displacement of the nose wheel. The damping element rotates in response to strut displacement, employing a co-axial arrangement of stator and rotor plates connected to the opposing electrodes in the control circuit. The vertical displacement is converted into rotation of the damper through a screw-nut mechanism. The ER fluid between the electrodes is thus engaged in shear along circumferential lines of action. This design results in a fast time response and a high ratio of strut forces achieved under ER- vs. zero-field control. Compact size and simplicity in fabrication are also attained. The analysis shows that when using an ER fluid of a yield stress of 7 kPa, the energy absorption efficiency of the landing gear can reach almost 100% at various sink rates.

## INTRODUCTION

The development of landing gear has come a long way, starting from bicycle-type wheels carried in cycle forks, wheels supported on rubber-and-spring devices, oleo-pneumatic shock absorbers, and to the later developments such as active or semi-actively-controlled landing gear [1-8].

A modern landing gear typically consists of a wheel, a brake, a motion damper, an energy storage medium, and a retraction mechanism. While each component deserves its own share of attention, this study will emphasize the damping function and, to a lesser extent, the energy storage or springing function. Vibrating forces and rigid body motions during landing and taxiing tend to hinder the pilots' manipulative and visual tasks, cause damage to the aircraft, and make the ride uncomfortable. The main functions of the damper are, of course, to absorb and dissipate energy during landing and taxiing.

During landing, the vertical kinetic energy of an aircraft is absorbed primarily by the tires and shock absorbers. Tires serve mainly as a spring for storing energy and low-pass filtering the pavement irregularities while the shock absorber package both stores and dissipates the bulk energy associated with vertical velocity and potential energy. The total reaction force from an oleo-pneumatic shock absorber is equal to the sum of the air spring force, the damping force associated with liquid pressure drop across the orifice, and other minor forces. The spring force increases with net deflection while the damping force is determined by the speed of the deflection. The deflection rate is typically the highest right at touchdown and then declines to zero as the aircraft settles toward (and perhaps overshoots) the static deflection state. Thus it is obvious that, with fixed orifice hardware, the damping forces will peak almost immediately upon tire impact, resulting in a nonuniform distribution of the energy absorption task over the full deflection transient or a low energy absorption efficiency. The energy absorption efficiency is defined as the ratio of the actual energy absorbed (stored in the spring plus dissipated through the damper) to the full area bounded by the maximum strut force and deflection ordinates.

An air spring is non-linear, and it is normally pre-pressurized in landing gear applications to reduce the required stroke needed to obtain maximum suspension forces. The preloading approach increases the storage efficiency (defined as the ratio of the actual energy storage to the full area bounded by the maximum spring load and deflection ordinates) by yielding a rather "boxy" force-deflection curve. If damping forces could be developed to yield comparably boxy force-deflection shapes, notwithstanding the declining velocity profile as deflection increased, dissipation efficiencies (defined as the ratio of the actual energy dissipated to the full area bounded by the maximum damping force and deflection ordinates) would likewise be improved.

In an oleo-pneumatic shock absorber, an active system generally utilizes a servo device to control the landing force, by pumping hydraulic oil into and out of one of the two hydraulic fluid chambers, or between them. The main effect of pumping oil in/out of the gas (air or nitrogen) chamber is to increase or decrease air spring stiffness while that of pumping oil in/out of the hydraulic chamber is to increase/decrease its

effective damping coefficient or force. Pumping oil between two chambers is equivalent to having an active orifice.

For example, McGehee and Leland of NASA Langley Research Center [7] used a microprocessor-controlled servo system to regulate landing gear forces by pumping hydraulic fluid in and out of the hydraulic chamber. During the landing, the oil was pumped out of the chamber to increase the travel of the gear. The enhanced device achieved an 11% drop in the peak landing force relative to the performance of the non-enhanced package. The active scheme was switched on only in a landing that would not bottom the passive gear. In another NASA study by Howell *et al.* [8], a series-hydraulically controlled nose gear for F-106B airplane was able to reduce the peak sprung mass acceleration by up to 47%.

This study is to explore the application of electrorheology to the real time control of damping forces that are transmitted through the landing gear. An electrorheologically controlled nose landing gear for an F-106B aircraft is proposed, designed and analyzed. ER technology pertains to special fluids that change their rheological properties in response to an electrical field [9]. The primary fluid property of interest is the apparent viscosity under shear, although the energized fluid assumes a Bingham-type solid state, with an associated elastic stiffness, as well. Considering a steady shear condition, the equivalent viscosity value can be increased by a factor of about ten to a hundred (depending on the shear rate), completely reversibly, at a rate of 1 to 2 kHz. The potential appeal of ER devices derives from their simplicity, speed, low cost, and the innovative functionalities that are made possible.

## AN ER LANDING GEAR

In approaching the design of an ER-based, semi-active suspension control, the ER component can be built as either a flow-mode, mixed-mode, or shear-mode type of damper [10]. Among the three conceptual types, the flow-mode damper is most similar to the traditional shock absorber except that it replaces the conventional orifice with an ER valve [11]. An analysis [10] indicates that the shear-mode damper achieves better dynamic response and more effective control than the flow- or mixed-mode types.

The general concept of the proposed design in this study is shown in Fig. 1. The control in the landing gear is realized through a medium of an ER fluid. The shear-mode damper uses, instead of translational plates, a plurality of rotational shearing disks (hot electrodes and cold electrodes), which form a total control (or shearing) surface area that is constant and independent of the relative position of the landing gear, resulting in a good control and a compact size. A translation-to-rotation device converts the translational motion of the gear into the rotational motion of the shear-mode damper, and vice versa.

In the specific design proposed in this study as shown in Fig. 2, a plurality of ground electrodes, separated from each other by a plurality of ground-electrode spacers, are mechanically fixed and electrically connected to a stator through two or more stator feather keys or other rotation-stops. The stator is grounded electrically and will be fixed rigidly onto the spindle of the wheels. A plurality of elevated-voltage or "hot" electrodes, separated from each other by a plurality of hot-electrodes spacers, is mechanically fixed and electrically connected to a rotator through two of more rotator feather keys or other rotation-stops. The rotator is mechanically supported by top and bottom bearings that can sustain both radial and axial loads. Inter-electrode gaps are filled with an ER fluid through top and bottom bleed-holes.

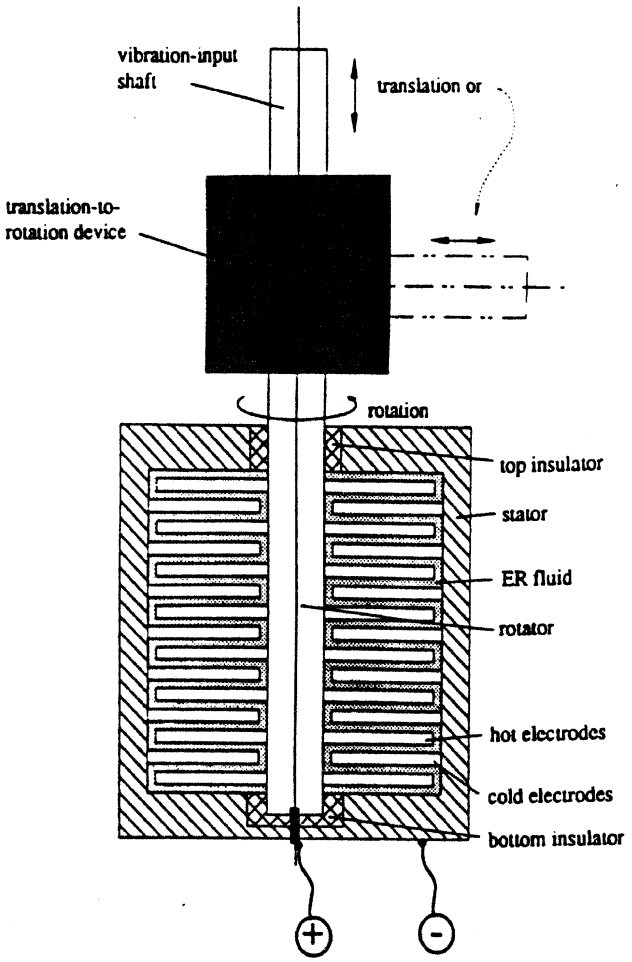


Fig. 1. The general concept of the proposed design.

The translational relative motion is converted through a screw-nut mechanism, with the screw machined on a shafted (rigidly connected to a cylinder) and the nut cut inside the rotator. The selection of the lead angle provides for the selection of the ratio of the shearing speed between disks in the shear-mode damper to the relative translational speed of a suspension as well as the selection of the ratio of the damping torque from the shear-mode damper to the damping force needed for the landing gear. One can also use a ball screw to obtain smoother power and motion transmissions. The elevated voltage can be supplied to the rotator through a carbon brush at the bottom instead of the fixed connection at the top as shown in Fig. 2.

The cylinder is charged (through gas/oil charge hole) with nitrogen gas and oil and will be connected to the sprung-mass. A pneumatic spring is thus easily integrated into the design, which makes the landing gear more compact and lighter than those semi-active or active systems that use a separate steel

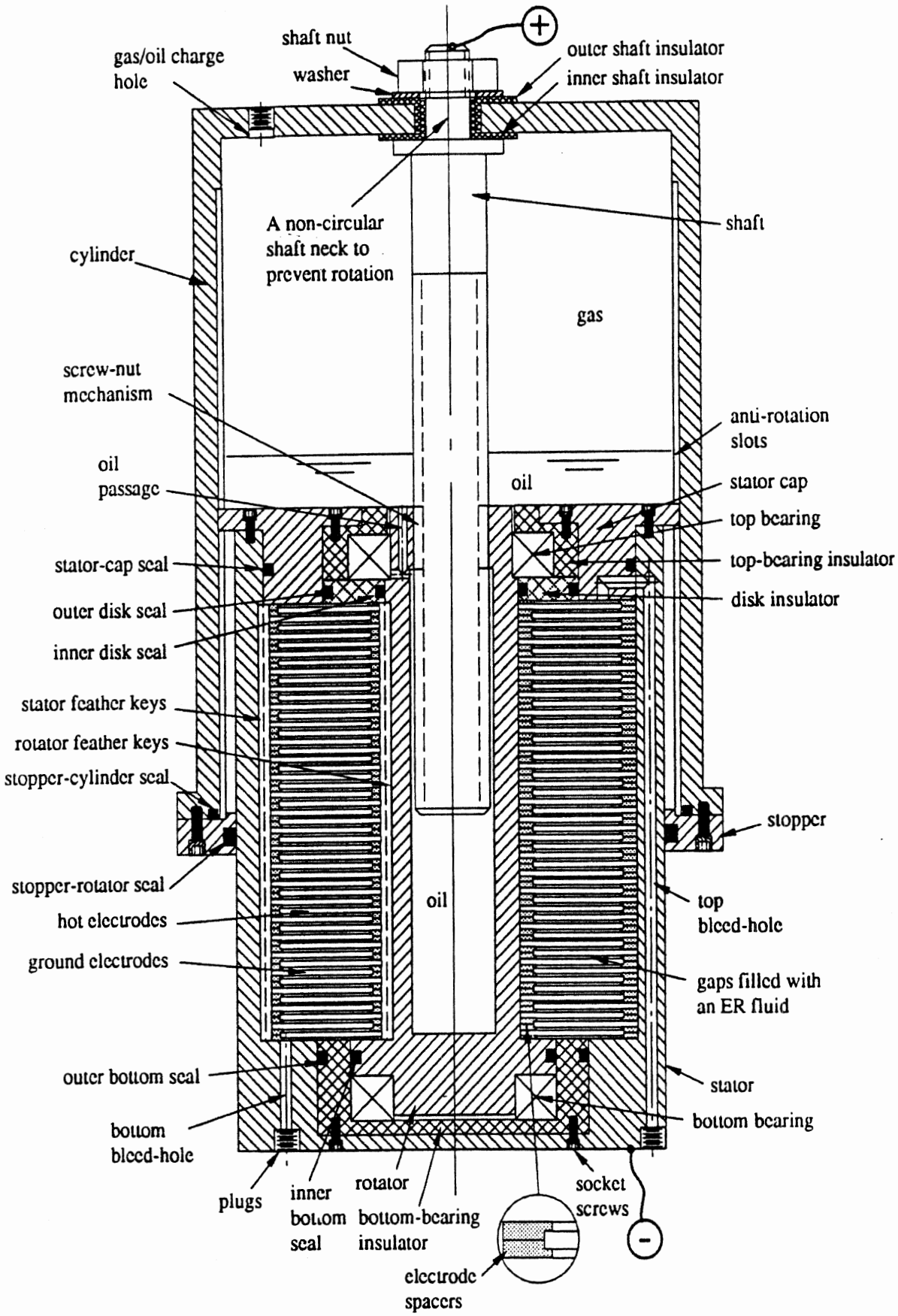


Fig. 2. The specific design of the proposed ER landing gear strut.

spring. The oil can lubricate the screw-nut mechanism, improve the sealing condition for the pneumatic spring, improve electric insulation, and enhance the heat transfer from the shear-mode damper. There are one or more oil passages through the top of the rotator, which can allow the oil either to flow freely into and out of a hole inside the rotator or, with a special design (e.g., adding one or more check valves in the passages) to introduce additional, non-ER damping when needed.

Two anti-rotation slots can be machined into the cylinder, together with two keys protruding in the radial direction from a stator-cap, to prevent relative rotation between the stator and the cylinder. This feature or other functionally similar features are needed when no rotational constraint exists between the sprung and unsprung masses.

Hot- and ground-electrode spacers can give sliding support for the ground- and hot-electrodes, respectively. The sliding support can guarantee the stability and accuracy of the gap size and prevent possible vibration in the electrodes. However, it may cause additional friction and wear, which can be reduced by designing a partial (around the circumference) sliding support. The non-sliding areas will also offer passages for the ER fluid to move in the axial direction during filling and bleeding. Otherwise, the passages have to be punched through the electrodes.

## MATHEMATICAL MODEL

For a small aircraft such as F-106B, a rigid body representation of the airframe is usually sufficient [12]. This study also ignores dynamics in horizontal direction, such as spin-up and spring-back reaction [13]. Further, the results presented are only for landing, without considering roll-out and taxing. The momentum equation for the sprung mass is thus simplified as

$$m_s a_s = -F_s - F_d + m_s g - F_l \tag{1}$$

where $m_S$ is the sprung mass, $a_S$ the sprung mass acceleration (positive downward), $F_S$ the spring force (positive during compression), $F_d$ the damping force (positive during compression), g the gravitation acceleration, and $F_l$ the lift. During a landing, the lift cancels the gravitational weight, and the last two terms in EQ (1) disappear.

The momentum equation for the unsprung mass is

$$m_u a_u = F_s + F_d + m_u g - F_t \tag{2}$$

where $m_U$ is the unsprung mass, $a_U$ the unsprung mass acceleration (positive downward), and $F_t$ the tire force (both tire spring and damping forces, positive during compression).

The pneumatic spring in the strut is filled with nitrogen gas and undergoes an adiabatic process during the landing, and the spring force is derived as

$$F_s = A_p\left[\frac{x_o^k(p_{og} + p_{atm})}{(x_o - \Delta x)^k} - p_{atm}\right] \tag{3}$$

with

$$\Delta x = x_s - x_u \tag{4}$$

where $A_p$ is the piston area, $p_{og}$ the hanging pre-charge (gage) pressure, $p_{atm}$ the atmosphere pressure, $x_o$ the hanging length of an equivalent gas cylinder (i.e. the hanging gas volume equals to $x_o$ times $A_p$), k the specific heat ratio of the gas, $x_S$ the sprung mass displacement, $x_U$ the unsprung mass displacement, and $\Delta x$ the deflection of the pneumatic spring. Both $x_S$ and $x_U$ are zero at the moment of tire impact, and they are positive displacing downward.

In a shear-mode damper, the influence of the inertia force is small [10], and the damping force in the strut can be approximated with a Newtonian damping force ($F_{dN}$) and an ER damping force ($F_{dER}$), corresponding to the effects of the plastic viscosity ($\eta$) and the yield shear stress ($\tau_y$), respectively, in the Bingham model (a simplistic but generally effective model of the ER fluids [14]). The two damping forces are derived as

$$F_{dN} = \frac{4\pi n\eta(r_o^4 - r_i^4)(f\tan\lambda + \cos\phi)}{hD_p^2\tan\lambda\,(\cos\phi\tan\lambda - f)}\Delta v \tag{5}$$

and

$$F_{dER} = \frac{\Delta v}{|\Delta v|}\frac{8\pi n(r_o^3 - r_i^3)(f\tan\lambda + \cos\phi)}{3D_p(\cos\phi\tan\lambda - f)}\tau_y \tag{6}$$

with

$$\Delta v = v_s - v_u \tag{7}$$

where n is the number of hot electrodes, h the gap size between the electrodes, $r_o$ and $r_i$ the outer and inner radii of the effective shearing surface of the electrodes, respectively. The parameter $D_p$ is the pitch diameter, $\phi$ the thread angle (standard at 29°), $\lambda$ the lead angle, and f the friction coefficient for the screw-nut mechanism. The variables $v_S$ and $v_U$ are the sprung and unsprung mass velocities, respectively, and $\Delta v$ is the strut deflection velocity. The Newtonian and ER damping forces here are completely uncoupled and additive, which will only provide a first-order estimation, yet convenient and insightful for a preliminary parametric study. However, a complete solution of the problem will demand a full solution of the fluid flow problem [15, 16].

Two tires (18×4.4×12ply) are mounted in parallel on the nose landing gear, and the force-deflection curve of each tire is as follows [17]

$$F_{ts} = [p_{tog} + 1.5\frac{w_t}{d_t}p_{to}(\frac{x_u}{w_t})^2 + 0.08p_{trg}]w_t\sqrt{w_t d_t}\, f_1 \tag{8}$$

where $F_{tS}$ is the single-tire spring force, $d_t$ the tire diameter (0.4483 m or 17.65 in), $p_{tog}$ the tire inflation gage pressure at zero vertical load (0.965 MPa or 140 psi), $p_{to}$ the tire inflation absolute pressure at zero vertical load (1.067 MPa or 154.7 psi), $p_{trg}$ the tire rated inflation gage pressure (1.551 MPa or 225 psi), and $w_t$ the maximum width of an undeflected tire (0.109 m or 4.3 in). The function $f_1$ is calculated as:

$$f_1 = 0.96\frac{x_u}{w_t} + \frac{0.216}{C_z}(\frac{x_u}{w_t})^2 \quad \text{for} \quad \frac{x_u}{w_t} \le \frac{10}{3}C_z \tag{9}$$

and

$$f_1 = 2.4(\frac{x_u}{w_t} - C_z) \quad \text{for} \quad \frac{x_u}{w_t} \ge \frac{10}{3}C_z \tag{10}$$

For type VII tires used in the landing gear, $C_z$ has a value of 0.03. In addition to the spring force shown in EQ (8), viscous damping force is added into the tire model with an assumed damping ratio of 0.02, which together with the combined stiffness of the two tires (951000 N/m, averaged over the first 2.3 cm deformation of the tire) and the unsprung mass, determine the damping coefficient. The tire damping has a significant effect on the interaction between the sprung and unsprung masses at the wheelhop frequency [18].

## CONTROL STRATEGY

The overall control goal during each landing is to reduce the peak landing force by achieving a boxy strut force-deflection curve of a minimum height, with a given adiabatic curve of the pneumatic spring and within the maximum stroke ($\Delta x_{max}$). The total energy to be absorbed (both dissipated and stored) $E_o$ is the kinetic energy at tire impact:

$$E_o = \frac{1}{2}(m_s + m_u)v_o^2 \tag{11}$$

where $v_o$ is the sink rate, i.e., the descending velocity at tire impact. To have a minimum height for the boxy force-deflection curve, one has to use as much stroke as possible. If one defines

$$F_{sc}\Delta x_c \equiv E_o \tag{12}$$

where

$$F_{sc} = A_p\left[\frac{x_o^k(p_{og} + p_{atm})}{(x_o - \Delta x_c)^k} - p_{atm}\right], \tag{13}$$

then the box delineated by $F_{st} = F_{sc}$ line and $\Delta x = \Delta x_c$ line will offer the most optimum control strategy (Fig. 3a) when $\Delta x_c < \Delta x_{max}$. When $\Delta x_c \geq \Delta x_{max}$, however, one has to let $F_{st} = E_o/\Delta x_{max}$ (Fig. 3b) because the limit of the maximum stroke. In the formulation, the relatively small amount of energy stored and dissipated in the tires is neglected.

With $F_{st}$ determined according to the control rule shown in Fig. 3, the controller is then to make sure that

$$F_{dER} = F_{st} - F_s - F_{dN} \quad \text{if } \Delta v > 0 \tag{14}$$

and

$$F_{dER} = 0 \quad \text{if } \Delta v \leq 0 \tag{15}$$

Equation (15) is based on the fact that an ER damper is a semi-active device and is physically not able to generate a positive damping force when the strut deflection velocity is negative. The ER damping force from EQ (14) is generally positive. A negative ER damping force can cause a larger discontinuity than no ER damping force at all. The strut deflection velocity does show negative values temporarily during a landing because of the wheel-hop phenomenon (see examples in the next section). Considering the energy absorption, it is desirable to keep the ER damper energized during short periods of negative strut deflection velocity. However, severer jerks (the derivative of the acceleration) caused by the negative damping force may be too high a price.

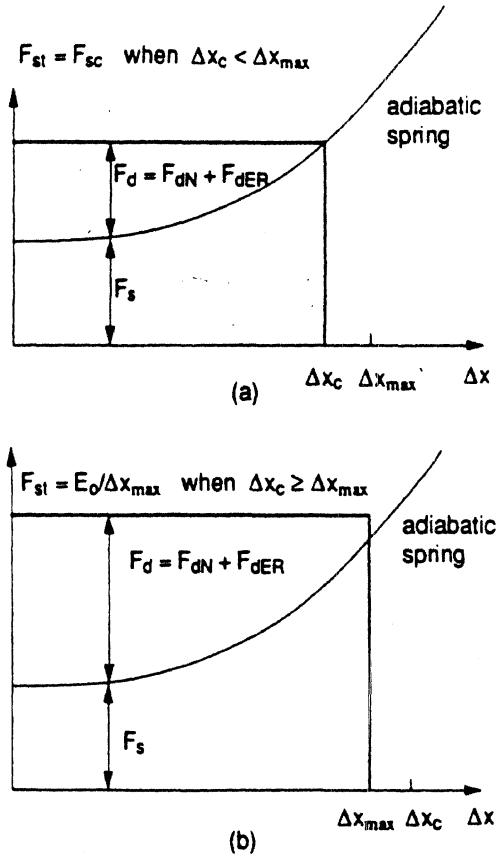


Fig. 3. The control strategy of the ER landing gear: (a) for soft and regular landings and (b) for hard landings.

Another practical problem with the above control strategy is that during a hard landing (a landing with a high sink rate), the ER damper may not always generate enough damping force dictated by EQ (14) because of, for example, the yield stress limit. In such a situation, the control strategy shown in Fig. 3 has to be modified into that shown in Fig. 4. The area under the modified $F_{st}$ curve (solid line) is equal to the area under the ideal $F_{st}$ curve (dotted line) in either Fig. 4a or Fig. 4b. The ER damper is fully energized during the early and most part of the stroke (curve p1-p2 in Fig. 4a or curve p4-p5 in Fig. 4b) to dissipate as much energy as possible. Depending on the total energy, the $\Delta x$ value at point p3 may extend to $\Delta x_{max}$ while point p2 may converge to point p3 in Fig. 4a. Similarly, point p5 may converge to point p6 in Fig. 4b, beyond which any extra energy will bottom up the landing gear.

To realize various control strategies discussed above, real time information of many variables are needed. The pneumatic spring force can be easily calculated using data from a pressure transducer. The real time Newtonian and ER damping forces are physically inseparable, and they together may be measured using one of a variety of sensors. The strut force can be derived from the sprung mass acceleration. The Newtonian and ER damping forces are difficult to predict precisely in a dynamic

situation, and an open-loop control of the ER damping force may not be robust.

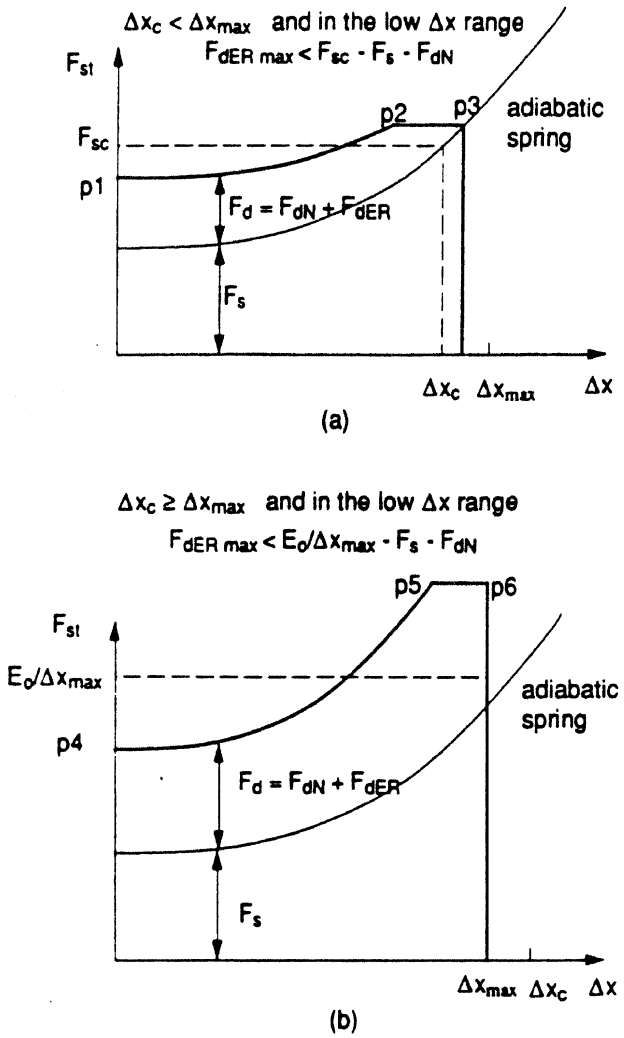


Fig. 4. The modified control strategy of the ER landing gear when the ER damping force is insufficient: (a) for soft and regular landings and (b) for hard landings.

## SIMULATION RESULTS

A computer code is developed using the mathematical model and control strategies discussed above. The momentum equations are integrated over the time domain, starting from tire impact and ending at the moment the sprung velocity ($v_S$) becomes zero.

The values of some of the major parameters are listed in Table 1. The piston diameter in the pneumatic cylinder of the ER damper is 13.5 cm instead of 8.255 cm (3.25 in) in the conventional design, and the hanging pre-charge gage pressure is accordingly changed from 758,423 Pa (110 psi) to 283,581 Pa (41.13 psi) to keep the same spring stiffness. Forty hot-electrodes are selected (i.e., n = 40), giving a total height of 16 cm for the column of the electrodes and ER fluid gaps. By adding bearings and other components at both ends, the total length of the stator will be in the same range as the strut stroke (23.5 cm). The maximum yield stress is chosen to be about 7 kPa, and ER fluids of a strength in this range has been reported [19-21]. At the maximum yield stress, the ER damping force $F_{dER}$ is 19.7 kN (4,440 lbf).

Table 1. Parameters used in the simulation.

| parameters | values |
|---|---|
| $\tau_{ymax}$ | 6895 Pa (1 psi) |
| h | 1 mm |
| $r_o$ | 6 cm |
| $r_i$ | 2 cm |
| $A_p$ | 0.0143 $m^2$ |
| $\eta$ | 0.1 $Ns/m^2$ (100 cP) |
| $m_s$ | 1020.6 kg (2250 lb) |
| $m_u$ | 65.77 kg (145 lb) |
| $\Delta x_{max}$ | 0.235 m (9.25 in) |
| k | 1.4 |
| $x_o$ | 0.276 m |
| $\lambda$ | 45° |
| $D_p$ | 3 cm |
| f | 0.1 |

Simulations are performed with three different sink rates: 0.76 m/s (2.5 ft/s), 1.37 m/s (4.5 ft/s), and 3.05 m/s (10 ft/s), which are normally considered to be soft, regular, and hard landings, respectively.

The displacements of the sprung and unsprung masses at a sink rate of 1.37 m/s (4.5 ft/s) are illustrated in Fig. 5, and the corresponding velocities are shown in Fig. 6. The sprung mass velocity decreases almost linearly with the time and reaches zero within 0.155 seconds (Fig. 6), when the strut deflection $\Delta x$ is about 0.097 m (Fig. 5). Both the displacement and velocity of the unsprung mass show a decaying sinusoidal oscillation at a frequency of about 20 Hz, a wheel-hop frequency. At the peaks of its oscillation, the unsprung mass velocity $v_u$ is higher than the sprung mass velocity $v_S$ (Fig. 6), resulting a negative strut deflection velocity $\Delta v$.

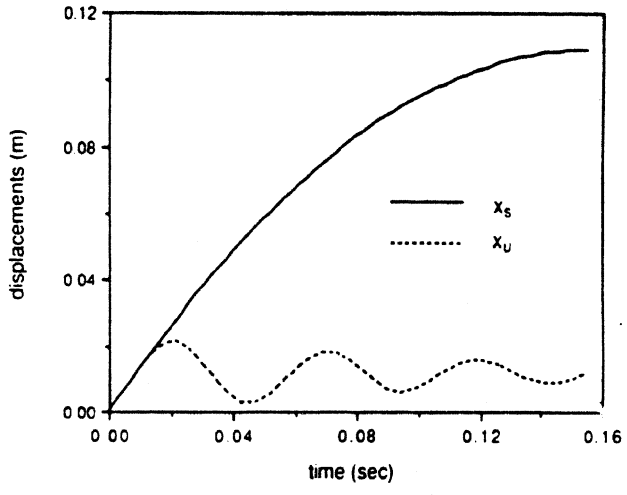


Fig. 5. The displacements of the sprung ($x_S$) and unsprung ($x_u$) masses at a sink rate of 1.37 m/s (4.5 ft/s).

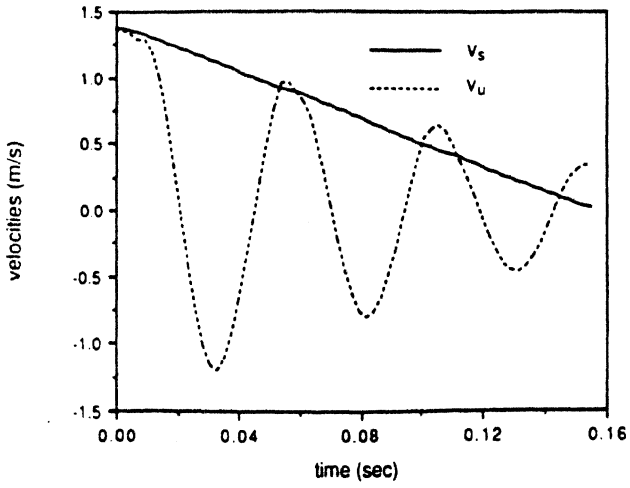


Fig. 6. The velocities of the sprung ($v_s$) and unsprung ($v_u$) masses at a sink rate of 1.37 m/s (4.5 ft/s).

The periodic variation in $\Delta x$ and $\Delta v$ causes a corresponding oscillation in the strut spring force $F_S$ and the Newtonian damping force $F_{dN}$ (Fig. 7). There is similarly a large, periodic total tire force Fs because of the wheel-hop phenomenon (Fig. 7). The ER damping force $F_{dER}$ is continuously regulated, resulting in an almost constant strut force $F_{st}$ except short periods when $F_{dER}$ has to be zero to avoid severe jerks in the presence of negative strut deflection velocity (Fig. 7). Because of the complete cancellation of the weight by the lift, the sprung mass deceleration, $-a_s$, is directly proportional to the strut force $F_{st}$ and is also boxy in shape (Fig. 8). The peak deceleration of the sprung mass at a sink rate of 1.37 m/s is 0.952g.

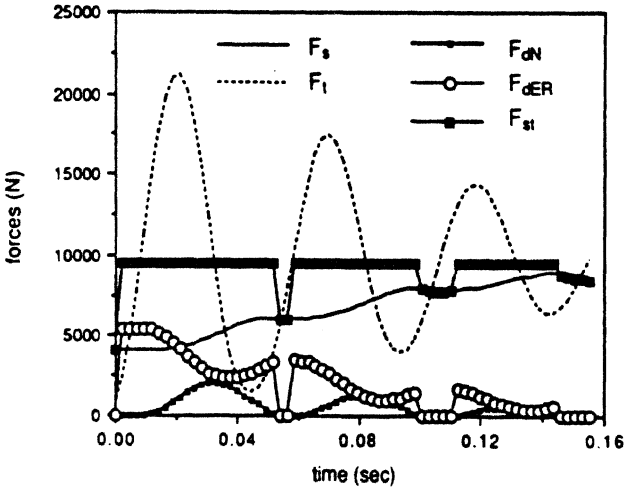


Fig. 7. Various forces at a sink rate of 1.37 m/s (4.5 ft/s).

The sprung mass decelerations at sink rates of 0.76 m/s (2.5 ft/s) and 3.05 m/s (10.0 ft/s) (Fig. 8) are also almost constant except the periodic disruptions caused by the negative strut deflection velocity. In the former case, there is even a short period, around 0.007 second, when the damping forces and the spring force are equal to zero, resulting a zero deceleration (Fig. 8). The peak sprung mass decelerations are 0.60g and 2.66g, and the strokes are 0.045 and 0.170 m at sink rates of 0.76 and 3.05 m/s, respectively.

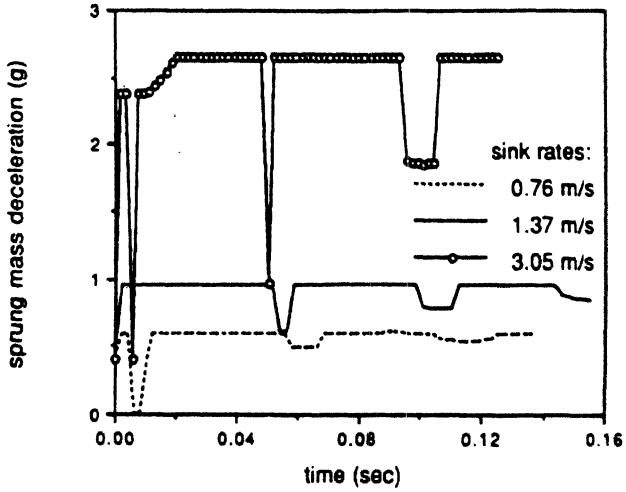


Fig. 8. The decelerations of the sprung mass at sink rates of 0.76 m/s (2.5 ft/s), 1.37 m/s (4.5 ft/s), and 3.05 m/s (10.0 ft/s).

## DISCUSSIONS

While jerks in the simulation results are undesirable, each of them lasts a short period of time (a few milliseconds), their effect on energy absorption is negligible, and the human uncomfortableness they induce may not be significant. The sharpness with which variables change with the time may not exist when one considers nonlinear factors and time delays in various components such as those involved in the fluid flow.

The parameter values in the simulation are identical to those used by Howell et al. [8] in a drop test of a F-106B airplane active control landing gear. Their results are listed in Table 2 along with those from this study at a sink rate of 1.37 m/s with the lift. Relative to their passive system, the reduction in the peak deceleration by their active system is about 32%, and the reduction by the ER system in this study is about 23%. The reduction in the peak deceleration in their study is however realized over a longer stroke (19.1 cm), while the reduction in this study is achieved over a much shorter stroke (9.7 cm). With the maximum stroke equal to 23.5 cm, the scheme in this study has much more room to accommodate higher sink rates. At a sink rate of 3.05 m/s (a hard landing), the ER system uses a stroke of only 17 cm, and no comparable test was performed by Howell et al. [8].

## SUMMARY

An electrorheologically controlled semi-active nose landing gear for an F-106B aircraft is proposed, designed, and analyzed. The adoption of the rotary shear-mode damper results in a fast time response and a high ratio of strut forces achieved under ER- vs. zero-field control. The use of the screw-nut mechanism and the integration of the pneumatic spring make it a compact and simple design. The analysis shows that when

using an ER fluid of a yield stress of 7 kPa, the energy absorption efficiency of the landing gear can reach almost 100% at various sink rates.

Table 2. The comparison among the experimental results of passive and active systems by Howell et al. [8] and the simulation result of the ER system in this study at a sink rate of 1.37 m/s with the lift.

| | passive by Howell et al. | active by Howell et al. | ER system in study |
|---|---|---|---|
| peak $a_s$ | - 1.23 g | - 0.84 g | - 0.95 g |
| stroke | 17.0 cm | 19.1 cm | 9.7 cm |

## NOMENCLATURE

| | |
|---|---|
| $a_s$ | sprung mass acceleration. |
| $a_u$ | unsprung mass acceleration. |
| $A_p$ | piston area. |
| $C_z$ | a constant in the tire force calculation. |
| $d_t$ | tire diameter. |
| $D_p$ | pitch diameter of the screw-nut mechanism. |
| $E_o$ | kinetic energy at the tire impact. |
| f | friction coefficient in the screw-nut mechanism. |
| $f_1$ | a function in the tire force calculation. |
| $F_d$ | strut damping force. |
| $F_{dER}$ | ER damping force. |
| $F_{dN}$ | Newtonian damping force. |
| $F_l$ | lift on the wings. |
| $F_s$ | strut spring force. |
| $F_{sc}$ | control strut force. |
| $F_t$ | tire force. |
| $F_{ts}$ | single-tire spring force. |
| g | gravitation acceleration. |
| h | gap size between the electrodes. |
| k | specific heat ratio of the gas. |
| $m_s$ | sprung mass. |
| $m_u$ | unsprung mass. |
| n | number of hot electrodes. |
| $p_{atm}$ | atmosphere pressure. |
| $p_{og}$ | hanging pre-charge gage pressure. |
| $p_{tog}$ | tire inflation gage pressure at zero vertical load. |
| $p_{to}$ | tire inflation absolute pressure at zero vertical load. |
| $p_{trg}$ | tire rated inflation gage pressure. |
| p1, p2, ... and p6 | some points in Fig. 4. |
| $r_i$ | inner radius of the effective shearing surface. |
| $r_o$ | outer radius of the effective shearing surface. |
| $v_o$ | sink rate. |
| $v_s$ | sprung mass velocity. |
| $v_u$ | unsprung mass velocity. |
| $w_t$ | maximum width of an undeflected tire. |
| $x_o$ | hanging length of an equivalent gas cylinder. |
| $x_s$ | sprung-mass displacement. |
| $x_u$ | unsprung-mass displacement. |
| $\Delta v$ | strut deflection velocity. |
| $\Delta x$ | strut deflection. |
| $\Delta x_c$ | control strut deflection. |
| $\Delta x_{max}$ | the maximum stroke. |
| $\phi$ | thread angle. |
| $\eta$ | plastic viscosity. |
| $\lambda$ | lead angle of the screw-nut mechanism. |
| $\tau_y$ | yield shear stress. |

## ACKNOWLEDGMENTS

The authors are grateful to NASA-Langley Research Center for the support of this research through grant NAG-1-1410. Thanks are also due to Mr. William E. Howell of NASA-Langley Research Center for his providing various technical data and insightful discussions.

## REFERENCES

[1] Wignot, J. E., Durup, P. C., and Gamon, M. A., Design formulation and analysis of an active landing gear-Vol. I Analysis, AFFDL-TR-71-80, Vol. 1, U.S. Air Force, 1971.

[2] Bender, E. K., Berkman, E. F., and Bieber, M., A feasibility study of active landing gear, AFFDL-TR-70-126, U.S. Airforce, 1971.

[3] McGehee, J. R., and Carden, H. D., A mathematical model of an active control landing gear for load control during impact and roll-out, NASA-TND-8080, NASA, 1976.

[4] McGehee, J. R., and Carden, H. D., Analytical investigation of the landing dynamics of a large airplane with a load-control system in the main landing gear, TP 1555, NASA, 1979.

[5] McGehee, J., and Dreher, R., Experimental investigation of active loads control for aircraft landing gear, TR No. 2042, NASA, 1982.

[6] Ross, I., and Edson, R., An electronic control for an electrohydraulic active control aircraft landing gear, NASA CR-3113, NASA, 1979.

[7] Wigotsky, V., Active landing gear smooths the ride, *Aerospace Am.*, 22: 42-4, 1984.

[8] Howell, W. E., McGehee, J. R., Daugherty, R. H., and Vogler, W. A., F-106B airplane active control landing gear drop test performance, SAE Technical Paper Series 901911, SAE, 1990.

[9] Filisko, F. E., Electrorheological materials: smart materials of the future, *Chemistry and Industry*, 10: 370-3, 1992.

[10] Lou, Z., Ervin, R. D., and Filisko, F. E., A preliminary parametric study of electrorheological dampers. In: ASME Fluids Engineering Division Meeting. ASME, New York, 1993, to-be-presented.

[11] Petek, N. K., An electronically controlled shock absorber using electrorheological fluid, Pub. No. 920275, SAE, Inc., Warrendale, PA, 1992.

[12] Tung, C. C., Penzien, J., and Horonjeff, R., The effects of runway unevenness on the dynamic response of supersonic transports, CR-119, NASA, 1964.

[13] Young, D. W., Aircraft landing gears--the past, present and future, *Proceedings of the Institution of Mechanical Engineers. Part D, Transport Engineering*, 200: 75-92, 1986.

[14] Lou, Z., Ervin, R. D., and Filisko, F. E., Behaviors of electrorheological valves and bridges. In: Tao, R., Ed., *Proceedings of the International Conference on Electrorheological Fluids: Mechanism, Properties, Structure,*

*Technology, and Applications*, World Scientific, River Edge, NJ, 1992, 398-423.

[15] Lou, Z., Ervin, R. D., and Filisko, F. E., The influence of viscometer dynamics on the characterization of an electrorheological fluid under sinusoidal electric excitation, *J. Rheology*, 37: 55-70, 1993.

[16] Wang, K. C., McLay, R., and Carey, G. F., ER fluid modelling. In: Carlson, J. D., Sprecher, A. F., and Conrad, H., Ed., *Electrorheological Fluids*, Proceedings of the Second International Conference on ER Fluids-1989. Technomic Pub. Co., Inc., Lancaster, 1990, 41-52.

[17] Smiley, R. F., and Horne, W. B., Mechanical properties of pneumatic tires with special reference to modern aircraft tires, TR R-64, NASA, 1960.

[18] Levitt, J. A., and Zorka, N. G., The influence of tire damping in quater car active suspension, *J. Dynamic Systems, Measurement, and Control*, 113: 134-137, 1991.

[19] Brooks, D. A., Electro-rheological effect adds muscle, *Control & Instrum.*, 14: 57-59, 1982.

[20] Stangroom, J. E., and Eckersley, J. S., Pipework snubbers based on electro-rheological fluids. In: *Pipework Design and Operation Conf.*, Bury St. Edmunds, U.K., Mech. Engng. Publications Ltd., Vol. IMechE Conf. Publications 1985-1, Paper C29/85, 1985, 279-284.

[21] Hartsock, D. L., Novak, R. F., and Chaundy, G. J., ER fluid requirements for automotive devices, *J. Rheology*, 35: 1305-1326, 1991.

# APPENDIX B

# A Preliminary Parametric Study of Electrorheological Dampers

Z. Lou[1]

R. D. Ervin

Transportation Research Institute,
The University of Michigan,
Ann Arbor, MI 48109

F. E. Filisko

Material Science and Engineering
Department,
The University of Michigan,
Ann Arbor, MI 48109

*In approaching the design of an electrorheology-based, semi-active suspension, the electrorheological component (ER damper) can be built as either a flow-mode, shear-mode, or mixed-mode type of damper. The source of damping force in the flow-mode is exclusively from flow-induced pressure drop across a valve, while that in the shear-mode is purely from the shear stress on a sliding surface. The dynamics of the fluid flow are included in the derivation of the zero-field damping forces. The control effectiveness is found to be strongly related to the dynamic constant (which is proportional to the square root of the vibration frequency) and, for shear- and flow-mode dampers, the ratio of the piston area to the cross-section of the ER control gap. To achieve the same performance, a flow-mode ER damper is not as compact and efficient as a shear-mode ER damper. With the same ER damping force, a mixed-mode damper is more compact than a shear-mode damper. However, the mixed-mode damper does not have as a low zero-field damping force as the shear-mode damper. The analysis is based on the assumption that the ER fluid is Bingham plastic.*

## Introduction

An electrorheological (ER) damper is a device that is able to generate a controllable damping force by employing an ER fluid. An ER fluid can change its rheological properties, most notably its effective viscosity. The wide range and the high bandwidth of the effective viscosity variation of ER fluids are two of the primary factors that have caused intense research and development activities in ER dampers. The ER damper studies so far have generally ignored the influence of the fluid dynamics, i.e., the unsteady nature of the fluid velocity, shear rates, and thus the damping force, which are all induced by the inertia of the fluid. Lou et al. (1992) have shown that the fluid inertia can limit the bandwidth of an ER valve to a level far below the bandwidth of the rheological variation of an ER fluid. Similar influence exists in ER dampers, many of which contain ER valves.

ER dampers can be classified as: flow-mode, mixed-mode, and shear-mode (Fig. 1). The configurations illustrated in Fig. 1 are generic concepts that contain simplified features to facilitate the design analysis. In practical hardware, for example, the cylinder is likely to be single-ended, rather than double-ended, and the ER control valve or area is likely to be comprised of multiple parallel or concentric plates. Among the three conceptual modes, the flow-mode damper is most similar to the traditional shock absorber except that is replaces the conventional orifice with an ER control gap or valve. The source of the damping force in this mode is exclusively from flow-induced pressure drop across the piston. The ER valve can be placed outside the cylinder (as in Fig. 1(*a*)) or within the piston component.

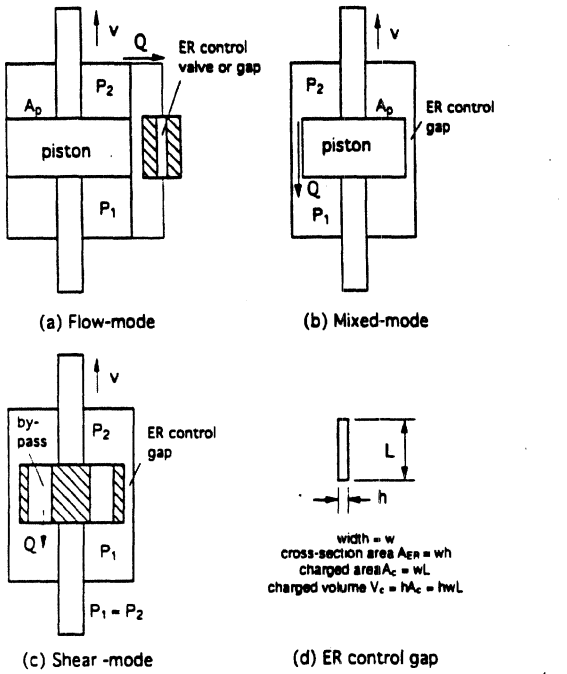


**Fig. 1 The generic concepts of the three modes of electrorheological dampers**

In the mixed-mode damper, the ER control is realized in the gap between the piston side-wall and the cylinder liner. The fluid shear stress at the shear surface also contributes to the damping force, while the flow-induced pressure drop is still present as a force component on the piston.

[1] Present address: Ford Motor Co., Electrical and Fuel Handling Div., McKean and Textile Roads, P.O. Box 922, Ypsilanti, MI 48197.

Contributed by the Fluids Engineering Division and presented at the Fluids Engineering Conference, ASME, June 20-23, 1993, Washington, D.C., of THE AMERICAN SOCIETY OF MECHANICAL ENGINEERS, FED-Vol. 164: Electrorheology Flows—1993, pp. 143-156. Manuscript received by the Fluids Engineering Division May 3, 1993; revised manuscript received November 1, 1993. Associate Technical Editor: R. Panton.

If a large bypass port is cut through the piston of a mixed-mode damper, the device becomes a simple shear-mode element. Since the fluid can flow freely through the by-pass, the pressure drop across the piston becomes negligible and only shear stresses developed along the wall contribute to the damping force.

The purpose of this study is to systematically analyze the dynamic performance of all three modes of ER dampers. Special attention is paid to (*a*) the relative magnitudes of the zero-field and ER components of the damping force under dynamic situation and (*b*) and their implication in the sizing and selection of the damping mode. For simplicity, ER fluids are assumed to be Bingham plastic. If ER fluids show a certain degree of elasticity, the assumption here will not result in significant errors for practical dampers that far out-stroke the elastic strain range and/or the low shear rate range. When the electric field strength is zero, an ER fluid is assumed to be Newtonian, with the zero-field viscosity being equal to the plastic viscosity of the Bingham model. Non-Newtonian behavior at zero-field has been reported though (Lou et al., 1990). The Bingham plastic assumption implies that the shear stress response to electric field changes is instantaneous and that the stress-shear rate relationship has no time dependency.

## Analysis

**Flow-Mode Dampers.** If the piston vibration (Fig. 1(*a*)) can be described as

$$v = v_p \sin \omega t = \omega x_p \sin \omega t \tag{1}$$

where $v$ is the piston velocity, $v_p$ the amplitude of $v$, $\omega$ the angular velocity, $t$ the time, and $x_p$ the amplitude of the piston displacement. From continuity, the amplitude of the (space-wise) mean velocity of the ER fluid in the ER valve is $(A_p/A_{ER})x_p\omega$, where $A_p$ is the piston cross-section area, and $A_{ER}$ is the ER valve cross-sectional area. The zero-field pressure drop for an equivalent steady flow of the same flow amplitude is

$$\Delta p_s = 12\eta \frac{LA_p}{h^2 A_{ER}} x_p \omega \tag{2}$$

where $L$ and $h$ are the length and gap size of the ER valve, respectively. The parameter $\eta$ is the zero-field or plastic viscosity. This pressure drop, frequently used in the literature of ER devices, does not account for the dynamic effect of a sinusoidal flow, which is fully presented in this study. The solution of an oscillatory flow of a viscoelastic medium between parallel planes induced by a sinusoidal pressure drop has been derived by Thurston (1959). The solution of an oscillatory flow induced by a sinusoidal flow rate or piston motion presented here is different only in phasic expression.

The dynamic pressure drop has a component induced by fluid inertia:

$$\Delta p_m = g_m \Delta p_s \sin\left(\omega t + \frac{\pi}{2}\right) \tag{3}$$

with

$$g_m = \frac{2}{3} h^{*2} \tag{4}$$

$$h^* = \frac{h}{2}\sqrt{\frac{\rho\omega}{2\eta}} \tag{5}$$

where $\rho$ is the density of the ER fluid. The dimensionless parameter $h^*$ is, if ignoring the constant $2\sqrt{2}$, the ratio of $h$ to $\sqrt{\eta/\rho\omega}$. The latter has the dimensions of length. It is related to the location of an overshoot in the mean velocity of an oscillatory flow in a flow-mode damper or to the penetration depth of an oscillatory shear flow in a shear-mode damper. One can thus consider $h^*$ as a dimensionless gap size. The parameter $h^*$ and its variations, including those in cylindrical flows, are called in the literature the kinetic Reynolds number, the Womersley number, dynamic constant, or dimensionless frequency. They are also related to the ratio of the flow time constant to the forcing function period (Lou and Yang, 1993). In this study, $h^*$ is named the dynamic constant instead of the dimensionless gap size because (*a*) the parameter appears only in a dynamic situation, (*b*) the practical gap size is generally in a narrow range around 1 mm, and (*c*) the frequency changes greatly in most ER fluid applications.

The functions $g_m$, called the dynamic factor of $\Delta p_m$, is 0 at $h^* = 0$ and rises proportionally with $h^{*2}$ (or with $\omega$ if other parameters in $h^*$ is fixed). Physically, the ratio of the amplitude of the inertia component of the dynamic pressure to the equivalent steady pressure drop is proportional to the frequency.

The dynamic pressure drop has another component that is induced by the wall shear stress:

## Nomenclature

$A_c$ = charged area
$A_{cf}$, $A_{cm}$, and $A_{cs}$ = flow-, mixed-, and shear-mode charged areas
$A_{ER}$ = ER valve cross-sectional area
$A_p$ = piston cross-sectional area
$A_1$, $A_2$, $A_3$, $A_4$, $A_{1um}$, $A_{2um}$, $A_{1om}$, and $A_{2om}$ = intermediate variables
$C$ = electric capacitance
$C_d$ = electric current density
$C_h$ = intermediate variable
$D_h$ = intermediate variable
$E_p$ = peak electric field strength
$F_{om}$ = mixed-mode total zero-field damping force
$F_{ERf}$ = flow-mode ER damping force
$F_{ERm}$ = mixed-mode ER damping force
$F_{ERs}$ = shear-mode ER damping force
$F_u$ = shear-mode zero-field (upper-plate) damping force
$f_{of}$ = flow-mode zero-field factor
$f_{om}$ = mixed-mode zero-field factor
$f_{os}$ = shear-mode zero-field factor
$g_l$ = dynamic factor of the shear-mode lower-plate stress
$g_m$ = dynamic factor of $\Delta p_m$
$g_o$ = dynamic factor of a flow-mode damper
$g_{om}$ = dynamic factor of a mixed-mode damper
$g_u$ = dynamic factor of (the upper-plate stress of) a shear-mode damper
$g_{um}$ = dynamic factor of the mixed-mode upper-plate stress
$g_w$ = dynamic factor of $\Delta p_w$
$h$ = gap size of an ER valve/gap
$h^*$ = dynamic constant
$L$ = ER valve/gap length
$P_{cp}$ = peak capacitive electric power
$P_{rp}$ = peak resistive electric power
$t$ = time

$$\Delta p_w = g_w \Delta p_s \sin(\omega t + \phi_w) \tag{6}$$

with

$$g_w = \frac{2}{3} h^* \frac{[(2C_h - C_h^2 - D_h^2)^2 + 4D_h^2]^{1/2}}{(2 - C_h)^2 + D_h^2} \tag{7}$$

$$\phi_w = \frac{\pi}{2} + tan^{-1}[2D_h/(2C_h - C_h^2 - D_h^2)] \tag{8}$$

$$C_h = \frac{\sin h^* \cos h^* + \sinh h^* \cosh h^*}{h^* [(\cosh h^* \cos h^*)^2 + (\sinh h^* \sin h^*)^2]} \tag{9}$$

$$D_h = \frac{\sin h^* \cos h^* - \sinh h^* \cosh h^*}{h^* [(\cosh h^* \cos h^*)^2 + (\sinh h^* \sin h^*)^2]} \tag{10}$$

The function $g_w$, called the dynamic factor of $\Delta p_w$, starts from 1.0 at $h^* = 0$, increases with $h^*$ slightly until about $h^* = 1$, and, then, rises almost proportionally with $h^*$ (or with $\sqrt{\omega}$ if other parameters in $h^*$ is fixed). Physically, the amplitude of the dynamic wall shear stress is approximately equal to that of the equivalent steady shear stress at low frequencies and grows larger at high frequencies. A solution of the wall shear rate at a low dynamic constant was presented by Thurston and Gaertner (1991).

The zero-field dynamic pressure drop $\Delta p_o$, the summation of its two components $\Delta p_w$ and $\Delta p_m$, is:

$$\Delta p_o = g_o \Delta p_s \sin(\omega t + \phi_o) \tag{11}$$

with

$$g_o = \frac{4h^{*2}}{3[(2 - C_h)^2 + D_h^2]^{1/2}} \tag{12}$$

$$\phi_o = \frac{\pi}{2} + \tan^{-1}[D_h/(2 - C_h)] \tag{13}$$

where $g_o$ and $\phi_o$ are the dynamic factor and the phase advance of the flow-mode damper, respectively. The primary value of $g_o$ is from $g_w$ at low frequencies and from $g_m$ at high frequencies. The factor $g_o$ remains close to one at low frequencies and rises proportionally with $h^{*2}$ (Fig. 2). Physically, $\Delta p_o$ is mainly to overcome the wall stress and the fluid inertia at low and high frequencies, respectively. The phase advance $\phi_o$ is 0 at $h^* = 0$ (steady state), 45 deg at about $h^* = 1$, and 90 deg as $h^*$ approaches infinite.

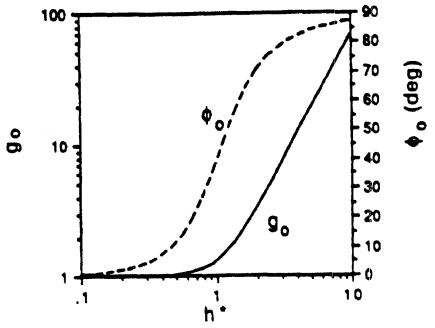


**Fig. 2 The dynamic factor $g_o$ and the phase advance $\phi_o$ of the zero-field pressure drop versus the dynamic constant $h^*$**

The above analysis has been for the zero-field situation. With the application of an electric field, a yield stress is induced. For a steady Couette flow within a narrow gap, the yield stress and the zero-field shear stress can be superposed. The linear summation is no longer valid under dynamic conditions and a numerical solution can be obtained by solving the fluid dynamic equation (Lou et al., 1993a). Analytical solutions for a dynamic Bingham fluid flow are not readily available, while numerical solutions are generally time-consuming. For a preliminary parametric study, a simplified, linear analytical approach is adopted here.

The ER pressure drop $\Delta p_{ER}$ is estimated to be

$$\Delta p_{ER} = 2\frac{L}{h}\tau_y \tag{14}$$

where $\tau_y$ is the yield stress. The time-dependency of electrorheology is not considered here, and $\Delta p_{ER}$ or $\tau_y$ involves only the amplitude of electrorheology. The ratio of $\Delta p_o$ to $\Delta p_{ER}$ is derived as

$$\frac{\Delta p_o}{\Delta p_{ER}} = f_{of} \sin(\omega t + \phi_o) \tag{15}$$

with

$$f_{of} = 6\frac{A_P}{A_{ER}}\frac{g_o}{\tau_y^*} \tag{16}$$

$$\tau_y^* = \frac{\tau_y}{\tau_o} \tag{17}$$

## Nomenclature (cont.)

$V_c$ = charged volume
$V_{cf}$, $V_{cm}$, and $V_{cs}$ = the flow-, mixed-, and shear-mode charged volumes
$v$ = piston velocity
$v_p$ = amplitude of $v$
$w$ = ER valve/gap width
$x_p$ = piston displacement amplitude
$\Delta p_{ER}$ = ER pressure drop
$\Delta p_m$ = pressure drop component induced by fluid inertia
$\Delta p_o$ = flow-mode zero-field pressure drop
$\Delta p_s$ = zero-field pressure drop for an equivalent steady flow of the same flow amplitude
$\Delta p_w$ = pressure drop component induced by the wall shear stress
$\epsilon$ = fluid dielectric constant
$\phi_l$ = phase advance of the shear-mode lower-plate stress
$\phi_o$ = flow-mode phase advance
$\phi_{om}$ = mixed-mode phase advance
$\phi_u$ = phase advance of (the upper-plate stress of) a shear-mode damper
$\phi_{um}$ = phase advance of the mixed-mode upper-plate stress
$\phi_w$ = phase advance of $\Delta p_w$
$\eta$ = zero-field viscosity
$\rho$ = fluid density
$\tau_l$ = shear-mode lower-plate shear stress
$\tau_o$ = equivalent to the zero-field shear stress between two parallel plates, with one of them fixed and the other plate moving at $v_p$
$\tau_u$ = shear-mode upper-plate shear stress
$\tau_{um}$ = mixed-mode upper-plate shear stress
$\tau_y$ = yield stress
$\tau_y^*$ = dimensionless yield stress
$\omega$ = angular velocity of the input vibration

$$\tau_o = \eta \frac{v_p}{h} \tag{18}$$

where $f_{of}$ is the zero-field factor of the flow-mode damper, a relative measure of the zero-field pressure drop. For the ER damper to be effective, $f_{of}$ has to be much less than one. The parameter $\tau_y^*$ is dimensionless; $\tau_o$ is equivalent to the zero-field shear stress between two parallel plates, with one of them fixed and the other plate moving at $v_p$.

The ER damping force on the piston of the flow-mode damper $F_{ERf}$ is calculated as

$$F_{ERf} = 2\frac{L}{h} A_p \tau_y \tag{19}$$

and it has to match the designed peak damping force. The compactness and efficiency of the device are important as well. The charged area $A_c$ (where the charged electrodes face each other) is calculated as

$$A_c = wL \tag{20}$$

where $w$ is the width of the ER valve. The charged volume $V_c$ (i.e., the volume between the charged electrodes) is calculated as

$$V_c = hA_c = wLh. \tag{21}$$

The damper electric capacitance $C$ is obtained as

$$C = \epsilon \frac{A_c}{h} \tag{22}$$

where $\epsilon$ is the fluid dielectric constant. Assuming a sinusoidal electric field strength with a peak value of $E_p$, one obtains the following peak capacitive electric power $P_{cp}$ and peak resistive electric power $P_{rp}$, respectively,

$$P_{cp} = \frac{1}{2}\epsilon\omega E_p^2 V_c \tag{23}$$

and

$$P_{rp} = C_d E_p V_c \tag{24}$$

where $C_d$ is the electric current density.

**Shear-Mode Dampers.** A practical shear-mode damper has a narrow gap whether it has a concentric or parallel arrangement of its electrodes. The fluid flow in a small gap can be approximated with a one-dimensional flow between two infinite parallel plates, with one plate (denoted arbitrarily as the lower-plate here) fixed and the other plate (the upper-plate) oscillating in its plane with a velocity

$$v = v_p \sin \omega t \tag{25}$$

Adapting the solutions of Schrag et al. (1965) to the current arrangement and a Newtonian fluid, the shear stress at the upper-plated $\tau_u$ is derived as

$$\tau_u = g_u \tau_o \sin(\omega t + \phi_u) \tag{26}$$

with

$$g_u = 2\sqrt{2}h^* \frac{\sqrt{A_1^2 + A_2^2}}{\sqrt{A_3^2 + A_4^2}}, \tag{27}$$

$$\phi_u = \frac{\pi}{4} + \tan^{-1}(A_2/A_1) - \tan^{-1}(A_4/A_3), \tag{28}$$

$$A_1 = \cosh 2h^* \cos 2h^*, \quad A_2 = \sinh 2h^* \sin 2h^*,$$

$$A_3 = \sinh 2h^* \cos 2h^*, \quad \text{and} \quad A_4 = \cosh 2h^* \sin 2h^* \tag{29}$$

where $g_u$ and $\phi_u$ are the dynamic factor and the phase advance of (the upper-plate stress of) the shear-mode damper, respectively. The dynamic factor $g_u$ is approximately equal to 1 when $h^* < 0.5$ and equal to $2\sqrt{2}h^*$ when $h^* > 0.5$ (Fig. 3). Therefore, $\tau_u$ increases with $h^*$.

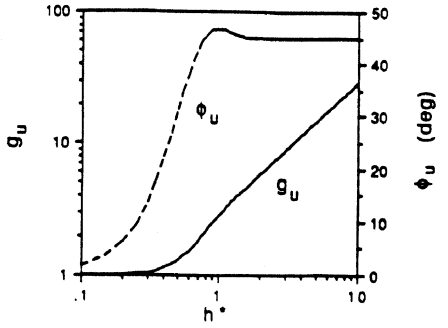


Fig. 3 The dynamic factor ($g_u$) and the phase advance ($\phi_u$) of the upper-plate shear stress of the shear-mode damper

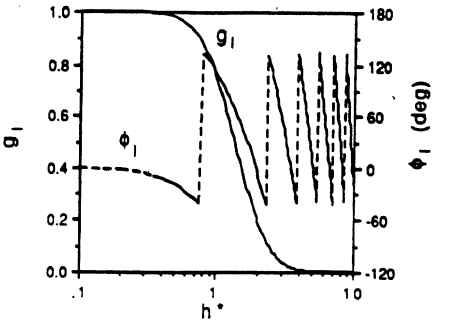


Fig. 4 The dynamic factor ($g_l$) and the phase advance ($\phi_l$) of the lower-plate shear stress of the shear-mode damper

The lower-plate shear stress $\tau_l$ is derived as

$$\tau_l = g_l \tau_o \sin(\omega t + \phi_l) \tag{30}$$

with

$$g_l = 2\sqrt{2}h^* \frac{1}{\sqrt{A_3^2 + A_4^2}} \tag{31}$$

$$\phi_l = \frac{\pi}{4} - \tan^{-1}(A_4/A_3) \tag{32}$$

where $g_l$ and $\phi_l$ are the dynamic factor and the phase advance of the lower-plate stress of the shear-mode damper, respectively. The dynamic factor $g_l$ is approximately equal to 1 when $h^* < 0.5$ and approaches 0 at high $h^*$ values (Fig. 4). Therefore, $\tau_l$ decreases with $h^*$. During a high-frequency oscillation, the shear waves does not fully reaches the lower-plate, and the majority of the energy is dissipated in the fluid volume immediately below the upper-plate.

As in the flow-mode damper, a simplified, linear analytical approach is adopted for dynamic flow of a Bingham fluid induced by an oscillating plate. In the shear-mode damper, no pressure drop is involved, and the damping force is directly related to the shear force on the upper-plate. The ER damping force in the shear-mode damper $F_{ERs}$ is estimated as

$$F_{ERs} = A_{cs}\tau_y. \tag{33}$$

where $A_{cs}$ is the charged area of the shear-mode damper. The zero-field (upper-plate) damping force $F_u$ is

$$F_u = A_{cs}\tau_o g_u \sin(\omega t + \phi_u) \tag{34}$$

The desired damping force of the system has to be matched by $F_{ERs}$, and $F_u$ has to be relatively small. The ratio of $F_u$ to $F_{ERs}$ is

$$\frac{F_u}{F_{ERs}} = f_{os} \sin(\omega t + \phi_u) \tag{35}$$

with

$$f_{os} = \frac{g_u}{\tau_y^*} \tag{36}$$

where $f_{os}$ is the zero-field factor of the shear-mode damper. For the damper to be effective, $f_{os}$ has to be much less than one.

**Mixed-Mode Dampers.** Because of the linear nature of the flow of a Newtonian fluid between two parallel plates, the velocity between the electrodes of a mixed-mode damper can be obtained by superposing those of the corresponding shear- and flow-mode dampers. The upper-plate shear stress $\tau_{um}$ is the summation of the shear stresses induced by Couette and Poiseuille flows:

$$\tau_{um} = \tau_o g_{um} \sin(\omega t + \phi_{um}) \tag{37}$$

with

$$g_{um} = \sqrt{A_{1um}^2 + A_{2um}^2} \tag{38}$$

$$\phi_{um} = \tan^{-1} \frac{A_{2um}}{A_{1um}} \tag{39}$$

$$A_{1um} = g_u \cos\phi_u + 6\frac{A_p}{A_{ER}} g_w \cos\phi_w$$

and

$$A_{2um} = g_u \sin\phi_u + 6\frac{A_p}{A_{ER}} g_w \sin\phi_w. \tag{40}$$

where $g_{um}$ and $\phi_{um}$ are the dynamic factor and the phase advance of $\tau_{um}$, respectively.

The total zero-field damping force $F_{om}$ is derived as

$$F_{om} = A_p g_o \Delta p_s \sin(\omega t + \phi_o) + A_c g_{um} \tau_o \sin(\omega t + \phi_{um}) \tag{41}$$

and the ER control force $F_{ERm}$ is as follows

$$F_{ERm} = 2\frac{L}{h} A_p \tau_y + A_c \tau_y \tag{42}$$

In ether of Eqs. (41) or (42), the first term on the right hand side is the force from the pressure drop, while the second term represent the force on the shearing surface.

The combination of Eqs. (41) and (42) gives

$$\frac{F_{om}}{F_{ERm}} = f_{om} \sin(\omega t + \phi_{om}) \tag{43}$$

with

$$f_{om} = \frac{g_{om}}{\tau_y^*} \tag{44}$$

$$g_{om} = \frac{\sqrt{A_{1om}^2 + A_{2om}^2}}{[2(A_p/A_{ER}) + 1]} \tag{45}$$

$$\phi_{om} = \tan^{-1} \frac{A_{2om}}{A_{1om}} \tag{46}$$

$$A_{1om} = 12(A_p/A_{ER})^2 g_o \cos\phi_o + g_{um} \cos\phi_{um} \tag{47}$$

$$A_{2om} = 12(A_p/A_{ER})^2 g_o \sin\phi_o + g_{um} \sin\phi_{um} \tag{48}$$

where $f_{om}$ is the zero-field factor, $g_{om}$ the dynamic factor, and $\phi_{om}$ the phase advance of the mixed-mode damper. Both $g_{om}$ and $\phi_{om}$ increase with $h^*$ (Fig. 5). The dynamic factor $g_{om}$ also increases with $A_p/A_{ER}$ because of the rising dominance of the flow action (Fig. 5(*a*)). The phase advance $\phi_{om}$ decreases with $A_p/A_{ER}$ at low $h^*$ and does the opposite at high $h^*$ (Fig. 5(*b*)). A mixed-mode damper becomes a shear-mode damper when $A_p/A_{ER}$ approaches zero, i.e., no more piston area.

**Flow-Mode Versus Shear-Mode.** In active damping control, one likes to generate a large ER damping force and keep the zero-field damping force as small as possible. For the same task, a shear-mode damper and a flow-mode damper therefore should have (*a*) the same ER damping force and (*b*) the same zero-field factor value. For the second requirement, one has

$$\frac{f_{of}}{f_{os}} = 1. \tag{49}$$

The substitution of Eqs. (15) and (36) into Eq. (49) gives

$$A_p = \frac{g_u}{6g_o} A_{ER}. \tag{50}$$

To meet the first requirement, one can derive from Eqs. (19), (20), (33), and (50) the following

$$\frac{V_{cf}}{V_{cs}} = \frac{A_{cf}}{A_{cs}} = \frac{3g_o}{g_u} \tag{51}$$

where $V_{cs}$ is the charged volume of the shear-mode damper, and $A_{cf}$ the charged area of the flow-mode damper. The both dampers are assumed to have the same gap size. The ratio $V_{cf}/V_{cs}$ is a good indicator of relative design merits of the two dampers because the charged volume is directly related to the size (Fig. 1(*d*)) and power requirement of a damper as shown in Eqs. (23) and (24). The ratio $V_{cf}/V_{cs}$, like $g_o$ or $g_u$, is a function of $h^*$ (see Fig. 6). The ratio $V_{cf}/V_{cs}$ is 3 at $h^* = 0$, decreases gradually to its minimum value of 1.35 around $h^* = 1$, and then increases linearly with $h^*$. To achieve the same performance, the flow-mode is not as compact and efficient as the shear-mode ER.

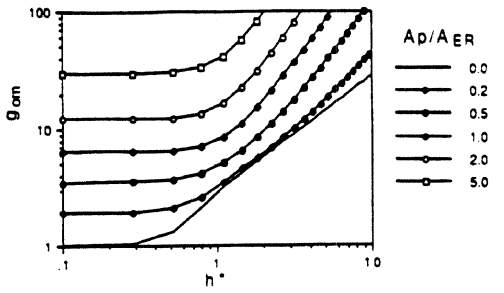


Fig. 5(*a*)

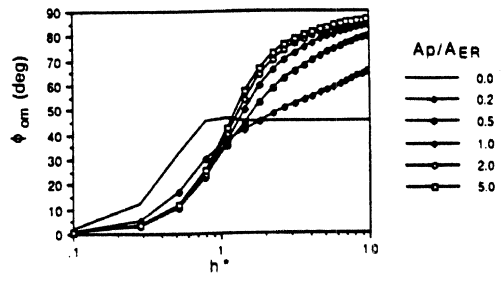


Fig. 5(*b*)

**Fig. 5** (*a*) The dynamic factor $g_{om}$ and (*b*) the phase advance $\phi_{om}$ of a mixed-mode damper versus the dynamic constant $h^*$ and the area ratio $A_p/A_{ER}$

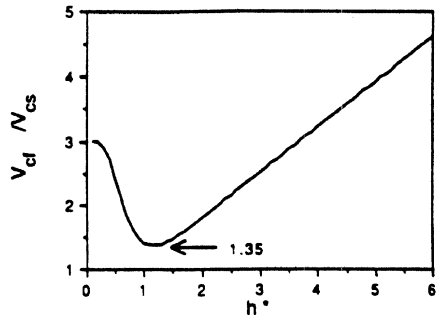


**Fig. 6** The ratio of the flow-mode charged volume ($V_{cf}$) to the shear-mode charged volume ($V_{cs}$) as a function of the dynamic constant $h^*$

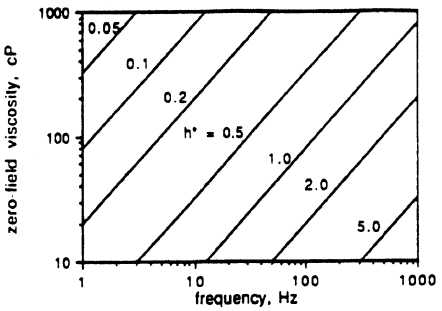


Fig. 7 The dynamic constant $h^*$ as a function of the vibration frequency ($=\omega/2\pi$) and the zero-field viscosity ($\eta$), with the ER control gap size $h=1$ mm and the ER fluid density $\rho=1000$ kg/m$^3$

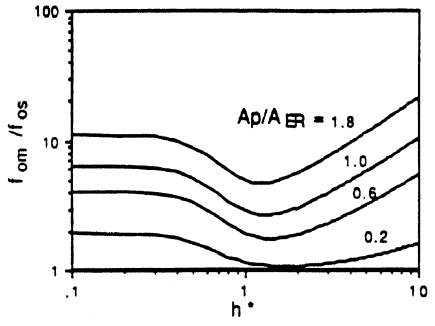


Fig. 8 The ratio of the zero-field factor of the mixed-mode damper $f_{om}$ to that of the shear-mode damper $f_{os}$ as a function of the dynamic constant $h^*$ and the area ratio $A_p/A_{ER}$

The significance of the dynamic constant $h^*$ is evident in Fig. 6. A practical range of $h^*$ is estimated using Eq. (5) and plotted in Fig. 7, where the fluid density $\rho$ and the gap size $h$ are chosen to be 1000 kg/m$^3$ and 1 mm, respectively. The frequency ranges from 1 to 1000 Hz, and $\eta$ ranges from 10 to 1000 cP in Fig. 7. In passenger cars, body natural frequencies are 1-2 Hz, the wheelhop frequency is around 15 Hz, and the engine mount natural frequency is 10-20 Hz (Morishita and Mitsui, 1992). The upper natural frequency limit of practical mechanical systems is probably 100 Hz. A middle-range value of the zero-field viscosity is 100 cP. For the chosen density and gap size, the dynamic constant $h^*$ varies from 0.05 to 5.0. Practical $\rho$ and $h$ values will not deviate too much from those chosen here, and the $h^*$ range in Fig. 7 is representative.

**Mixed-Mode Versus Shear-Mode.** For the ER damping force of a mixed-mode damper $F_{ERm}$ and that of a shear-mode damper $F_{ERs}$ to be equal, one obtains

$$\frac{V_{cm}}{V_{cs}}=\frac{A_{cm}}{A_{cs}}=\frac{1}{2(A_p/A_{ER})+1} \tag{52}$$

where $V_{cm}$ and $A_{cm}$ are the charged volume and area of the mixed-mode damper, respectively. The gap size $h$ is assumed to be the same. With a positive $A_p/A_{ER}$, $V_{cm}/V_{cs}<1$. With the same ER damping force, the mixed-mode damper is therefore more compact than the shear-mode damper.

The ratio of the zero-field factor of the mixed-mode damper $f_{om}$ to that of the shear-mode damper $f_{os}$ is equal to $g_{om}/g_u$ because of Eqs. (36) and (44). The ratio $f_{om}/f_{os}$ is a function of $h^*$ and $A_p/A_{ER}$, and is always greater than one for a positive $A_p/A_{ER}$ (Fig. 8). The mixed-mode damper therefore does not have as a low zero-field damping force as the comparable shear-mode damper.

## Discussions

The above analysis shows that one should avoid the flow-mode and use the shear-mode. There are two physical reasons for the conclusion. First, with a limited ER induced increase in the shear stress, a device should operate at as a low shear rate as possible to reduce the zero-field damping force and increase its effective control. The yield stress may even decreases with the shear rate (Klass and Martinek, 1967; Lou et al., 1990), which further enhances the need for a low shear rate. Second, the fluid inertia and the unsteady wall shear stress (which is higher than the steady wall shear stress) significantly increase the zero-field damping force. A flow-mode damper generally has higher shear rate and acceleration, especially with a large $A_p/A_{ER}$, than a shear-mode damper.

In the analysis, the cylinder component of a damper is fixed while the piston component vibrates. Both the components of many practical dampers can move. In most of these cases, there is a large disparity in the amplitudes of the motion for the two components, and the analysis in this study is valid. Otherwise, more appropriate boundary conditions have to be used for a finer analysis although the general conclusion from this study may still apply, at least to the first order accuracy.

For the purpose of generality, the assigned vibration in this study is sinusoidal. Road surface profiles for an automobile damper, for example, is not so. Through the use of the power spectral density function, however, one can present the surface profiles in forms of sine wave.

Shear-mode dampers can be further divided into rotary and translational types, either of which can have its own variations in the way electrodes are arranged.

The damper in Fig. 1(*c*) is only one possible version of the translational type of shear-mode dampers, where the electrodes are arranged concentrically. Electrodes can also be parallel plates. Multiple electrodes are generally used to achieve a compact design. Because of the translational motion, the cylinder in Fig. 1(*c*) has to be longer than the piston to keep a constant charged area. This results in a significant amount of idling surface on the cylinder at any moment.

A rotary-type shear-mode damper is able to reduce the extra surface area by having all the surface area engaged all the time. One possible version is to have a plurality of rotational shearing disks along the rotation axis (Lou et al., 1993b). An alternative is to have multiple concentric electrodes around the rotation axis. A translation-to-rotation device is needed if the motion to be damped is translational. ER fluids in shear-mode dampers are under a minimum, if any, pressure. Low pressure simplifies many design problems, especially the sealing problem. Among shear-mode dampers, a rotary damper has an additional advantage over a translational damper because the former can avoid sealing a reciprocating sliding surface, which is more prone to entrapping the solid phase of an ER fluid.

The ER fluid used in the analysis is Bingham plastic and has a time constant far smaller than those of the dampers. A practical ER fluid may not follow an ideal Bingham plastic model. As long as the practical fluid has a relatively Newtonian rheology at zero-field, a fast time response, and an effective yield stress (i.e., a finite shear stress increment at the working shear-rate range) when energized, the results from this study still apply because of the nature of the analysis in this study. The analysis is base on (1) the flow dynamics at zero-field and (2) the achievable stress increment when energized. If the ER response is close to or slower than those of the dampers, one needs to include the flow dynamics of the energized fluid as well.

## Conclusions

In this study, the dynamics of the fluid flow is included in the derivation of the zero-field damping forces of the flow-, shear-, and fixed-mode ER dampers based on an ER fluid that is Bingham plastic. The main results of the study are as follows:

- The zero-field pressure drop in a flow-mode damper is mainly to overcome the wall shear stress at low frequencies. At high frequencies (with the dynamic constant $h^*$ greater than one), the zero-field pressure counters pri-

marily the fluid inertia, and it increases with the frequency or $h^{*2}$. It also has a significant phase advance relative to the vibration at high frequencies. The level of ER control decreases with the ratio of the piston area to the ER valve cross-section $A_p/A_{ER}$.

- The zero-field pressure drop in a shear-mode damper also has to counter the fluid inertia at high frequencies. When the dynamic constant $h^*$ is greater than 0.5, the zero-field pressure increases with $h^*$ or the square root of the frequency.
- The behavior of the zero-field pressure drop in a mixed-mode damper is between those of a shear- and a flow-mode damper, and it is a function of the area ratio $A_p/A_{ER}$. The mixed-mode damper becomes a shear-mode damper when the ratio $A_p/A_{ER}$ approaches zero.
- To achieve the same performance, a flow-mode ER damper is not as compact and efficient as a shear-mode ER damper.
- With the same ER damping force, a mixed-mode damper is more compact than a shear-mode damper. However, the mixed-mode damper does not have as a low zero-field damping force as the shear-mode damper.

## Acknowledgments

The authors wish to acknowledge the financial support from the NASA-Langley Research Center, the U.S. Army Tank-Automotive Command (TACOM), Aeroquip Corporation, BASF, Chrysler Corporation, Ford Motor Company, Monroe Automotive Equipment Co., Naval Underwater Systems Center, Nissan Motors, and Tremec Trading Company.

## References

Klass, D. L., and Martinek, T. W., 1967, "Electroviscous Fluids I. Rheological Properties," *Journal of Applied Physics*, Vol. 38, pp. 67–74.

Lou, Z., Ervin, R. D., and Filisko, F. E., 1990, "The Feasibility of Using Electro-Rheological Fluids in Aircraft Flight Controls—Phase 1 Report," UM-TRI-90-10, The University of Michigan Transportation Research Institute, Ann Arbor.

Lou, Z., Ervin, R. D., and Filisko, F. E., 1992, "Behaviors of Electrorheological Valves and Bridges," *Proceedings of the International Conference on Electrorheological Fluids: Mechanism, Properties, Structure, Technology, and Applications*, Tao, R., ed., World Scientific, River Edge, NJ, pp. 398–423.

Lou, Z., Ervin, R. D., and Filisko, F. E., 1993a, "The Influence of Viscometer Dynamics on the Characterization of an Electrorheological Fluid Under Sinusoidal Electric Excitation," *Journal of Rheology*, Vol. 37, pp. 55–70.

Lou, Z., Ervin, R. D., Filisko, F. E., and Winkler, C. B., 1993b, "An Electrorheologically Controlled Semi-Active Landing Gear," SAE Technical Paper Series, No. 931403, SAE, Warrendale, PA (Also: "Electrorheologically Controlled Landing Gear," *Aerospace Engineering*, June 1993, pp. 17–22).

Lou, Z., and Yang, W. J., 1993, "A Computer Simulation of the Non-Newtonian Blood Flow at the Aortic Bifurcation," *Journal of Biomechanics*, Vol. 26, pp. 37–49.

Morishita, S., and Mitsui, J., 1992, "An Electronically Controlled Engine Mount Using Electro-Rheological Fluid," SAE Technical Paper Series, No. 922290, SAE, Inc., Warrendale, PA.

Schrag, J. L., Guess, J. F., and Thurston, G. B., 1965, "Shear-Wave Interference Observed by Optical Birefringence Induced in a Viscous Liquid," *Journal of Applied Physics*, Vol. 36, pp. 1996–2000.

Thurston, G. B., 1959, "Theory of Oscillation of a Viscoelastic Medium Between Parallel Planes," *Journal of Applied Physics*, Vol. 30, pp. 1855–1860.

Thurston, G. B., and Gaertner, E. B., 1991, 'Viscoelasticity of Electrorheological Fluids During Oscillatory Flow in a Rectangular Channel," *Journal of Rheology*, Vol. 35, pp. 1327–1343.

# APPENDIX C

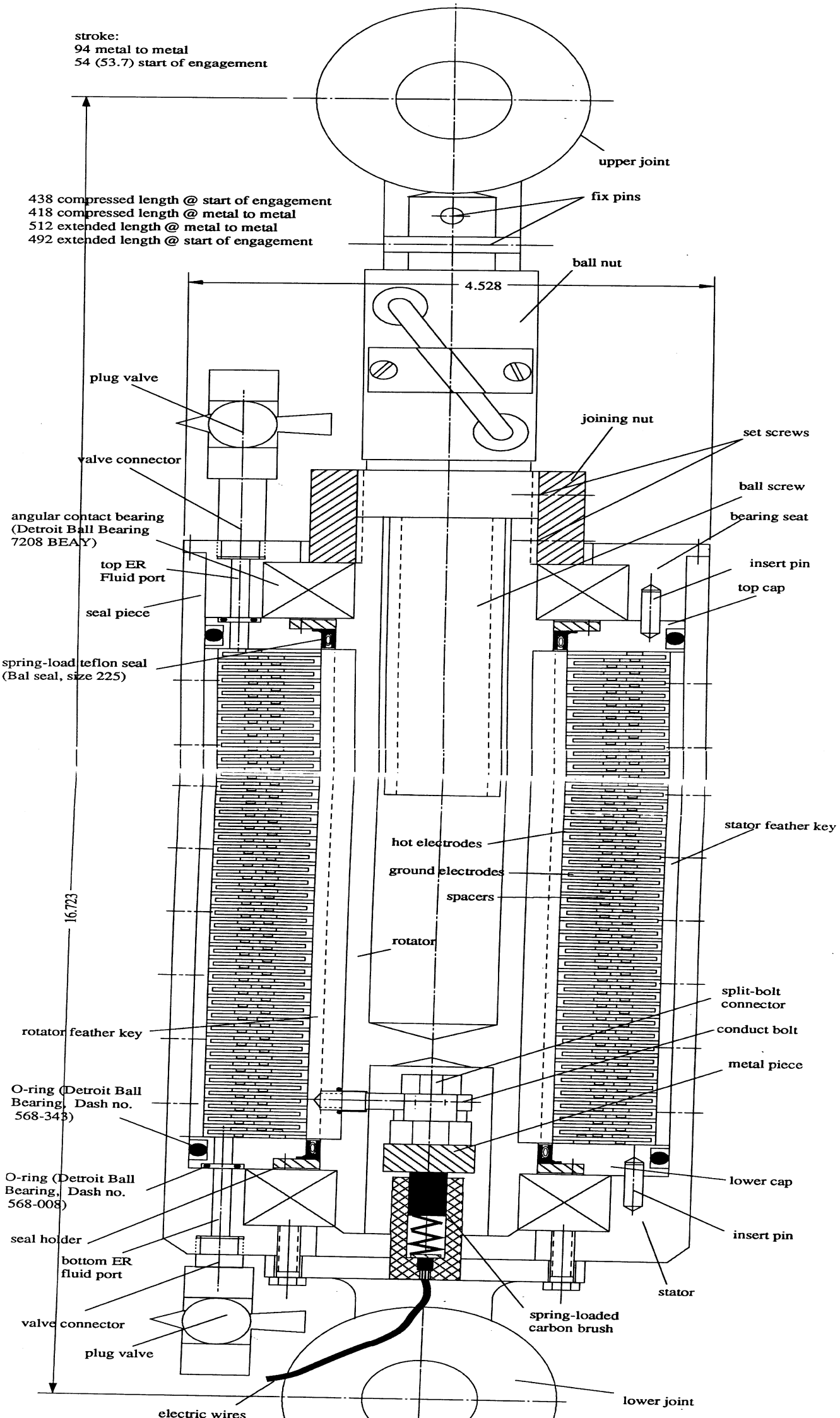
stroke:
94 metal to metal
54 (53.7) start of engagement
438 compressed length @ start of engagement
418 compressed length @ metal to metal
512 extended length @ metal to metal
492 extended length @ start of engagement
16.723
upper joint
fix pins
ball nut
4.528
plug valve
joining nut
set screws
valve connector
ball screw
angular contact bearing
(Detroit Ball Bearing
7208 BEAY)
bearing seat
top ER
Fluid port
insert pin
top cap
seal piece
spring-load teflon seal
(Bal seal, size 225)
stator feather key
hot electrodes
ground electrodes
spacers
rotator
split-bolt
connector
rotator feather key
conduct bolt
metal piece
O-ring (Detroit Ball
Bearing, Dash no.
568-343)
O-ring (Detroit Ball
Bearing, Dash no.
568-008)
lower cap
insert pin
seal holder
bottom ER
fluid port
stator
valve connector
spring-loaded
carbon brush
plug valve
lower joint
electric wires

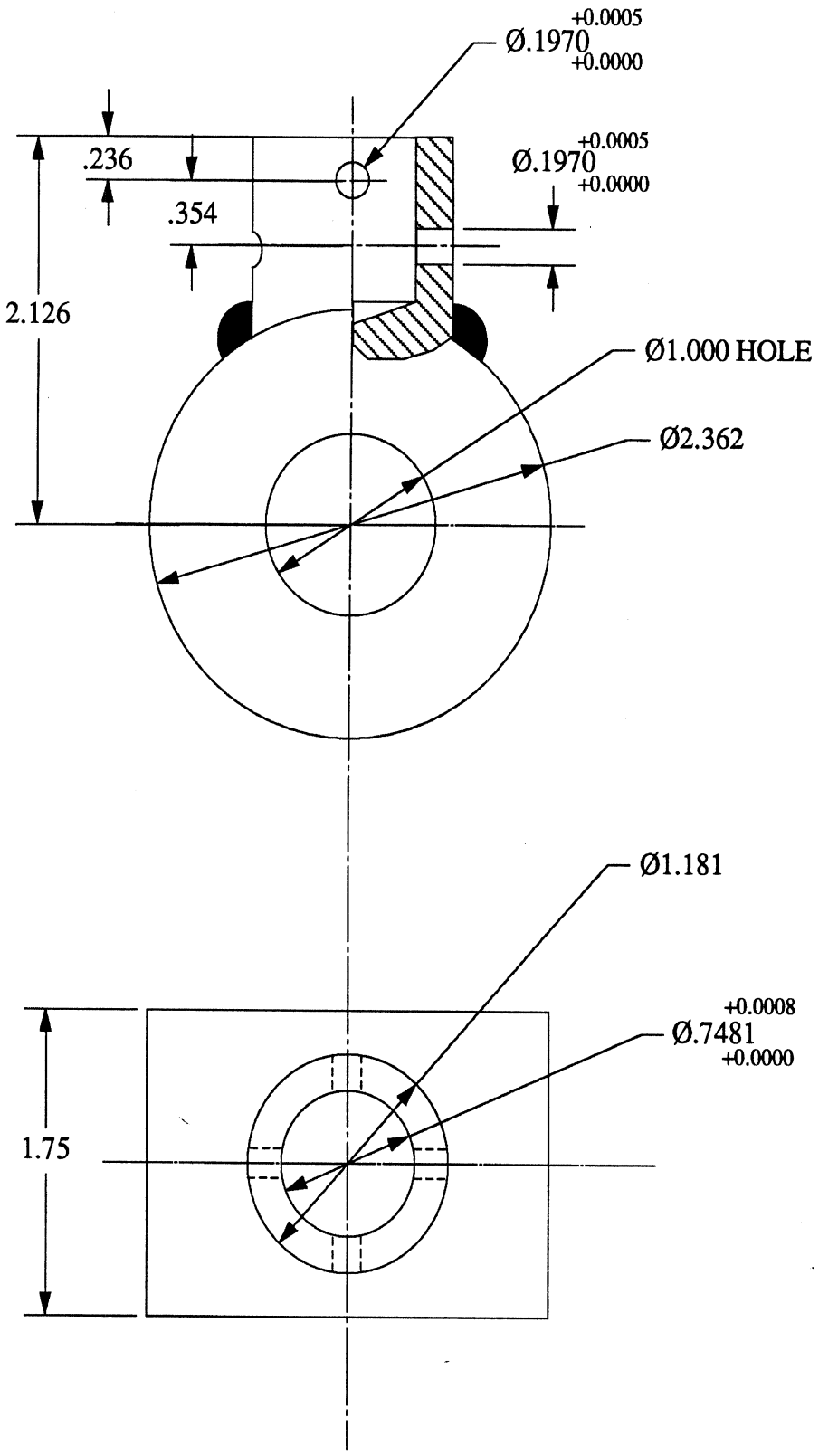


| Upper joint | Grade 12.9 Alloy steel | 1 |
|---|---|---|
| Part name | Material | Qty |

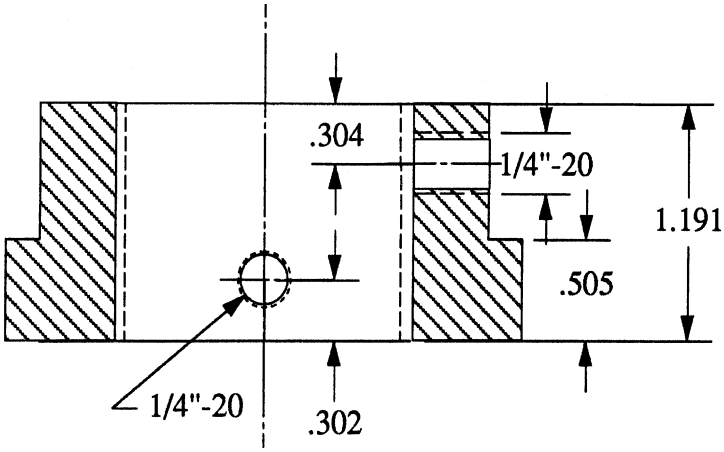


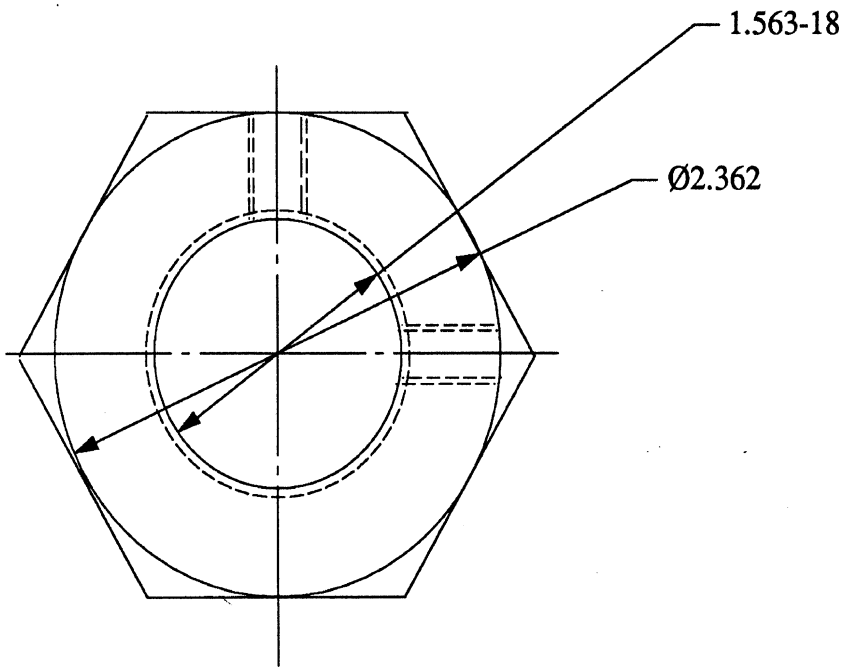


| Joining nut | Grade 12.9 Alloy steel | 1 |
|---|---|---|
| Part name | Material | Qty |

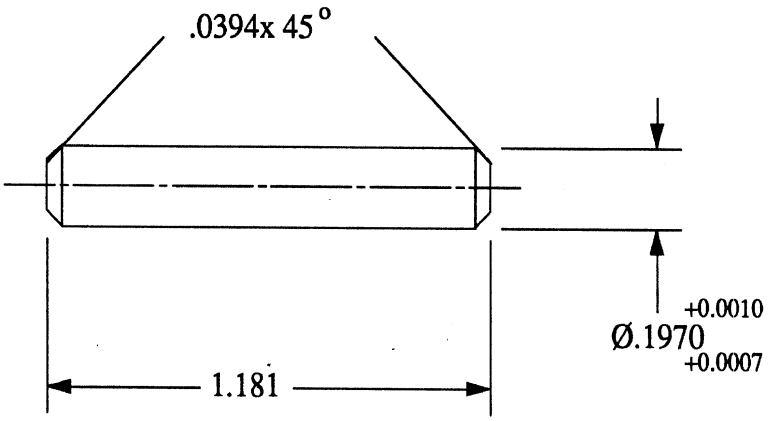


Scale : 2:1

| Pin | Grade 12.9 Alloy steel | 2 |
|---|---|---|
| Part name | Material | Qty |

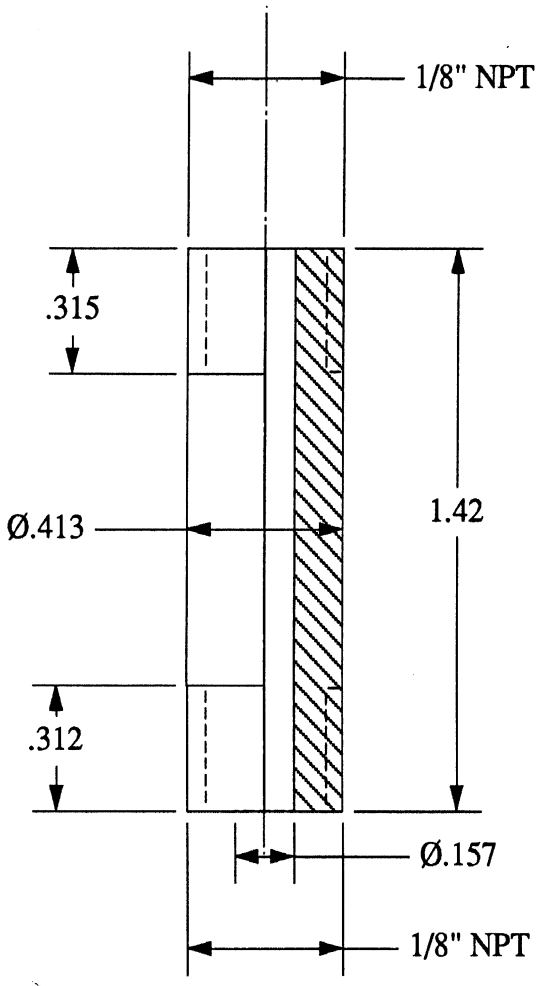


Scale : 2:1

| Valve connector | 303 Stainless steel | 1 |
|---|---|---|
| Part name | Material | Qty |

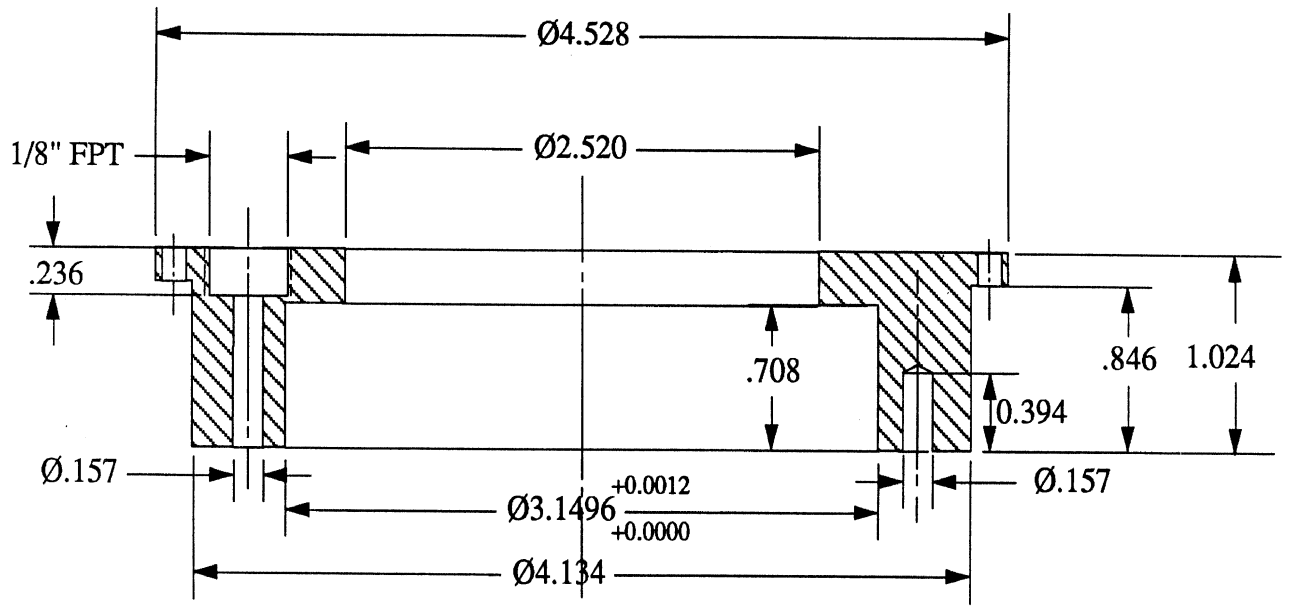


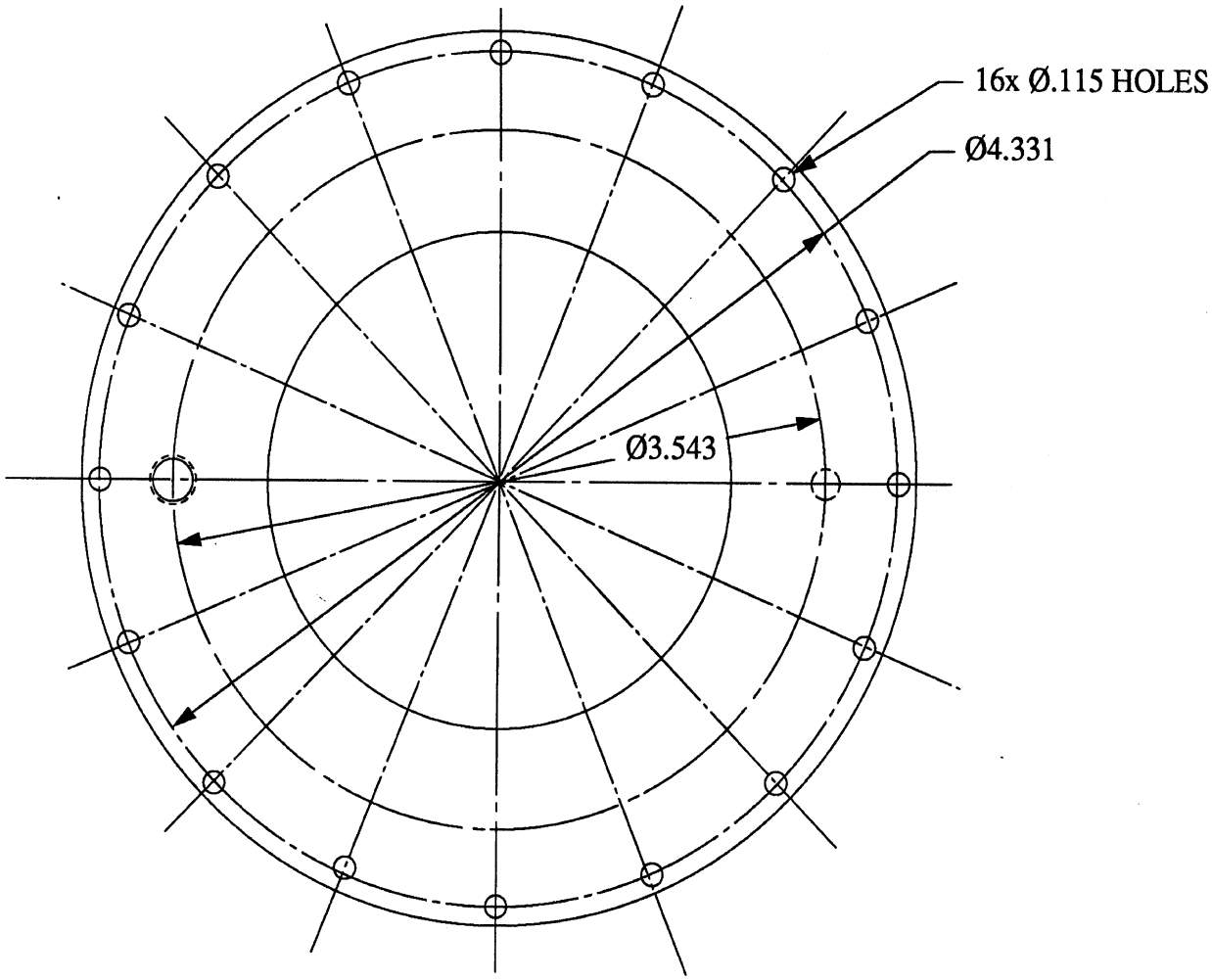


| | | |
|---|---|---|
| Bearing seat | 303 Stainless steel | 1 |
| Part name | Material | Qty |

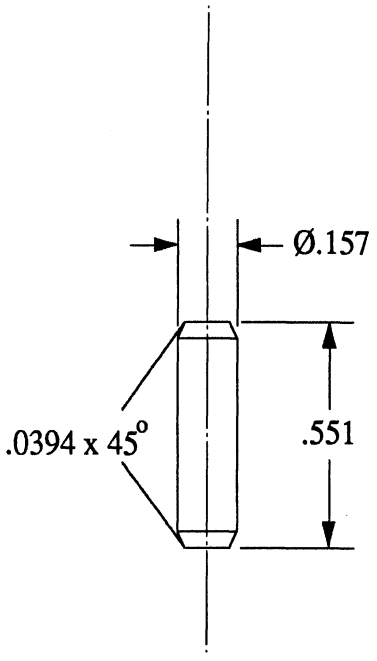


Scale: 2:1

| Part name | Material | Qty |
|---|---|---|
| Insert pin | 303 Stainless steel | 2 |

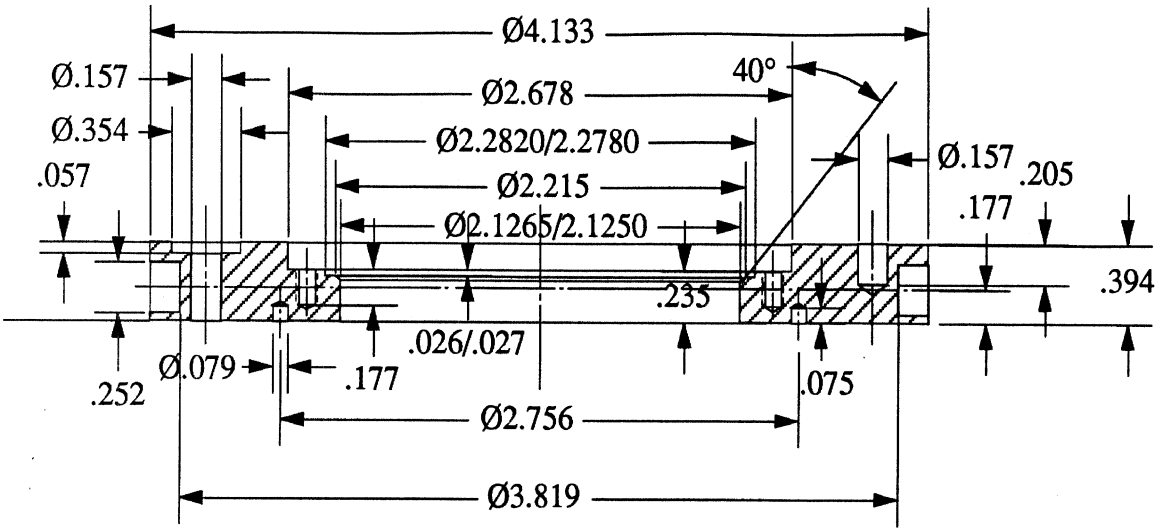


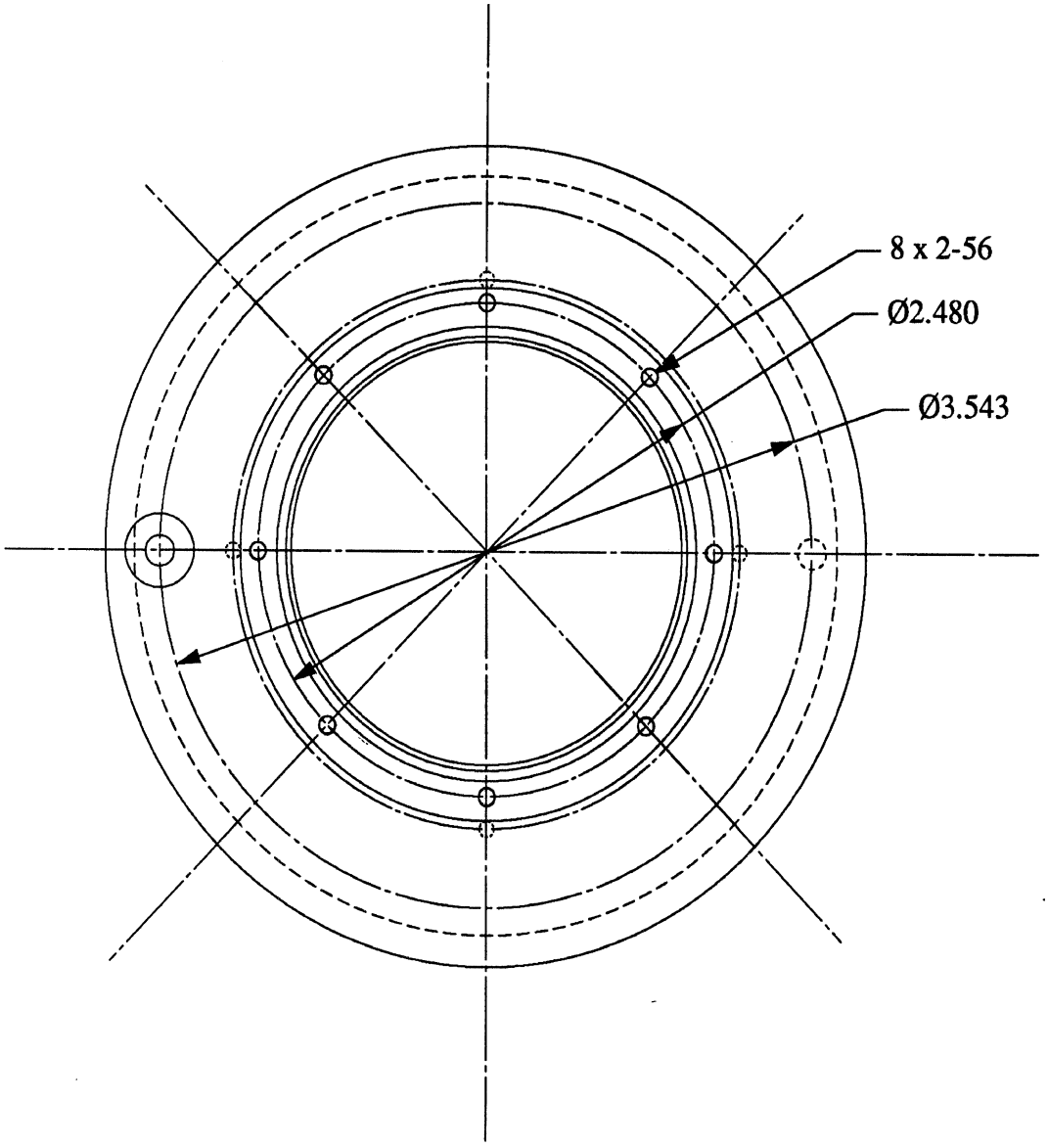


| Cap | 303 Stainless steel | 2 |
|---|---|---|
| Part name | Material | Qty |

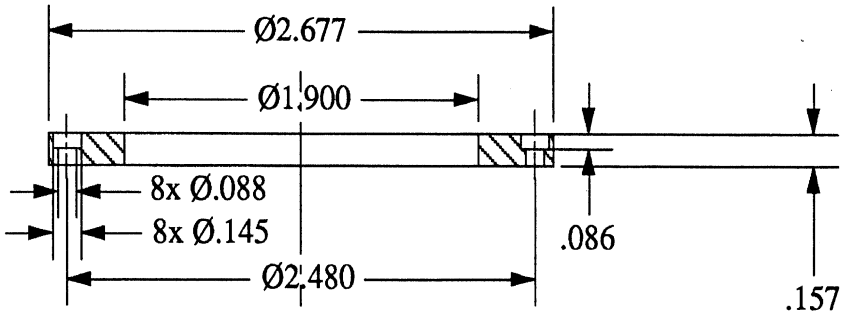


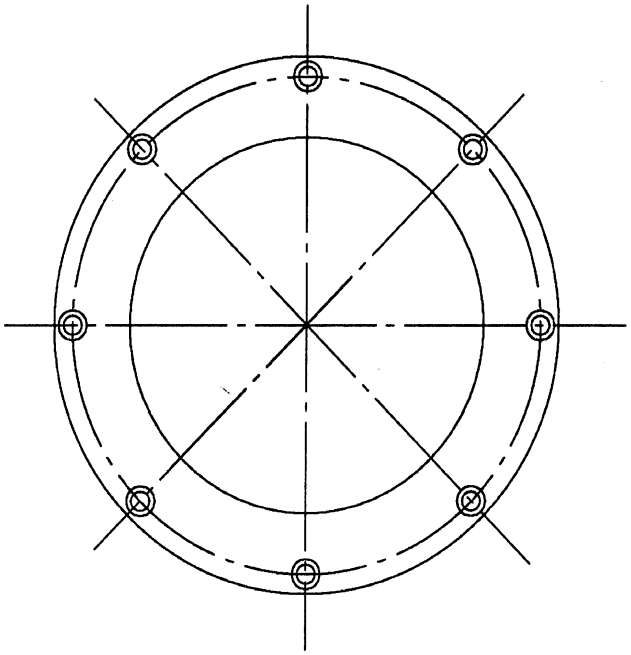

| Seal holder | 303 Stainless steel | 2 |
|---|---|---|
| Part name | Material | Qty |

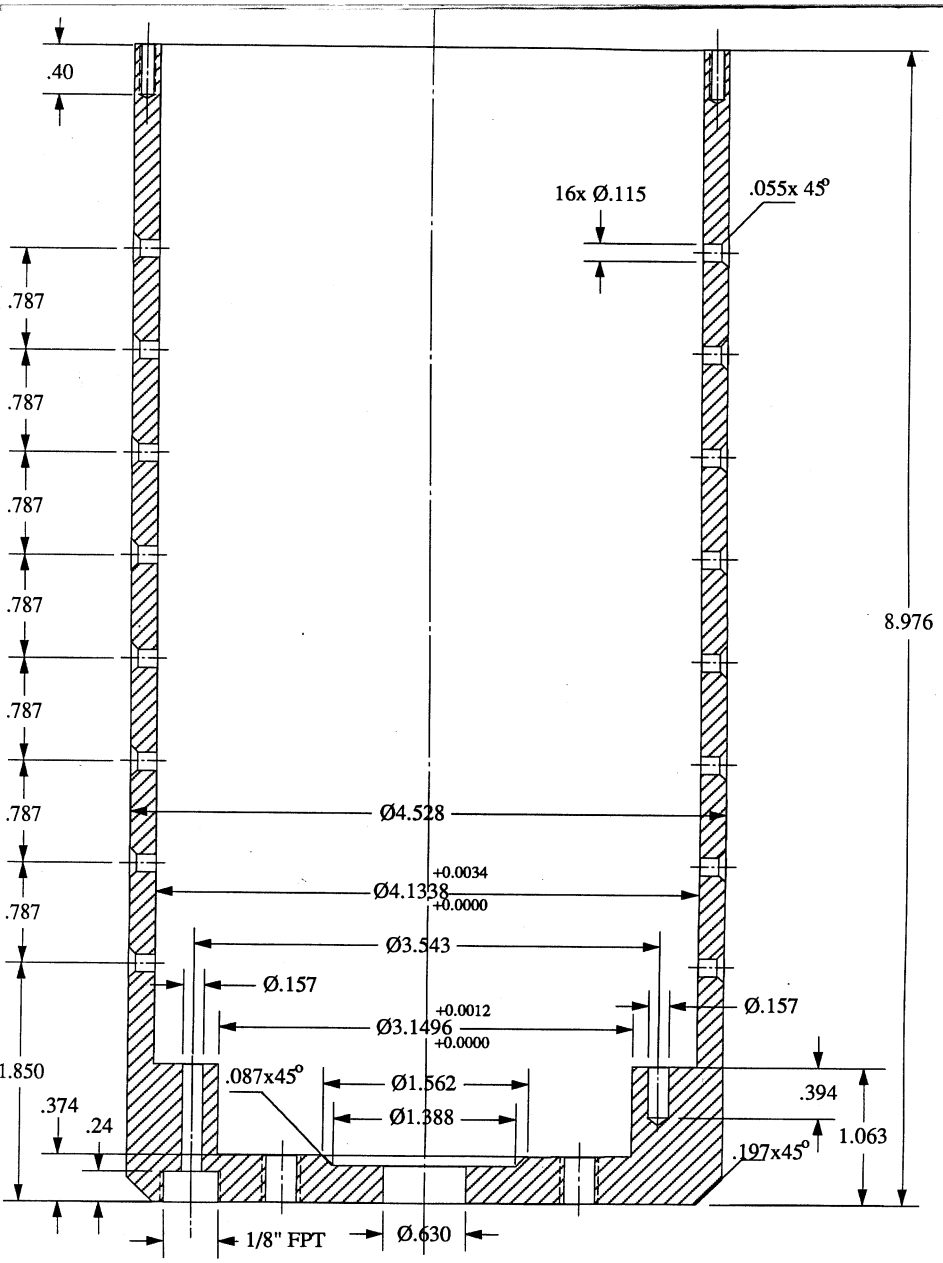


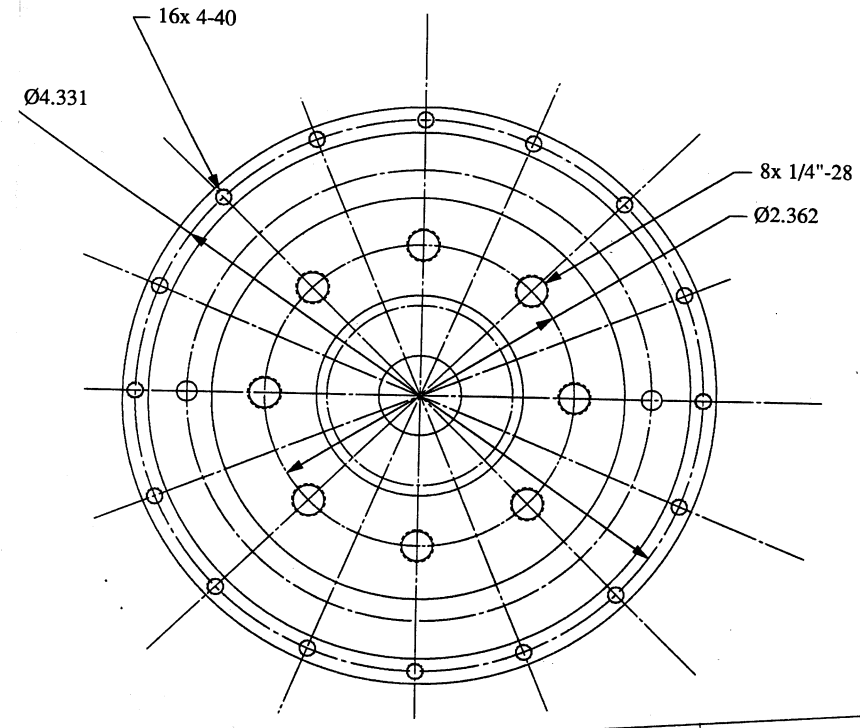


| Stator | 303 Stainless steel | 1 |
|---|---|---|
| Part name | Material | Qty |

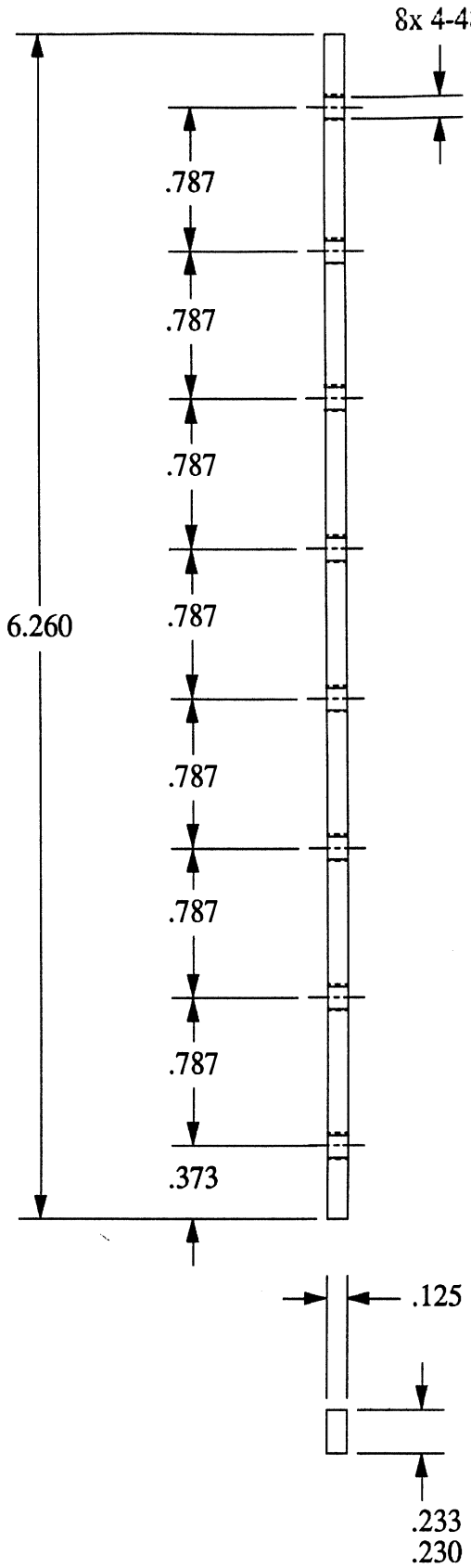


All corners R 0.02

| Stator feather key | 303 Stainless steel | 2 |
|---|---|---|
| Part name | Material | Qty |

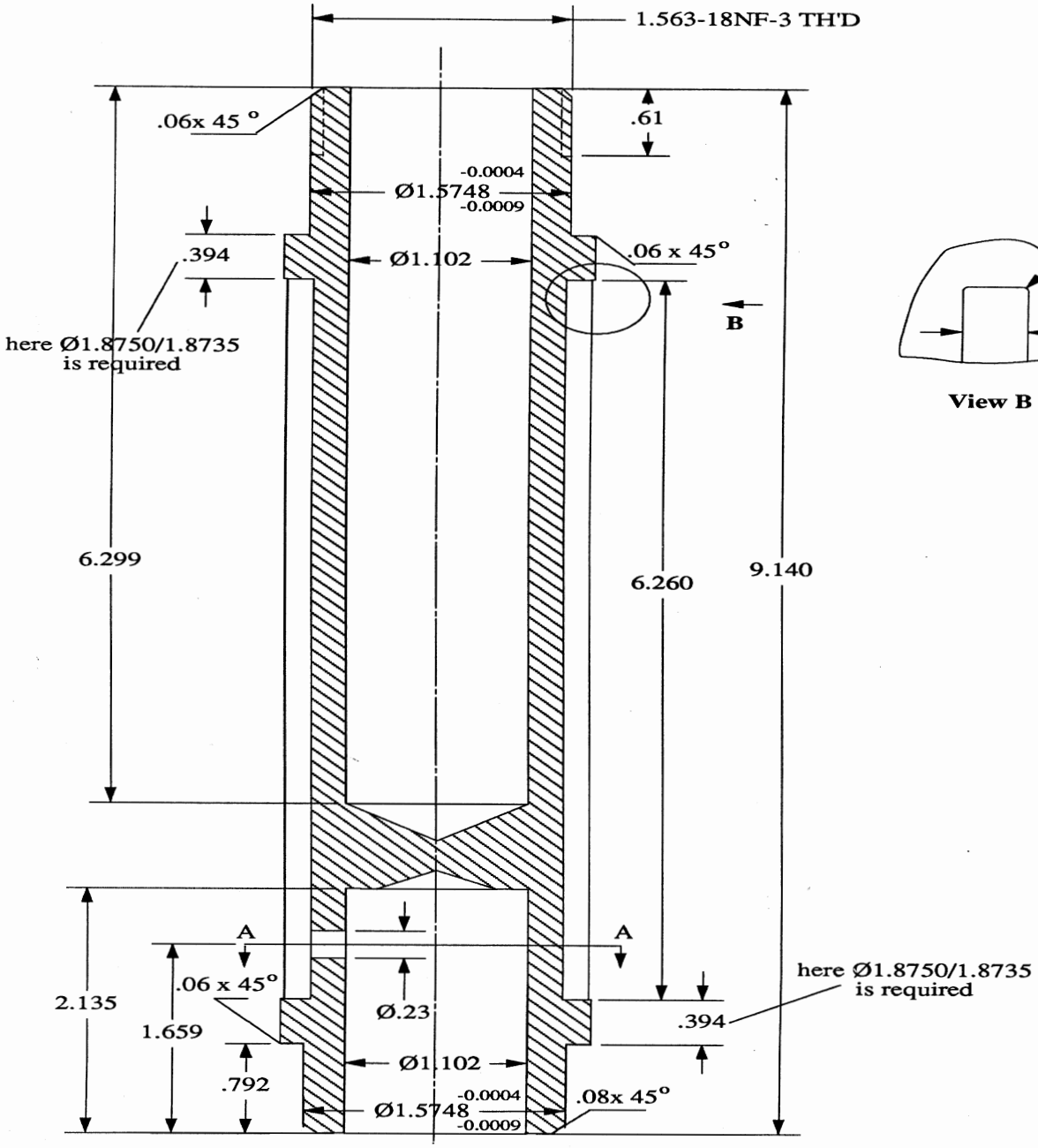





**View B**

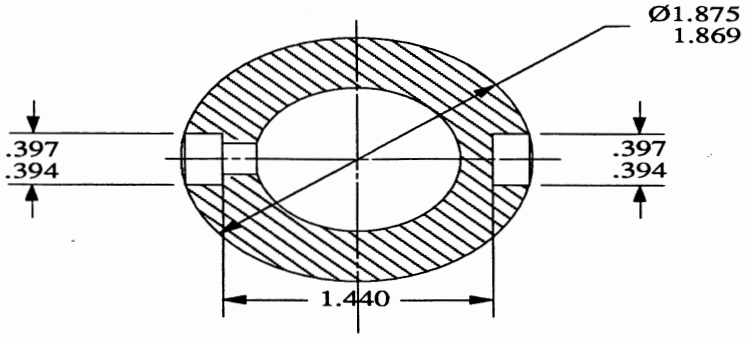


**View A-A**

All corners R 0.02

| Part name | Material | Qty |
|---|---|---|
| Rotator | Glass epoxy G-11 | 1 |

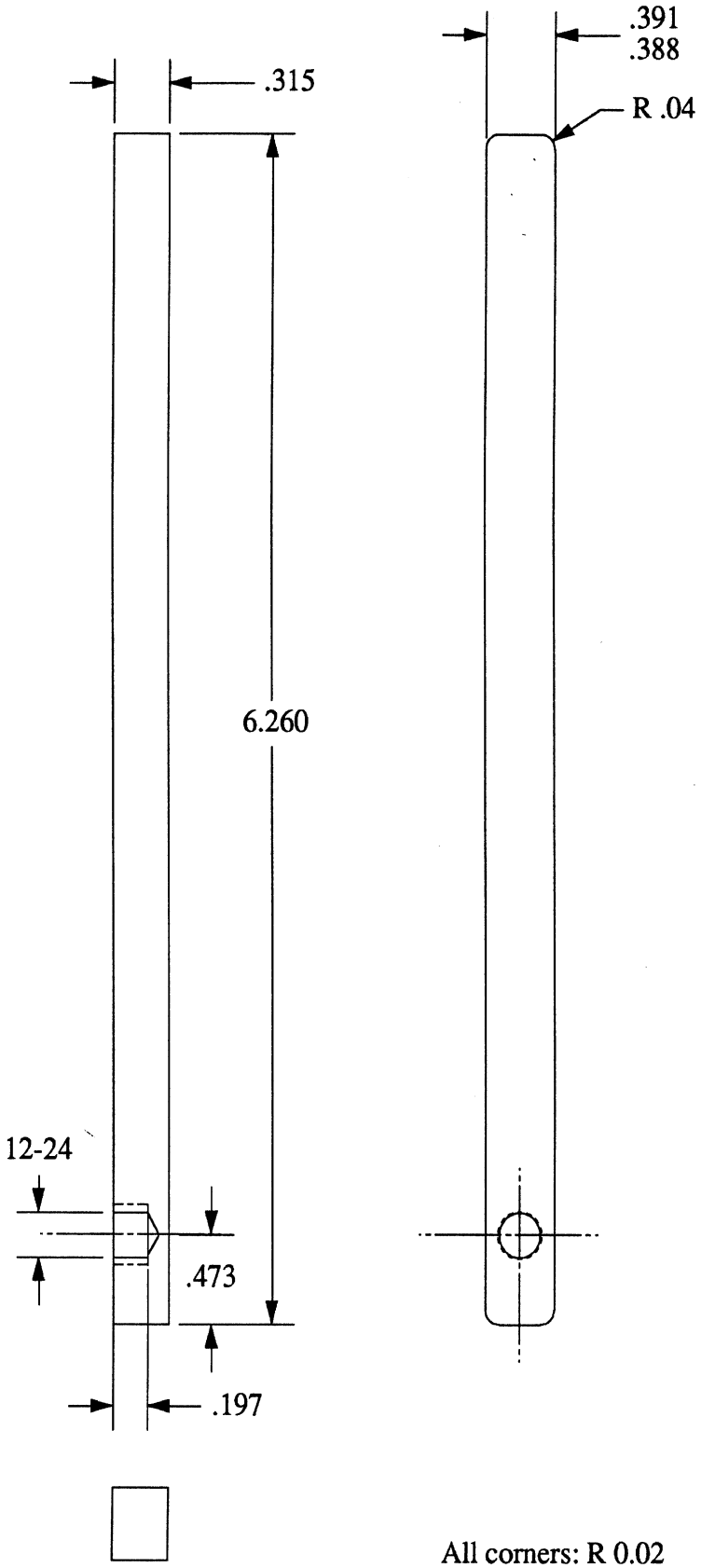


All corners: R 0.02

| Rotator feather key | 303 Stainless steel | 2 |
|---|---|---|
| Part name | Material | Qty |

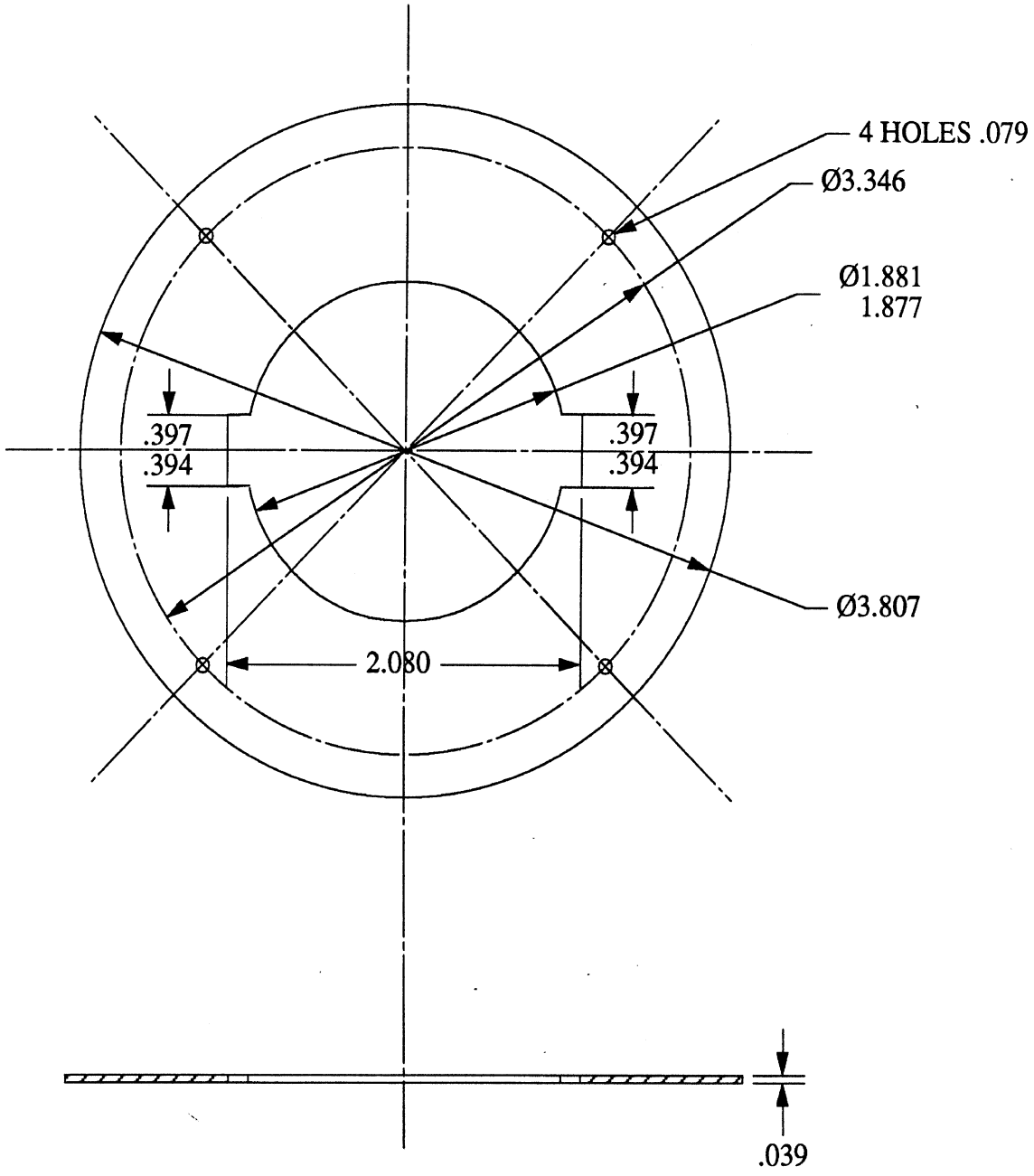


All corners: R 0.02

| Part name | Material | Qty |
|---|---|---|
| Hot electrode | Stainless steel 18-8 | 40 |

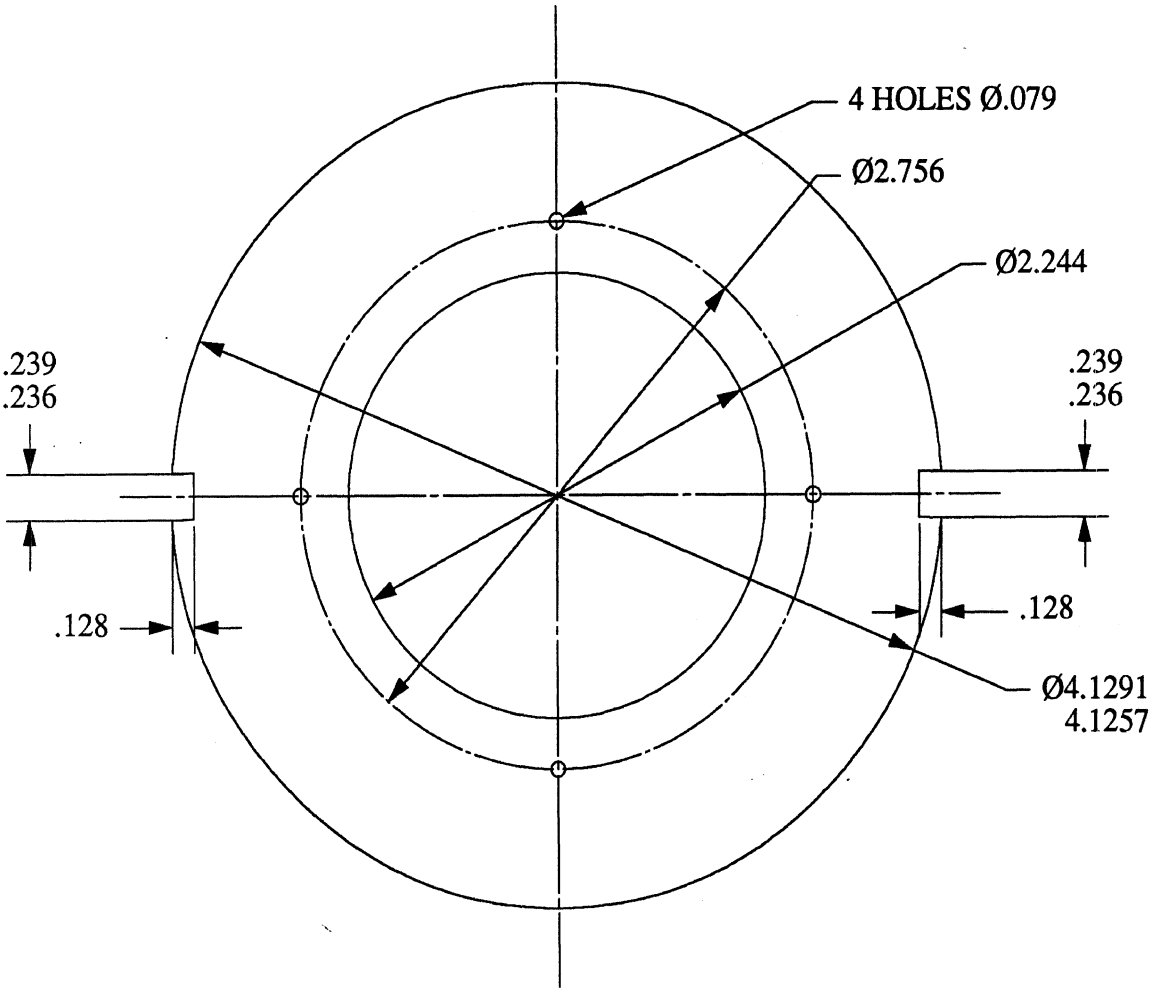


All corners: R 0.02

Thickness: .039

| Ground electrode | Stainless steel 18-8 | 39 |
|---|---|---|
| Part name | Material | Qty |

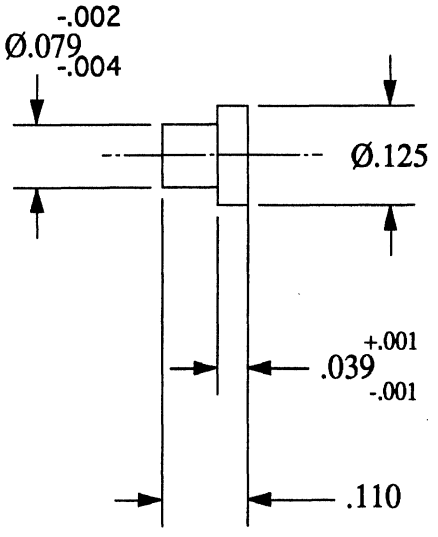


Scale: 4:1

| Spacer | Delrin | 320 |
|---|---|---|
| Part name | Material | Qty |

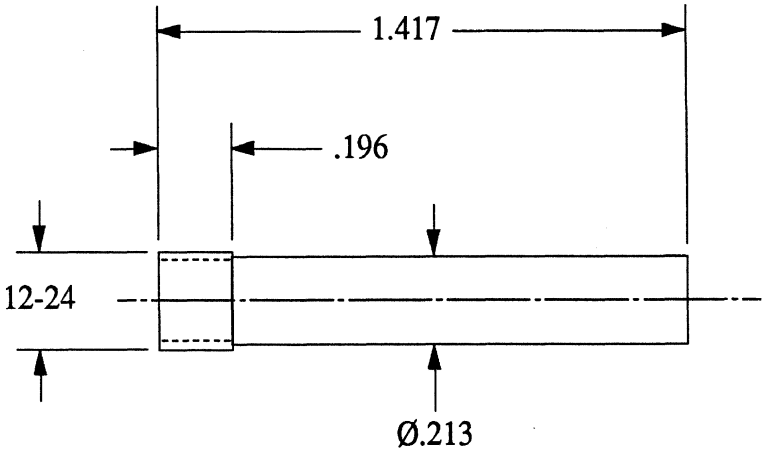


Scale: 2:1

| Part name | Material | Qty |
|---|---|---|
| Conduct bolt | Brass | 1 |

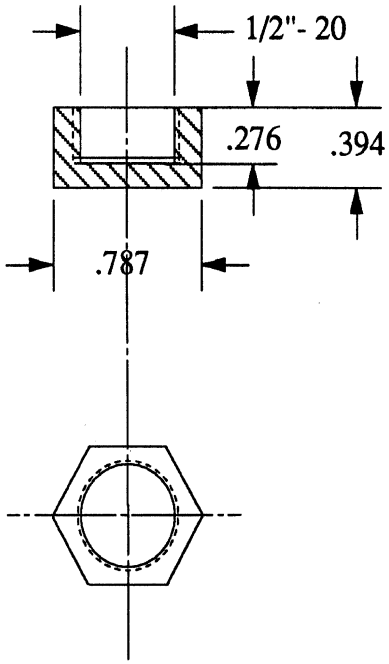


| Part name | Material | Qty |
|---|---|---|
| Metal piece | Brass | 1 |

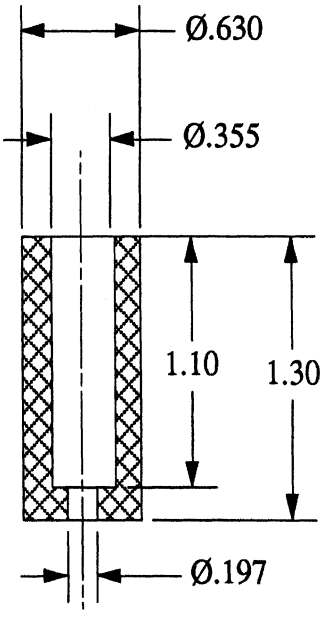


| Brush holder | Glass epoxy G-11 | 1 |
|---|---|---|
| Part name | Material | Qty |

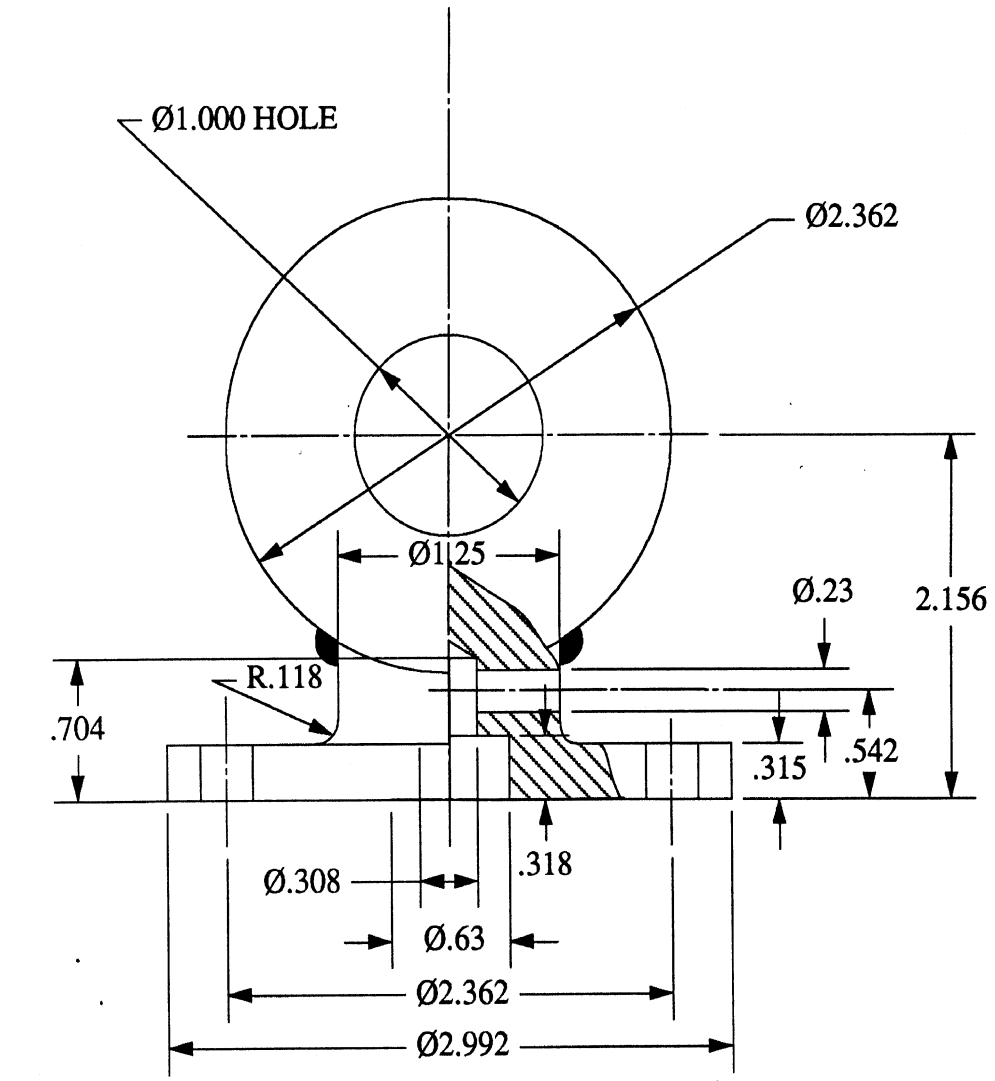


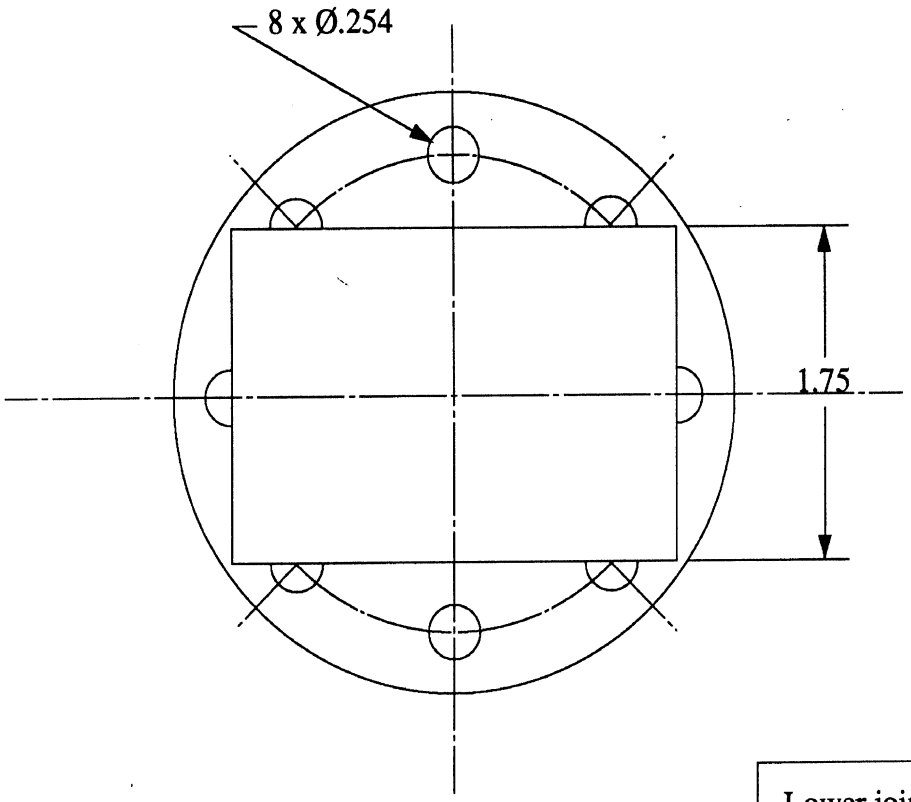


| Lower joint | Grade 12.9 Alloy steel | 1 |
|---|---|---|
| Part name | Material | Qty |